TECHNISCHE UNIVERSITÄT MÜNCHEN

Lehrstuhl für Ernährungsphysiologie

Phenotyping of PEPT1-deficient mice on the background of a high fat-diet induced obesity

Dominika Johanna Kolodziejczak

Vollständiger Abdruck der von der Fakultät Wissenschaftszentrum Weihenstephan für Ernährung, Landnutzung und Umwelt der Technischen Universität München zur Erlangung des akademischen Grades eines

Doktors der Naturwissenschaften

genehmigten Dissertation.

Vorsitzender: Univ.-Prof. Dr. D. Haller

Prüfer der Dissertation:

1. Univ.-Prof. Dr. H. Daniel
2. Univ.-Prof. Dr. J. J. Hauner

Die Dissertation wurde am 29.03.2012 bei der Technischen Universität München eingereicht und durch die Fakultät Wissenschaftszentrum Weihenstephan für Ernährung, Landnutzung und Umwelt am 18. 10. 2012 angenommen.

Table of content

List of figures V
List of tables VI
Abstract 1
Zusammenfassung 2

Introduction 3
1 Anatomy and physiology of the gut 3
1.1 The intestinal tube 3
1.2 Mucosa 4
2 Peptide transport 5
2.1 SLC 15 family 5
2.2 SLC15A1 – PEPT1 6
2.2.1 Tissue localization 6
2.2.2 Gene polymorphism 8
2.2.3 Molecular structure 8
2.2.4 Transport mechanism 9
2.2.5 Substrate specificity 10
2.2.6 Regulation 10
3 Sodium-proton exchange 12
3.1 SLC9A family 13
3.2 SCL9A3 – NHE3 13
4 PEPT1 and lipid metabolism in *Caenorhabditis elegans* 14
4.1 The link between PEPT1 and lipid metabolism 14
4.2 Interplay between NHE3 and PEPT1 15
5 Aim of the project 17

Methods 18
1 Mouse husbandry, handling and sample collection 18
1.1 Animals 18
1.2 Mouse husbandry 18
1.3 Genotyping 18

1.4 Dietary intervention study 19
1.5 Data sampling during study 20
1.6 Collection of plasma and tissue samples 21
2 Feces analyzes 21
2.1 Intestinal transit time 21
2.2 Bomb calorimetry: energy intake by food and fecal energy excretion 22
2.3 Fourier-Transform infrared spectroscopy (FT-IR) 22
2.4 Analysis of free fatty acids by gas chromatography-mass spectrometry 23
3 Lipid analyzes in plasma, liver and caecum content 23
3.1 Triglyceride analysis in liver and caecal content 24
3.2 Non-esterified fatty acid (NEFA) analysis 24
3.3 Phospholipid (PL) analysis 25
4 Plasma analysis 25
4.1 General and lipid parameters in plasma 25
4.2 Insulin analysis in plasma 25
4.3 Leptin analysis in plasma 26
4.4 Pancreatic lipase and amylase activity in plasma 26
4.5 Amino acid analysis 26
5 Histology 26
5.1 Mounting samples in paraffin 26
5.2 Hemalum and Eosyn (H&E) staining 28

Results 29
1 Physiological analyzes of wild-type and *Pept1*$^{-/-}$ mice on High Fat Diet 29
1.1 Body weight and food and water intake 29
1.2 Body composition 31
1.3 Locomotor activity, energy expenditure and respiratory quotient 33
1.4 Organ parameters 35
2 Feces and caecum analyzes 39
2.1 Feces excretion and transit time 39
2.2 Fecal energy excretion 39
2.3 Fourier-Transform infrared spectroscopy (FT-IR) analysis of feces and caecal content 40

2.4 Caecal lipid analysis 43
2.5 Free fatty acids in caecal content – GC/MS analysis 43
3 Liver lipids 46
4 Blood parameters 47
4.1 Lipid parameters 47
4.2 General chemistry 49
4.3 Insulin concentration 51
4.4 Leptin concentration 51
4.5 Pancreatic lipase and amylase activity 52
4.6 Amino acid analysis 53
5 Interaction of PEPT1 and NHE3 56
5.1 Inhibitory effect of amiloride 56
5.2 S1611 treatment does not inhibit NHE3 57
5.3 Fat mass analysis during amiloride and S1611 treatment 57

Discussion 60
1 Metabolic syndrome 60
2 The *Pept1*$^{-/-}$ mouse – phenotypes on standard chow and high protein diet 60
3 C57BL/6 mice – an obesity prone model for diabetes and metabolic Syndrome 62
4 *Pept1*$^{-/-}$ mice are partially resistant to high fat diet-induced obesity 62
4.1 *Pept1*$^{-/-}$ mice showed lower weight gain despite similar energy intake 62
4.2 The *Pept1*$^{-/-}$ mouse – increased energy excretion due to changes in in gut microbiota? 63
4.3 Lower body weight are not due to changes in locomotor activity 64
4.4 WT and *Pept1*$^{-/-}$ mice on HFD – suffering from NAFLD? 66
4.5 Amino acid and impaired bile acid secretion – leading to maldigestion or malabsorption 68
4.6 Adaptation to HFD leads to morphological changes in the small Intestine 69
5 Lipid accumulations due to impaired NHE3 activity? 71

Conclusion 74

Appendix – Composition of diets **75**
Abbreviations **76**
References **81**
Acknowledgement **90**
CV **92**
Erklärung **95**

List of figures

Fig.1: Structure of the small intestine 1
Fig. 2: Model of human PEPT1 secondary structure 8
Fig. 3: Schematic view of peptide transport across the brush-border membrane 9
Fig. 4: Functional link between the sodium-proton exchanger NHE3 and intestinal free fatty acid uptake 16
Fig. 5: Mean body weight, food, energy and water intake of *Pept1*$^{-/-}$ and WT mice on CD and HFD 30
Fig. 6: Body composition of *Pept1*$^{-/-}$ and WT mice 32
Fig. 7: Weight and size of various tissues 33
Fig. 8: Cumulative locomotor activity in *Pept1*$^{-/-}$ and WT mice 34
Fig. 9: Energy expenditure, O_2 consumption and CO_2 production in *Pept1*$^{-/-}$ and WT mice 35
Fig. 10: Percentage of various tissues per body weight in *Pept1*$^{-/-}$ and WT mice 37
Fig. 11: Villi length and length of small and large intestine of *Pept1*$^{-/-}$ and WT mice 38
Fig. 12: Weekly feces excreted by *Pept1*$^{-/-}$ and WT mice 39
Fig. 13: Fecal energy content and total fecal energy excretion of *Pept1*$^{-/-}$ and WT mice 40
Fig. 14: Caecum and feces analysis of *Pept1*$^{-/-}$ and WT mice on CD and HFD 41
Fig. 15: Cluster analysis of fecal nutrient content of *Pept1*$^{-/-}$ and WT mice 42
Fig. 16: Lipid analysis of caecal content of *Pept1*$^{-/-}$ and WT mice 43
Fig. 17: Analysis of free fatty acids in caecal content of *Pept1*$^{-/-}$ and WT mice 44
Fig. 18: Triglyceride, phospholipid and non-esterified fatty acid concentration of *Pept1*$^{-/-}$ and WT mice 46
Fig. 19: Plasma lipid parameters in *Pept1*$^{-/-}$ and WT mice 48
Fig. 20: Non-esterified fatty acids and phospholipid concentrations in plasma of *Pept1*$^{-/-}$ and WT mice 49
Fig. 21: ALT and AST concentrations in plasma of *Pept1*$^{-/-}$ and WT mice 50
Figure 22: Plasma insulin concentrations in plasma of *Pept1*$^{-/-}$ and WT mice 51
Figure 23: Plasma leptin concentrations in plasma of *Pept1*$^{-/-}$ and WT mice 52

Figure 24: Enzymatic activity of pancreatic lipase and amylase in *Pept1*$^{-/-}$ and WT Mice 53
Figure 25: Concentration of free amino acids in plasma of *Pept1*$^{-/-}$ and WT mice 55
Figure 26: Mean body weight, food and water intake of WT mice treated with Amiloride 56
Figure 27: Mean body weight, food and water intake of WT mice treated with S1611 57
Figure 28: NMR analysis of fat and lean mass of WT mice treated with Amiloride 58
Figure 29: NMR analysis of fat and lean mass of WT mice treated with S1611 59
Figure 30: Structure of amiloride 71
Figure 31: Structures of specific NHE3 inhibitors 72

List of tables

Table 1: SLC15 – The proton-coupled oligopeptide family 6
Table 2: Tissue and cellular localization and function of PEPT1 7
Table 3: Tissue and cellular localization and function of NHE3 14
Table 4: Primer sequences for genotyping of *Pept1*$^{-/-}$ and WT mice 19
Table 5: Body composition of *Pept1*$^{-/-}$ and WT mice 31
Table 6: Percentage of organ weight per body weight in *Pept1*$^{-/-}$ and WT mice 36
Table 7: Plasma lipid parameters of *Pept1*$^{-/-}$ and WT mice on CD and HFD 47
Table 8: General plasma parameters of *Pept1*$^{-/-}$ and WT mice on CD and HFD 50
Table 9: Concentration of pancreatic enzymes of *Pept1*$^{-/-}$ and WT mice 52
Table 10: Concentrations of plasmic amino acids in *Pept1*$^{-/-}$ and WT mice 54

Abstract

The intestinal peptide transporter PEPT1 transports most of the 8000 different di- and tripeptides and a large number of peptidomimetics. Transport is energized by an inwardly directed electrochemical proton gradient that is generated and maintained by the (i) Na^+/H^+ antiporter NHE3 in the apical membrane and the (ii) Na^+/K^+ ATPase in the basolateral membrane of enterocytes. In the nematode *Caenorhabditis elegans* lacking *pept-1* a highly increased fat accumulation was observed and animals displayed abnormal fatty acid patterns. By using specific inhibitors it was shown that the increase in intestinal fatty acid absorption in worms also depends on NHX-2, a homolog of the mammalian Na^+/H^+ antiporter NHE3 [1]. However, when WT and *Pept1*$^{-/-}$ mice were fed a high fat diet, only WT animals showed an obese phenotype. Surprisingly both genotypes had increased lipid parameters in plasma and liver samples. While WT mice adapted to the higher dietary fat content by increasing villus height *Pept1*$^{-/-}$ mice on HFD had a reduced villi length and IL-6 concentrations indicating an impaired intestinal cell proliferation. These mice had also lowered concentrations of taurine that may lead to a reduced bile acid production and secretion. As a result cholesterol degradation may be reduced leading to an increased fecal energy excretion. Furthermore, while *Pept1*$^{-/-}$ mice fed a control diet showed enlarged caeca indicating a high bacterial growth, *Pept1*$^{-/-}$ animals on high fat diet had smaller caeca suggesting a reduced bacterial growth. Fat utilization by bacteria is low and therefore energy excretion is consequently high.
All data indicate that *Pept1*$^{-/-}$ mice on HFD have a maldigestion, i.e. reduced concentrations of pancreatic enzymes and bile acids and changes in gut microbiota, and a malabsorption, i.e. decreased villus height in the small intestine.

Zusammenfassung

Der intestinale Peptidtransporter PEPT1 transportiert die meisten der 8000 verschiedenen Di- und Tripeptide, aber auch eine große Anzahl von Peptidmimetika. Der Transport wird ermöglicht durch eine nach innen gerichteten elektrochemischen Protonengradienten. Dieser wird erzeugt und aufrechterhalten von (i) dem Na^+/H^+ Antiporter NHE3 in der apikalen und (ii) der Na^+/K^+-ATPase in der basolateralen Zellmembran der Enterozyten. Erhöhte Lipidakkumulation und Veränderungen in der Fettsäurezusammensetzung wurden in einem *pept1*-defizienten *Caenorhabditis elegans* beobachtet. Durch Versuche mit einem spezifischen Inhibitor konnte gezeigt werden, dass die erhöhte Fettsäureabsorption in diesen Wurm abhängig ist von NHX-2, einem Homolog zu dem Na^+/H^+ Antiporter NHE3 in Säugern. Das deutet darauf hin, dass PEPT1 und NHE3 sowohl in die Peptid- als auch in die Fettsäureaufnahme involviert sind. Wurden Wildtyp- und *Pept1*$^{-/-}$ -Mäuse mit einer fettreichen Diät gefüttert, zeigten nur Wildtyp-Mäuse einen adipösen Phänotyp. Jedoch hatten beide Genotypen erhöhte Lipidwerte im Blutplasma als auch in der Leber. WT-Mäuse zeigten eine Anpassung an den höheren Fettgehalt der Nahrung, indem die Darmvilli länger wurden. Im Gegensatz dazu hatten *Pept1*$^{-/-}$ -Mäuse verkürzte Darmvilli und eine erniedrigte Konzentration von IL-6, was auf eine reduzierte intestinale Zellproliferation hindeutet. Diese Tiere hatten auch niedrigere Konzentrationen der Aminosäure Taurin, was zu einer reduzierte Produktion und Sekretion von Gallensäuren führen kann. Eine mögliche Folge davon wäre ein reduzierter Abbau von Cholesterin und damit eine erhöhte fäkale Energieausscheidung. Zudem hatten *Pept1*$^{-/-}$-Mäuse auf der Kontrolldiät vergrößerte Caeca, was auf verstärktes Bakterienwachstum hinweist. Dagegen hatten *Pept1*$^{-/-}$-Mäuse auf der fettreichen Diät kleine Caeca, was ein reduziertes Bakterienwachstum vermuten läßt.

Diese Daten geben einen möglichen Hinweis darauf, dass *Pept1*$^{-/-}$ -Mäuse auf der fettreichen Diät unter einer Maldigestion (reduzierte Konzentrationen von pankreatischen Enzymen und Gallensäuren, veränderte Darmflora) und Malabsorption (verkürzte Villi im Dünndarm) leiden.

Introduction

1 Anatomy and physiology of the gut

1.1 The intestinal tube

The murine intestine is a 40-50 cm long tube [2] that is divided in two main parts: small and large intestine. Both are separated from each other by the caecum. The small intestine itself is 29-39 cm long [2] and is subdivided in three parts – duodenum, jejunum and ileum. The caecum is highly populated by diverse bacteria [3, 4] which contribute to the digestion of nutrients. The large intestine is relatively short when compared to the small intestine – only 9-14 cm [2]. It can be further subdivided into colon and rectum.

The major role of the small intestine is the uptake of various nutrients from the chyme that is released by the stomach. This uptake is mediated via a number of transporters, e.g. peptide transporter, amino acid transporter, glucose transporter etc. which are located on the apical side of epithelial cells in the gut. Dietary nutrients are then absorbed by the portal vein or the lymphatics and transported to their target organs such as liver, brain or muscles. To fulfill its absorbent function the gut has a mean surface of 1.41 m^2 [5]. This is achieved by (i) circular folds of the murine gut wall and (ii) evaginations of the mucosa called villi [6]. The intestinal wall is composed of four different layers (Figure 1) that contribute to further digestion of the chyme and to the uptake of nutrients: the innermost layer that surrounds the lumen is called the **mucosa**. It comes in direct contact with the chyme and is therefore responsible for secretion of hormones and enzymes and absorption of nutrients (small intestine) and water (large intestine). The mucosa can be further divided into the epithelium, the *Lamina propia* and the *Muscularis mucosae*. The **submucosa** is a thin layer of connective tissue between the mucosa and the muscularis. It includes large blood vessels, lymphatics and the enteric nervous system branching into the musoca as well as into the muscularis. The latter one contains the Meissner´s plexus, an enteric nervous plexus on the inner surface of the muscularis. The **muscularis** consists of an inner circular and an outer longitudinal muscular layer. Both together enable coordinated contractions called peristalsis: the inner layer

propels the food through the gastrointestinal tract and the longitudinal layer shortens the tract. In between these two muscle layers is the Auerbach´s plexus. The outermost tissue is the **serosa** that is composed of a connective tissue and a secretory epithelial layer (mesothelium). It is responsible for secretion of lubricating fluid which reduces friction from muscle movement.

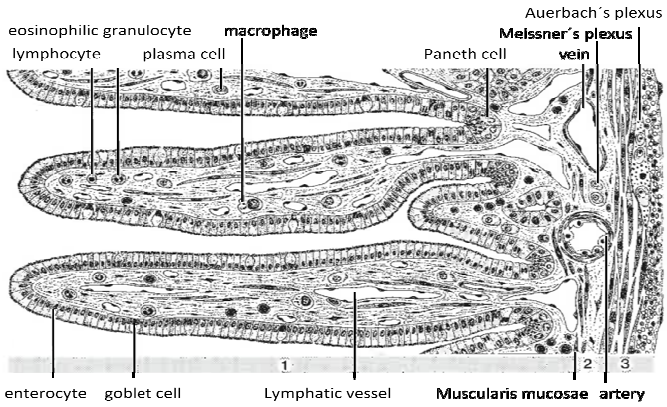

Figure 1: Structure of the small intestine. 1. Mucosa 2. Submucosa 3. Muscularis (from Storch and Welsch, 1999, modified)

1.2 Mucosa

The intestinal barrier is formed by the mucosa. It is an epithelial monolayer that is organized into crypt-villus units and has an intraluminal pH value of 6.1 to 6.8 [7-9]. Proliferating cells are limited to the crypt where the pool of multipotent stem cells is located [10]. These stem cells differentiate into four different cell types: goblet cells, paneth cells, enteroendocrine cells and enterocytes [11]. During differentiation cells migrate from the bottom of the crypts to the villous tip – only paneth cells remain at the base of the crypts. Reaching the villous tip, cells become apoptotic and are shed into the lumen where they are digested. Whether a cell differentiates into a paneth cell, an enterocyte or another cell type is influenced by various factors, e.g. transcription factors, secretion factors or the extracellular matrix [10]. This cycle of migration, differentiation and mortality takes 3 – 5 days [12]. **Goblet cells** secrete mucins that dissolve in water to form the mucus. Mucus has various functions: in the esophagus it serves as lubricant for food, in the stomach it protects against the highly acidic environment and in the intestinal tract it functions as a barrier against infectious agents, e.g. bacteria, viruses and fungi. **Paneth cells** are secretory cells

localized at the bases of intestinal crypts (crypts of Lieberkühn) [13]. This type of cells contributes to intestinal defense against micro-organisms by secreting antimicrobial substances, e.g. lysozyme, intestinal phospholipase A2 and defensins [14, 15]. Most **enteroendocrine cells** are found in the islets of Langerhans, but they are also found in the intestinal tract. They have the ability to secrete different hormones: Glucagon (α cells), insulin and amylin (β cells), somatostatin (δ cells) and ghrelin (ε cells) are secreted from the pancreas whereas gastrin (G cells of stomach, duodenum and pancreas), cholecystokinin (I cells of duodenum), motilin (M cells of duodenum and jejunum), gastric inhibitory peptide (GIP) (K cells of duodenum and jejunum), Glucagon-like peptide 1 (GLP-1) and Glucagon-like peptide 2 (GLP-2) (L cells of ileum and colon) are released from the gut itself. **Enterocytes** represent the major cell population along the villus [16]. These are polarized columnar cells with a height of about 30 µm [17]. The apical side, facing the gut lumen, is covered by microvilli that enlarge the intestinal surface 13 – 19 times [17]. Their functions include the uptake of ions (Na^+, Ca^{2+}, Mg^{2+} and Fe^{3+}), water, sugar, peptides and amino acids, lipids and vitamin B12. The uptake of these compounds is mediated via a number of transporters in the apical brush-border membrane. On the basolateral side these substances are released into the bloodstream or the lymphatics.

2 Peptide transport

During the 1970´s, the active absorption of short peptides was shown in mammalian gut epithelial cells. At this time it was believed to be driven by a transmembrane Na^+ gradient. In the 1980´s it was proven to be energized by an inwardly driven proton gradient across brush-border membranes – but still the transporters remained unknown. Just in the mid 1990´s the underlying transporters were identified. Today we know that the transport of peptides across membranes into cells is performed by specific, energy-dependent transporters. They are found in all kind of organisms from bacteria to humans [18].

2.1 SLC15 family

The **s**o**l**ute **c**arrier (SLC) family is a group of membrane transport proteins with more than 300 members that are organized into 47 groups [19]. Peptide transporters

belong to the SLC15 family. It is also called the Proton-coupled Oligopeptide Transporter (POT) super family or the Peptide Transporter (PTR) family [18]. Members of the mammalian POT-family are electrogenic transporters that utilize the proton-motive force for the transport of short chain peptides and peptido-mimetics across the plasma membrane. So far, four members in this super family have been identified: PEPT1 (SLC15A1), PEPT2 (SLC15A2), PHT2 (SLC15A3) and PHT1 (SLC15A4). The proteins of this super family vary in size between 450 and more than 700 amino acids. All members are predicted to have 12 transmembrane domains (TMD) with N- and C-termini facing the cytosol [20]. The characteristics of each member are summarized in Table 1.

Table 1: SLC15 – The proton-coupled oligopeptide family (modified from [20])

Human gene name	Protein name	Predominant substrates	Tissue distribution and (sub-) cellular expression	Human gene locus
SLC15A1	PEPT1	Di- and tripeptides, protons, β-lactam antibiotics	Intestine, kidney, apical, lysosomal membrane	13q33-q34
SLC15A2	PEPT2	Di- and tripeptides, protons	Kidney, lung, brain, mammary gland, bronchial epithelium	3q13.3-q21
SLC15A3	PHT2	Histidine, di- and tripeptides, protons	Lung, spleen, thymus, (faintly brain, liver, adrenal gland, heart)	11q12.1
SLC15A4	PHT1	Histidine, di- and tripeptides, protons	Brain, retina, placenta	12q24.32

2.2 SLC15A1 - PEPT1

PEPT1 (SLC15A1) was the first mammalian peptide transporter cloned from rabbit intestine in 1994 [21, 22].

2.2.1 Tissue localization

Human PEPT1 was shown to be expressed in a number of various tissues as shown in Table 2 - mainly being expressed in the apical membrane of enterocytes in the small intestine [22, 23]. In humans, the highest mRNA levels were found in duodenum with decreasing levels towards the ileum [24]. Ford et al. showed that PEPT1 is nearly absent or expressed at very low levels under normal healthy

conditions in human colonic mucosa [25]. However, PEPT1 expression was changed in patients suffering from short-bowel syndrome (SBS), chronic ulcerative colitis and Crohn´s disease. Under these inflamed conditions PEPT1 mRNA and protein levels were shown to be up regulated [26, 27]. But newest data of our group demonstrate PEPT1 mRNA and protein expression in murine colon also under normal conditions without inflammation (unpublished data). Several groups found PEPT1 expression also in the S1 segment of the proximal tubule in kidney [23, 28, 29] and even in zebrafish [30]. Furthermore transport activity was detected in renal lysosomal membranes to transport peptides from the cytosol into lysosomes [31] and in liver cells where peptides were translocated from lysosomes into the cytosol after protein degradation [32]. Additonally, PEPT1 is expressed in the nuclei of vascular smooth muscle cells of the pancreas [33, 34]. Newest data also show PEPT1 expression (mRNA and protein level) and transport activity in human nasal epithelium [35].

Table 2: Tissue and cellular localization and function of PEPT1 (modified from [36])

Tissue	Localization	Species	Function	Reference
Bile duct	Apical membrane of cholangiocytes	Mouse		[37]
Kidney	Present depending on organism	Rat, zebrafish, human to be clarified	Probably minor or no role in the reabsorption of di- and tripeptides and peptidomimetics	[23, 24, 28, 30, 38-40]
Liver	Lysosomal membrane	Rats	Transport of small peptides from lysosome to cytoplasm after protein degradation	[32]
Nasal epithelium	Nasal epithelial cells	Human		[35]
Reproductive organs	Present with very low expression in Sertoli cells	Rat, mouse		[41]
Pancreas	Lysosomes of acinar cells	Rat		[33, 34]
Small intestine	Brush-border membrane in epithelial cells of duodenum, jejunum, ileum	Human, rat, mouse	Absorption of di- and tripeptides and peptidomimetics	[22-24, 42]

In mice, PEPT1 was detected in the brush-border membrane of enterocytes in the small intestine [42]. Additionally, its expression has been shown in apical membrane of cholangiocytes of the bile duct [37] and in Sertoli cells of the testes [41].

2.2.2 Gene polymorphism

The gene encoding hPEPT1 is located on chromosome 13q33-34 and contains 23 exons and 22 introns. As this gene is conserved it shows only little genetic polymorphisms among ethnic groups. Zhang et al. performed a genetic screening of 44 ethnically diverse individuals and indentified nine non-synonymous and four synonymous coding-region single-nucleotide polymorphisms (SNPs) [43]. Among these SNPs only one single SNP (P586L) leads to significantly reduced transport activity.

2.2.3 Molecular structure

The mammalian PEPT1 proteins are highly homologous with 707 aa (rabbit) [22], 708 aa (human) [44], 709 aa (mouse) [45] and 710 aa (rat) [46], respectively. The protein is composed of 12 TMD with both termini facing into the cytosol. It is predicted to have a big extracellular loop between TMD 9 and 10 (Figure 2) and TMD 1-4 and 7-9 were shown to be critical for substrate affinity [47-49]. Human PEPT1 is highly glycosylated and contains two protein kinase C (PKC) binding sites [44].

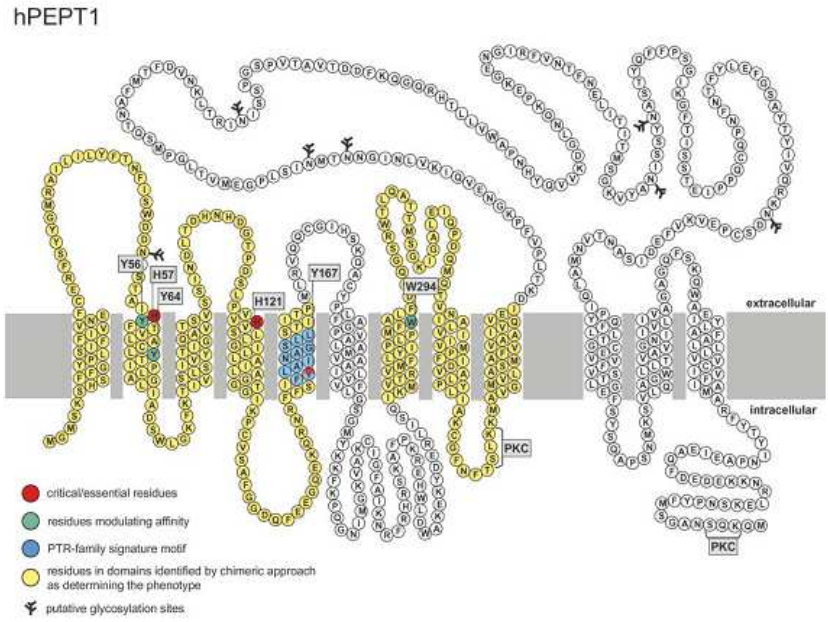

Figure 2: Model of the human PEPT1 secondary structure. Amino acid residues and protein domains with importance for the transport process are highlighted: Residues that alter substrate specificity or are essential for transport activity (red, green) and the signature motif of the POT-transporter family (blue). (from [50]).

2.2.4 Transport mechanism

In 1983 Ganapathy and Leibach demonstrated that intestinal peptide uptake is driven by an inwardly directed proton gradient [51] with an acidic microclimate (pH 6.1 to 6.6) on the luminal surface of the epithelial cells [7]. This gradient is generated and maintained by the (i) Na^+/H^+ antiporter NHE3 in the apical membrane and the (ii) Na^+/K^+ ATPase in the basolateral membrane of enterocytes [52] (Figure 3). The import of peptides is a well ordered and simultaneous procedure in which the proton binds first to PEPT1 but substrate and proton are imported together [53].

PEPT1 has a broad substrate spectrum with preference to substrates with no net charge. These compounds are imported with a 1:1 stoichiometry in proton to substrate flux [54]. For di- and tripeptides with glutamate or aspartate residues, two protons are required to translocate the substrate into the enterocyte. In this case the second proton is believed to protonate the side chain carboxyl group prior to transport [54, 55]. PEPT1 translocates cationic peptides containing arginine or lysine groups preferentially in their neutral form but in addition also in the charged form. This happens in a 1:1 stoichiometry in both cases. It was shown by Amesheh and colleagues that PEPT1 preferentially recognize zwitterionic dipeptides [56].

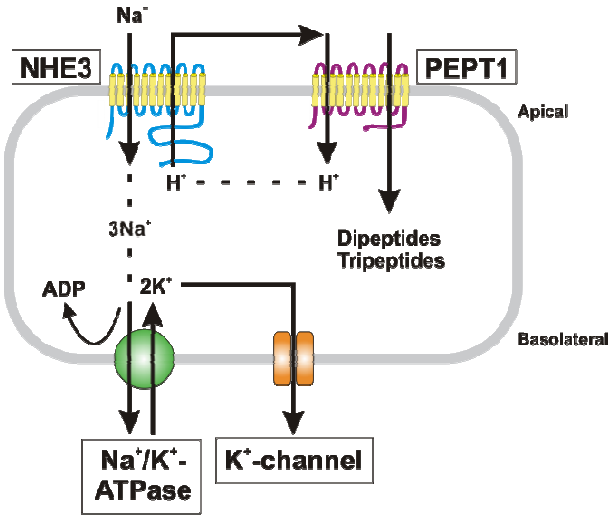

Figure 3: Schematic view of peptide transport across the brush-border membrane. PEPT1 transports di- and tripeptides together with protons (H^+) into epithelial cells. This leads to an intracellular acidification. To counteract this acidification the sodium-proton exchanger NHE3 exports H^+ in a 1:1 ratio out of the cell and imports sodium ions (Na^+) into the cell. Imported Na^+ leave the cell in exchange for potassium ions (K^+) via the Na^+/K^+-ATPase on the basolateral side. Potassium ions are finally pumped out by a K^+- channel.

2.2.5 Substrate specificity

Natural di- and tripeptides

Human PEPT1 (hPEPT1) has broad substrate specificity and transports most of the 400 di- and 8000 tripeptides resulting from breakdown of dietary protein in the intestinal lumen. But it does not translocate any single amino acids, tetrapeptides or larger peptides.

Translocation of peptides occurs stereospecific in the sense that PEPT1 has a much higher affinity to di-and tripeptides formed of L-amino acids than the ones containing D-amino acids [57]. Peptides solely consisting of D-stereoisomers will not be transported by PEPT1 [58]. Additionally, peptides consisting only of basic amino acids may not be transported by PEPT1 [59, 60].

Due to its cyclic structure that is conformational inflexible peptides containing proline in either the N-terminal or C-terminal position have demonstrated differences in transport affinity. Modifications, e.g. methylation or acetylation, in the N-terminal amino group or C-terminal carboxyl group of peptides lead to a reduced affinity for PEPT1 [61] and to a total loss of affinity when one or both of these groups is removed. The decrease in affinity is higher for modifications at the N-terminus [59].

Essential structural features for peptides to be transported by PEPT1 are: (i) L-amino acids, (ii) acidic or hydrophobic function at the C-terminus, (iii) a weakly basic group in the α-position at the N-terminus, (iv) a ketomethylene or acid amine bond and (v) a trans conformation of peptide bonds [36].

Xenobiotics

Beside di- and tripeptides, PEPT1 can transport a large number of drugs, e.g. amino β-lactam antibiotics of cephalosporin and penicillin classes (cefadroxil), selected ACE-inhibitors (captopril, enalapril), peptidase inhibitors (bestatin), anti-virals (acyclovir, ganciclovir) and prodrugs (L-DOPA) [62, 63].

2.2.6 Regulation

PEPT1 was shown to be regulated chronically as well as acutely by a variety of factors including its substrates, diet or disease.

Signal transduction:

In the human colon carcinoma cell line Caco-2, it was shown that treatment with phorbol esters (activator of protein kinase C) decreased Gly-Sar uptake. This was accompanied by a decrease in V_{max} and an unaltered K_m. This effect could be blocked by using an inhibitor of the protein kinase C, staurosporine [64]. Also cholera toxin inhibited the activity of PEPT1 by decreasing V_{max}. This inhibitory effect was blocked by inhibitors of protein kinase A and C [65].

PEPT1 substrates:

Upon expression to Gly-Sar, PEPT1 mRNA and protein levels in Caco-2 cells increased three and two folds, respectively. Also the uptake of another dipeptide (Gly-Gln) was increased two fold due to an increase in V_{max} but no changes in K_m [66]. Another study showed that Gly-Phe or phenylalanine alone could increase PEPT1 expression by stimulating the promoter activity [67].

Hormones:

Insulin is the most important metabolic hormone. In Caco-2 cells, it was shown to increase Gly-Gln uptake by increasing V_{max}. Also protein levels were increased due to release of PEPT1 from a cytoplasmic pool [68]. Buyse and colleagues showed that leptin increased Gly-Sar and cephalexin uptake in Caco-2 cells with an increased V_{max} but unaffected K_m [69]. Contrary to these two hormones, thyroid hormone T3 was found to reduce Gly-Sar uptake in Caco-2 cells by decreasing V_{max} [70]. Furthermore, it was shown that PEPT1 mRNA, protein and Gly-Sar uptake are decreased in hyperthyroid rats [71].

Inflammation:

Patients suffering from the short bowel syndrome were shown to have five-fold increased PEPT1 mRNA levels when compared to healthy subjects [27]. Additionally, patients with Crohn´s disease and ulcerative colitis have an induced PEPT1 expression in their colon. During these diseases, bacteria (e.g. *Escherichia coli*) secrete peptides like formyl-Met-Leu-Phe (fMLP) that act as chemotactic attractants to recruit neutrophils to the sites of inflammation [26]. As a possible mechanism of upregulation of PEPT1 in the colon, Vavricka and colleagues demonstrated that tumor necrosis factor α (TNF-α) and interferon γ (IFN-γ) could increase hPEPT1

protein density and transport activity of Gly-Sar [72]. An infection with the protozoa *Cryptosporidium parvum* is thought to be responsible for the intestinal malabsorption syndrome. It has been demonstrated in rats, that during the time of infection PEPT1 protein levels and activity were reduced but returned to normal levels after clearance of the parasites [73].

Diet:

Hindlet and colleagues could demonstrate that feeding mice a hypercaloric diet (35 % fat) over a period of four weeks resulted in 50 % decrease of PEPT1 mRNA and 30 % decrease in protein of PEPT1. This finally led to a 46 % reduced Gly-Sar uptake [74] when compared to control mice fed a laboratory chow (3 % fat). These observations were accompanied by a parallel two-fold decrease in leptin receptor expression.

Fasting:

After one day of fasting, rats had a three-fold increase in mRNA expression and a two-fold increase in PEPT1 protein levels and V_{max} in Gly-Gln uptake [75]. A fasting period of two days resulted in increased PEPT1 mRNA amount and transport activity in the upper and middle intestinal regions [76]. Other studies showed that different intestinal regions respond differently to total parenteral nutrition (TPN). It was demonstrated by Ihara and colleagues, that mRNA and protein levels were increased in the jejunum after a ten day administration of TPN [77]. A follow-up study showed no differences in the duodenum but increased mRNA levels in the ileum after rats have been given TPN for seven days [78]. Although the underlying mechanism remains unclear yet, Shimakura and colleagues proposed that peroxisome proliferator-activated receptor alpha (PPAR-α) induces PEPT1 expression by increasing mRNA levels [79].

3 Sodium-Proton-Exchange

Since the intracellular pH is important for cell division and development of multicellular organisms, cells have developed various pH-regulating mechanisms. The first sodium-proton exchanger was described in kidney tissue by Murer and colleagues [80].

3.1 SLC9A family

The **s**ol**u**te **c**arrier (SLC) family is a group of membrane transport proteins with more than 300 members that are organized into 47 groups [19]. Sodium-proton exchangers (NHE) belong to the SLC9A family. Members of this family are driven by an inwardly-directed sodium (Na^+) gradient [81, 82]. The human SLC9A family consists of 9 members, NHE1-9 (SCL9A1-9), that are organized in two isoforms: plasma membrane (NHE1-5) and intracellular, organellar isoforms (NHE6-9). The first group is further subdivided in NHEs that (i) resident permanently in the plasma membrane (NHE1, 2, 4) [83, 84] and (ii) the ones that cycle between the plasma membrane and recycling endosomes (NHE3, 5) [85-87]. The organellar isoforms include NHE6 that is located in recycling endosomes [88-90], NHE7 in the *trans*-Golgi network [91, 92], NHE9 in late endosomes and NHE8. But the intracellular localization of NHE8 is not yet determined [93, 94].
Of all these sodium-proton exchangers, NHE1-3 and 7 are present in all organs of the gastrointestinal tract and NHE6 is found in pancreas and liver. Contrary to this, NHE4 and 5 do not seem to be expressed in the intestine.
The proteins of this super family vary in size between 645 and 848 amino acids and consist of two domains: (i) the N-terminal transport domain (~ 500 aa) is responsible for the exchange of Na^+ for H^+ in a 1:1 stoichiometry and (ii) the C-terminal domain that is involved in the regulation of NHEs by growth factor and protein kinase. All members are predicted to have 12 TMD with an extracellular N- and an intracellular C-terminus whereby the plasma membrane-associated isoforms have longer C-termini.

3.2 SLC9A3 - NHE3

The human NHE3 gene is located on chromosome 5p15.3 and was shown to be expressed in a number of various tissues as shown in Table 3 – mainly being expressed in the gastrointestinal tract and kidney. In humans, NHE3 was reported to be expressed in the brush-border membrane of duodenum, jejunum and ileum as well as in colon, gall bladder and kidney (for review see [95]).
In mice, NHE3 is located on chromosome 13. Its expression was demonstrated to be higher in the epithelial cells of the colonic surface rather than in crypts [96].

Furthermore, murine NHE3 is expressed in canalicular cells of hepatocytes and on cholangiocytes [97].

Functional analysis of mammalian NHE3 showed it is the major protein involved in Na^+ and fluid reabsorption in the proximal tubule of kidney but also Na^+ absorption in ileum. This happens via an exchange of Na^+/H^+ with a 1:1 stoichiometry. Therefore, NHE3 regulates the systemic electrolyte, acid-base and water homeostasis [98].

Table 3: Tissue and cellular localization and function of NHE3

Tissue	Localization	Species	Reference
Stomach	Apical membrane of parietal cells	Rat	[99]
Duodenum	Brush-border	Human, rat	[100, 101]
Jejunum, Ileum	Brush-border	Human, rabbit, rat	[100, 102]
Colon	Brush-border	Human, rabbit, mouse	[96, 102]
Gallbladder	Cholangiocytes	Mouse, rat, rabbit, prairie dog	[97, 103, 104]
Liver	Canalicular membranes of hepatocytes	Mouse, rat	[97]

Human NHE3 can be inhibited by amiloride (IC_{50}=283 µM), cariporide (IC_{50}=900 µM), S1611 (IC_{50}=0.05 µM), S2120 (IC_{50}=0.07 µM), S2121 (IC_{50}=0.61 µM) and S3226 (IC_{50}= 0.02 µM) [105]. Furthermore, it was shown in studies with rats that inhibition of NHE3 with the specific inhibitors S1611 and S3226 leads to an increased duodenal bicarbonate secretion and saponification of free fatty acids. As a consequence, these free fatty acids are not absorbed by the intestinal epithelial cells [106]. From these findings, we hypothesize that NHE3 counteracts a diet-induced obesity by influencing intestinal fatty acid absorption with its action on the “fatty acid flip-flop”, the pH regulation and bicarbonate secretion.

4 PEPT1 and lipid metabolism in *Caenorhabditis elegans*

4.1 The link between PEPT1 and lipid metabolism

In the nematode *Caenorhabditis elegans,* it was demonstrated that a deletion of PEPT1 leads to drastic changes in the worm. These include amino acid deficiency, a reduced growth and a reduction of progeny by 60 % [1]. Additionally, Spanier and colleagues showed that *pept1(lg601)* worms (PEPT1 knockout worm) had a 2-fold increased amount of body fat and also larger fat granules in intestinal cells when

compared to wild-type worms. mRNA analysis of *pept1(lg601)* worms revealed 1653 genes with more than 1.5-fold up-regulation in expression. Major pathways affected by these changes were the lipid and fatty acid metabolism, cell signaling and amino acid metabolism [1], e.g. peroxisomal protein involved in fatty acid oxidation. When analyzing fatty acid composition the overall concentration of saturated fatty acids (SFA) remained unchanged but there was an increase in C16:0 fatty acids. Furthermore, levels of monounsaturated fatty acids (MUFA) were ~50 % higher and polyunsaturated fatty acids (PUFA) were ~45 % lower in *pept1(lg601)* than in wild-type *C. elegans*. The decrease in PUFA levels went along with a down-regulation of genes involved in elongation and desaturation of PUFAs.

4.2 Interplay between NHE3 and PEPT1

Intestinal di- and tripeptide uptake via PEPT1 is an electrogenic proton-coupled symport that is driven by an inwardly directed proton gradient. As a continuous H^+ uptake would lead to an intracellular acidification, this gradient has to be maintained by exporting protons back into the intestinal lumen. This process is performed by the (i) Na^+/H^+ antiporter NHE3 in the apical membrane and the (ii) Na^+/K^+ ATPase in the basolateral membrane of enterocytes.

In *C. elegans*, experiments with a fluorescent-labeled C12 fatty acid (BODYPI-C12) demonstrated a highly increased uptake of this fatty acid in *pept1(lg601)* worms. This was also observed in wild-type worms incubated for 1 h with 1 mM of the PEPT1 antagonist Lys-[z-NO_2]-Val. Keith Nehrke showed a functional coupling of PEPT1 (formerly OPT-2) and NHX-2 (homologue to NHE3) in regulation of the intracellular pH (pH_{ic}). NHX-2 was shown to be responsible for recovery of pH_{ic} after acidification resulting from di- and tripeptide uptake via PEPT1 [96]. Additionally, studies in human intestinal cells revealed that sodium-proton exchangers maintain the pH homeostasis [107] and therefore enable proton-dependent peptide uptake. Inhibition of these exchangers leads to an intracellular acidification that abolishes peptide uptake via PEPT1. A process directly influenced by changes in the proton gradient is the uptake of free fatty acids via the “fatty acid flip-flop” mechanism [108] (Figure 4). Initially, fatty acids are released from their transport protein, protonated and inserted in the outer leaflet of the plasma membrane with the carboxylic group facing the intestinal lumen. In this form it crosses the membrane resulting in a re-orientation of

the carboxylic group to the cytosolic site. After deprotonation the fatty acid leaves the inner leaflet of the plasma membrane and binds to intracellular fatty acid binding proteins (FABP).

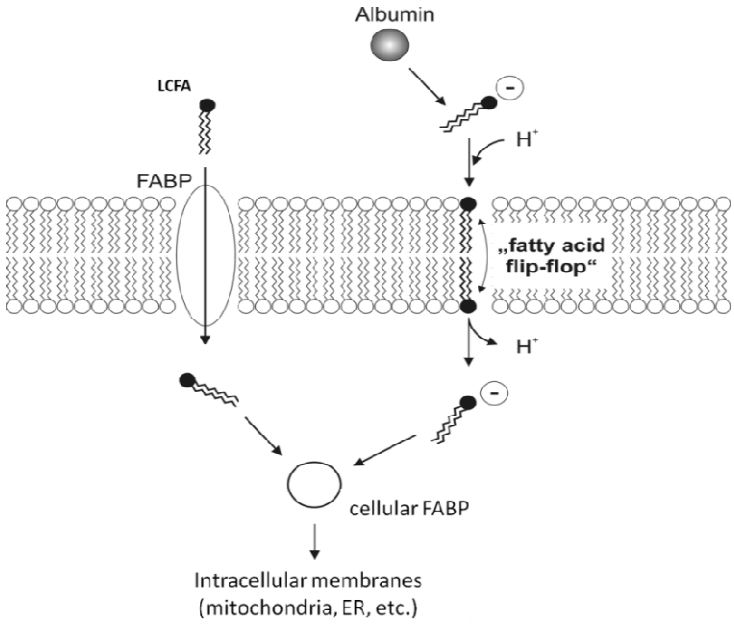

Figure 4: Functional link between the sodium-proton exchanger NHE3 and intestinal free fatty acid uptake. Right: Long chain fatty acids (LCFA) are released from their transport protein albumin. They move to the plasma membrane where they are protonated. Uncharged fatty acids can cross the plasma membrane via the “fatty acid flip-flop” mechanism. At the inner side of the plasma membrane they are deprotonated, bind to cellular fatty acid binding proteins (FABP) and are transported to intracellular membranes (mitochondria, ER, etc.). Protons (H^+) are co-transported with each fatty acid into the cell. This leads to a decrease in intracellular pH. **Left:** Fatty acid binding proteins inside the plasma membrane represent another transport mechanism for LCFA into the cells.

It was shown, that uptake of BODIPY-C12 was drastically reduced in wild-type and *pept1(lg601)* worms when the *nhx-2* gene was silenced by RNAi. These worms had a reduced fat content and smaller fat granules [1]. A decrease in BODIPY-C12 uptake was also seen after 1 h incubation with 1 µM of the specific NHE3 inhibitor, S3226. These data confirms results from Nehrke who reported a lean phenotype in *nhx-2*(RNAi) *C. elegans* [109] and proves a functional interaction between the intracellular pH homeostasis and fatty acid uptake.

5 Aim of the project

PEPT1 (SLC15A1) is primarily found in the brush border membrane of enterocytes in the small intestine but also with lower levels in other tissues. In humans, the highest mRNA levels were found in duodenum and decreasing towards the ileum. It is a unique feature of PEPT1 to transport almost all of the 8000 different di- and tripeptides that can be released by breakdown of dietary protein in the intestinal lumen. Beside di- and tripeptides PEPT1 also transports a large number of drugs, including β-lactam antibiotics, peptidase inhibitors, anti-virals and prodrugs. Transport is energized by an inwardly directed electrochemical proton gradient and an acidic microclimate on the luminal surface of the epithelial cells. This proton gradient is generated and maintained by the (i) Na^+/H^+ antiporter NHE3 in the apical membrane and the (ii) Na^+/K^+ ATPase in the basolateral membrane of enterocytes.
In the model organism *Caenorhabditis elegans* lacking the intestinal peptide transporter *pept-1* a highly increased fat accumulation was observed and animals displayed abnormal fatty acid patterns. That the increase in intestinal fatty acid absorption in worms also depends on NHX-2, a homolog of the mammalian Na^+/H^+ antiporter NHE3, was demonstrated by use of specific inhibitors and down-regulation of the gene. The findings, however, supported the notion that PEPT1 and the transmembrane proton gradient essentially affect intestinal uptake of both peptides and fatty acids and moreover, that the fat absorption might be influenced by PEPT1.

The aim of the project was to explore a possible interplay between PEPT1 and lipid homeostasis in mammals. We assessed whether a PEPT1-deficient mouse line shows phenotypic changes when fed a normal high carbohydrate control diet or a high-fat diet that causes diet-induced obesity (DIO) in wild-type animals. Additionally, we wanted to address the question whether the interplay between NHE3 and PEPT1 is also found in mammals. Therefore, WT and *Pept1*$^{-/-}$ mice were treated with amiloride and S1611 to inhibit NHE3 activity. We monitored weight gain, food and water intake as well as body fat and lean mass composition.

Methods

1 Mouse husbandry, handling and sample collection

1.1 Animals

Wild-type C57/BL6 mice were raised in our SPF animal facility. *Pept1*$^{-/-}$ were purchased from Deltagen (San Carlos, California, USA). Further breeding of these knockout animals was carried out in house.

1.2 Mouse husbandry

All animals were kept at 22 ± 2 °C and a 12:12 hrs light/dark cycle under SPF conditions. Mice had access to water and a standard chow (Ssniff, Soest, Germany) *ad libitum*. For the experiment homozygous C57BL/6 (*Pept1*$^{+/+}$) and *Pept1*$^{-/-}$ mice, respectively, were mated to obtain entirely homozygous litter. All procedures in this study were performed according to the German guidelines for animal care and approved by the state ethics committee under reference number 55.2-1-54-2531-39-10 and 55.2-1-54-2532-45-11.

1.3 Genotyping

Mice were genotyped by PCR screening with primers (sequences see Table 4) directed against the *Pept1* wild-type allele and the LacZ cassette that is inserted in the targeted allele, respectively. Tail biopsies were digested o/n at 65 °C with proteinase K (0.5 mg/ml proteinase K, 50 mM KCl, 10 mM Tris-HCl, 0.1 mg/ml gelatine, 0.45 % Nonidet NP-40, 0.45 % Tween 20, pH 8.3). Afterwards, proteinase K was heat inactivated at 95 °C. PCR was performed using 1 µl of the digested sample that contained genomic DNA. PCR products were run on a 1.5 % agarose gel. A band of 213 bps indicated the product of the wild-type allele and a band of 360 bps indicated the product of the targeted allele.

Table 4: Primer sequences for mice genotyping of *Pept1*$^{-/-}$ and WT mice

Primer pair	direction	Sequence (5´- 3´)	Amplicon size [bp]
62970 WT	Forward	AGT GTG GGC TGG TGA GAC ACG TGT C	213
62971	Reverse	CAG GGG GCG AGA GAA ACA GAG TTA G	
3195 Neo	forward	GGG CCA GCT CAT TCC TCC CAC TCA T	360
62971	Reverse	CAG GGG GCG AGA GAA ACA GAG TTA G	

1.4 Dietary intervention study

High-fat diet feeding study:

During the dietary intervention study male wild-type (WT) and *Pept1*$^{-/-}$ mice received purified diets with a low (13 energy %) or high (48 energy %) fat content. For each diet and genotype 15 animals were studied. The formulation of each diet is to be found in the appendix. 6 weeks old male mice were placed separately in cages and the standard chow was changed to the experimental diet. The feeding trial was carried out for 12 weeks and animals had access to tap water and food *ad libitum*.

NHE3 inhibition study:

Since there is no literature available for longtime inhibition of NHE3, we first looked for the lowest effective dose of amiloride (general sodium-channel inhibitor) and S1611 (specific NHE3 inhibitor).

During the NHE3 inhibition study, 3x 15 male WT mice (6 weeks of age) were separated into three groups of 5 mice (15 mice per inhibitory substance): (i) control group, (ii) 1st treated group and (iii) 2nd treated group. All three groups were fed a 48 % high-fat diet for the first two weeks of the study. Both treated groups received either amiloride or S1611 (kind gift from Sanofi-Aventis GmbH, Frankfurt, Germany) in the drinking water at weeks 3 (5 and 10 µg/ml) and 5 (20 and 30 µg/ml). At weeks 4 and 6, mice had a recovery phase with no supplement in the water. The feeding trial was carried out for 8 weeks and animals had access to tap water and food *ad libitum*.

1.5 Data sampling during study

Weight gain, food and water consumption:

Body weight and food and water consumption were monitored once a week between 9.00 and 9.30 a.m. for a period of 12 weeks (feeding study) or 8 weeks (NHE3 study). Feces of every mouse were collected at week 4, 8 and 12 for calorimetric analyzes.

Locomotor activity:

After 4 weeks on the experimental diet 5 mice of each group were housed for three days in special feeding-drinking-activity cages (TSE-Systems, Bad Homburg, Germany) to monitor the activity of each mouse. This system enables to detect the activity in x-, y- and z-direction. It consists of sensor frames with 32 light barriers on the longitudinal and 16 light barriers on the breadth side. Furthermore, there are sensors in the holding device for food and water containers that allow measuring the frequency and amount of food and water consumption. All cages are connected to a computer with LabMaster V2.8.3 software (TSE-Systems, Bad Homburg, Germany) which records and visualizes all measurements for 24 h per day. During that analysis mice received food and water *ad libitum.*

Indirect calorimetry:

After 4 weeks on the experimental diet 5 mice of each group were housed for three days in special calorimetry cages (TSE-Systems, Bad Homburg, Germany) to monitor the oxygen consumption and carbon dioxide production. During that analysis mice received food and water *ad libitum.*

NMR analysis:

Mice from the NHE3 study underwent a weekly scan to detect changes in body fat and lean mass composition. Animals from the HFD feeding study were scanned at weeks 4, 8, and 12. Therefore mice were put in a restrainer that was locked at both ends and measured in a LF50H BCA-Analyzer using the m^+ software (Bruker Optics, Ettlingen, Germany).

1.6 Collection of plasma and tissue samples

Blood samples were taken under isofluran anesthesia by puncturing the retro-orbital sinus with heparin coated capillaries (Neolab, Heidelberg, Germany). To obtain plasma for further analysis, blood was collected in Li-Heparin coated tubes (Sarstedt, Nuembrecht, Germany). Collected samples were centrifuged at 3000 g for 10 min within 1 h to prevent possible degradation. All plasma samples were stored at –80 °C until they were analyzed.

For collection of tissue samples mice were dissected and organ weights were determined on a precision balance with 15 male mice per genotype and diet. Organ weights are expressed in relation to body weight.

Small pieces of the intestine (proximal and distal part of small intestine, colon), liver and epididymal adipose tissue were put in an eppendorf tube containing 500 µl of 4 % paraformaldehyde for histological analyzes. The remaining samples were put in an eppendorf tube and frozen directly in liquid nitrogen. For long term storage samples were kept at – 80°C.

2 Feces analysis

To determine whether the two genotypes show differences in absorption or digestion of nutrients, we performed fecal analysis for energy content and detailed composition of excreted nutrients. For this purpose, feces samples of five individual mice per group were collected at week 4, 8 and 12 during the study. Each sample was dried for two days in an oven at 50 °C and fecal dry weight was recorded.

2.1 Intestinal transit time

Gastrointestinal transit time was determined according to Koopman and colleagues (1978). Briefly, 10 steel balls of 0.5 mm in diameter were given by gavage at 1900 on two subsequent days. On each day, during the following 10 h, the feces of individual mice was collected every 30 min and examined for occurrence of the balls. The median recovery time of the 10 steel balls was taken as the gastrointestinal transit time. Since the experiment was performed on two subsequent days, the final transit time was calculated as median from the values of both days.

2.2 Bomb calorimetry: energy intake by food and fecal energy content

Determination of the calorific value was performed with an automated oxygen bomb calorimeter 6300 (Parr Instrument GmbH, Frankfurt, Germany). The calorimeter uses the isoperibolic technique were the jacket temperature is kept constant while the temperature in the bomb (reaction chamber) changes after burning the sample.
For analysis 0.9-1.1 g of feces or food pellets were grinded and pressed. The pellets were put onto a high sensitive scale and the exact mass was recorded. Afterwards each pellet was placed in a small bucket and a thread was tied around the ignition wire. The sample was placed in the bomb calorimeter and measurement was started after entering the exact mass of the sample. Results are presented in kJ/g feces dry weight.
Total energy intake, total fecal energy excretion and energy assimilation were calculated according to the following formulas:

Total energy intake (kJ) = food intake (g) x energy content in food (kJ/g)

Total energy excretion (kJ) = feces excreted (g) x fecal energy (kJ/g)

Energy assimilation (kJ) = Energy intake (kJ) – energy excretion (kJ)

2.3 Fourier transform infrared spectroscopy (FT-IR)

To identify the fecal components and quantify amounts of carbohydrates, proteins and lipids, feces samples were analyzed with FT-IR spectroscopy. For analysis the FT-IR spectrometer Tensor 27 (Bruker Optik GmbH, Ettlingen, Germany) was used. Mouse feces were homogenized and the powder was loaded on an aluminum 96-well plate. The spectrometer was pre-cooled by liquid nitrogen. Each sample was measured in five replicates and data was analyzed using the OPUS software (Bruker Optik GmbH, Ettlingen, Germany).

2.4 Analysis of free fatty acids by gas chromatography-mass spectrometry

To measure free fatty acids, caecal content was lyophilized for 20 h under vacuum. Metabolites were extracted from 10-30 mg of lyophilized caecal content with 500 µl of ice-cold methanol. After samples were incubated for 10 min at 4 °C on a shaker, they were centrifuged for 5 min at 4 °C and 14,000 x g. Supernatant was transferred into a new tube and dried using a vacuum concentrator (SPD 111V SpeedVac, Thermo Savant).Since gas chromatography-mass spectrometry (GC-MS) requires a derivatization step, a variation of the two-step technique was performed. To protect carbonyl moieties via methoximation, 20 µl of pyridine containing 40 mg/ml methoxyamine hydrochloride were added to the dried pellets and incubated for 90 min at 30 °C. Derivatization of acidic protons was carried out by treatment for 30 min at 37 °C with the addition of 32 µl MSTFA (N-methyl-N-trimethylsilyl-trifluoroacetamide). As internal standard, paracetamol was added to each sample. 1 µl of the derivatized sample was injected on the column in a splitless mode. GC was run on a 30 m long VF-5ms capillary column (0.25 mm inner diameter, 25 µm film thickness) (VARIAN, Palo Alto, USA) at a constant flow of 1 ml/min helium. Temperature program started at 70 °C for 1 min followed by continuous heating of 10 °C/min until reaching a final temperature of 330°C that was held for 8 min. Analysis was carried out on a HP 7890 gas chromatograph (deactivated spit/splitless liners) coupled to a Quadropole (Agilent 5975) mass analyzer with scan rates of 5 s^{-1} and mass ranges of 70 to 600 Da. Chromatograms were further processed using the MetaboliteDetector software 2.06.

3 Lipid analysis in plasma, liver and caecum content

To investigate the differences between wild-type and knockout animals we first preformed a lipid screening in plasma, liver and caecum content samples. This screening included the detection of general blood lipid parameters, triglycerides, phospholipids and non-esterified fatty acids in plasma and liver.

3.1 Triglyceride analysis in liver and caecal content

Triglycerides in liver were measured with the TRIGLYCERIDES liquicolor^{mono} kit (HUMAN, Wiesbaden, Germany) according to manufacturer´s specifications. Since this kit is used to usually measure triglycerides in serum or plasma some modification were performed to analyze liver and caecal content samples.

Liver and caecal content preparation:
Caecal content was lyophilized for 20 h under vacuum conditions. Liver samples were homogenized in liquid nitrogen. 20-50 mg of dried caecal content or homogenized liver were solubilized by adding 500 µl of 0.9 % NaCl. Homogenates were put on a horizontal mixer for 10 min at RT in a thermo block (Eppendorf, Hamburg, Germany). The sample was divided for detection of the protein concentration and for further triglyceride analysis. These homogenates were also used for phospholipid and non-esterified fatty acid (NEFAs) analysis. 200 µl of the suspension were transferred in a fresh eppendorf tube and mixed with 500 µl of 0.5 M ethanolic KOH. Samples were shaken in a thermo block for 30 min at 71 °C and 1 ml of 0.15 $MgSO_4$ was added. The fluids were centrifuged for 10 min at RT and 13000 g. The supernatant was used for triglyceride analysis.

Triglyceride (TG) analysis:
10 µl of the supernatant and standard, respectively, were mixed with 1 ml of RGT reagent and incubated for 10 min at RT. RGT reagent alone was used as blank. Samples were measured at 500 nm wavelength. Results are presented in mg TG/g protein.

3.2 Non-esterified fatty acid (NEFA) analysis

Non-esterified fatty acid (NEFAs) were measured with the NEFA-HR(2) kit (Wako Chemicals GmbH, Neuss, Germany). Preparation of reagents and analysis was carried out according to manufacturer´s instructions. For liver analysis the homogenate containing 0.9 % NaCl from triglyceride preparation was used.

3.3 Phospholipid (PL) analysis

Phospholipids (PL) concentrations in plasma and liver were detected using the LabAssay™Phospholipid kit (Wako Chemicals GmbH, Neuss, Germany). The assay was carried out on a microplate using duplicates for analysis. Color reagent and the standard were prepared according to manufacturer´s instructions. For liver analysis the homogenate containing 0.9 % NaCl from triglyceride preparation was used.

4 Plasma analysis

4.1 General and lipid parameters in plasma

General blood parameters were analyzed with a Piccolo® xpress Chemistry Analyzer using the Piccolo® General Chemistry 13 Reagent Disc (HITADO, Möhnesee, Germany). This panel can measure levels of the following parameters: alanine aminotransferase (ALT), albumin, alkaline phosphatase (AP), amylase, aspartate aminotransferase (AST), calcium, creatinine, estimated glomerular filtration rate (eGFR, calculated), gamma glutamyltransferase (GGT), glucose, total bilirubin, total protein, blood urea nitrogen (BUN) and uric acid.
Blood lipid parameters were measured with the Piccolo® Lipid Panel Reagent Disc (HITADO, Möhnesee, Germany). With this panel the following parameters are measured: total cholesterol, high-density lipoprotein cholesterol (HDL), triglycerides, low-density lipoprotein cholesterol (LDL, calculated), very low-density lipoprotein cholesterol (VLDL, calculated), total cholesterol/HDL ratio (calculated).
For analysis 100 µl of Li-Heparin plasma was pipeted into the hole in the middle of the panel and inserted into the Piccolo® xpress Chemistry Analyzer. Data was directly printed by the machine in mg/dL or U/L.

4.2 Insulin analysis in plasma

Quantitative determination of plasma insulin level was performed using the Ultra Sensitive Mouse Insulin ELISA Kit (Crystal Chem Inc., Downers Grove, Illinois, USA). The assay was carried out on a microplate using duplicates for analysis. All reagents and the procedure were performed according to manufacturer´s instructions.

4.3 Leptin analysis in plasma

Plasma leptin concentrations were determined using the Mouse Leptin ELISA Kit (Crystal Chem Inc., Downers Grove, Illinois, USA). The assay was carried out on a microplate using duplicates for analysis. All reagents and the procedure were performed according to manufacturer´s instructions.

4.4 Pancreatic lipase and amylase activity in plasma

Pancreatic lipase is the primary lipase that hydrolyzes triglycerides to monoglycerides and free fatty acids. It is secreted into the duodenum from the pancreas and in small amounts also by the salivary glands, gastric, pulmonary and intestinal mucosa. Serum concentrations are normally very low. During disease, e.g. acute or chronic pancreatitis or obstruction of the pancreatic duct, the pancreas may begin to autolyse and releases then enzymes including pancreatic lipase into the serum.
Pancreatic Lipase concentrations were measured using the Lipase assay (Diazyme Europe GmbH, Dresden, Germany). Everything was prepared and performed according to manufacturer´s instructions.

4.5 Amino acid analysis

Amino acid composition in plasma was analyzed with the AA 45/32 Starter Kit (Applied Biosystems Deutschland GmbH, Darmstadt, Germany). Everything was performed according to manufacturer´s instructions.

5 Histology

5.1 Mounting samples in paraffin

After the organs were removed small samples from adipose tissue were put in 4 % paraformaldehyde directly and kept o/n at 4 °C. The next day samples were washed twice with 500 µl PBS and put in 70 % ethanol until further proceeding. Tissue

samples were put in plastic cassettes and dehydrated for embedding in paraffin according to the following protocol:

Chemicals for dehydration	Time [min]	Temperature [°C]
70 % ethanol	60	40
80 % ethanol	60	40
95 % ethanol	60	40
95 % ethanol	60	40
100 % ethanol	60	40
100 % ethanol	60	40
100 % ethanol	60	40
100 % xylene	60	40
100 % xylene	60	40
paraffin	60	58
paraffin	60	58
paraffin	60	58
paraffin	60	58

Dehydrated samples were mounted in a paraffin block and 5 µm slices were cut for different staining. Sections were collected in a 37 °C pre-warmed water bath, transferred onto microscope slides and dried o/n at 37 °C in a drying oven.

For different staining the paraffin was removed according to the protocol:

Chemicals for rehydration	Time [min]
100 % xylene	4
100 % xylene	4
100 % ethanol	4
96 % ethanol	3
80 % ethanol	3
Bluing in tab water	2

Samples were stained directly.

5.2 Hemalum and Eosyn (H&E) Staining

H&E staining was used to access morphological changes in tissue after feeding of different diets. Paraffin sections (5 µm) were stained with Mayer´s Hemalum and Eosyn Y 0.5 % alcoholic solution with phloxin.

Chemicals for staining	Time [min]
Mayer´s Hemalum 50% in water	1
Bluing in tab water	3
96 % ethanol	0.5
Eosyn Y 0.5% alcoholic solution with Phloxin	5
80 % ethanol	Short
96 % ethanol	Short

To prevent re-dyeing microscope slides were directly dried by shaking in the hand. Afterwards the samples were covered with mounting medium (Dako North America Inc., Carpinteria, USA) and a cover slip (Roth, Karlsruhe, Germany). Subsequently, the sample was dried deprived from light. The samples were analyzed using a DMI4000B transmitted light microscope (Leica, Wetzlar, Germany) with the Leica Application Suite V3.0.0.

Results

1 Physiological analyzes of wild type and *Pept1*$^{-/-}$ mice on a High Fat Diet

During the study the following parameters were monitored: weight gain, food and water intake, oxygen consumption, activity, body length, rectal body temperature.

1.1 Body weight and food and water intake

Prior to feeding the high-fat diet (HFD), the body weight was not significantly different between *Pept1*$^{-/-}$ mice and wild-type (WT) animals at 6 weeks of age. After 12 weeks on the HFD, genotype-specific differences were observed. *Pept1*$^{-/-}$ mice on HFD showed a significantly reduced body weight (35.86 ± 1.40 g) when compared to WT mice (42.78 ± 1.16 g). Animals fed for 12 weeks with the control diet (CD) showed no significant genotype-specific differences in body weight: *Pept1*$^{-/-}$ mice had a final weight of 26.45 ± 0.51 g and WT mice showed a body weight of 28.72 ± 0.51 g (Figure 5A & 5B). The weight gain during the feeding period was as followed: (i) *Pept1*$^{-/-}$ mice on HFD gained 15.03 ± 0.93 g, (ii) WT mice on HFD gained 19.60 ± 1.01 g, (iii) PEPT1$^{-/-}$ mice on CD gained 5.06 ± 0.28 g and (iv) WT mice on CD gained 4.57 ± 0.49 g. The lower weight gain of *Pept1*$^{-/-}$ mice was accompanied by a slightly reduced food and energy intake (Figure 5B & 5C). There were also no genotype-specific but diet-specific differences in drinking behavior. Animals of both genotypes fed the CD had a significantly higher water intake when compared to the mice on HFD (Figure 5D).

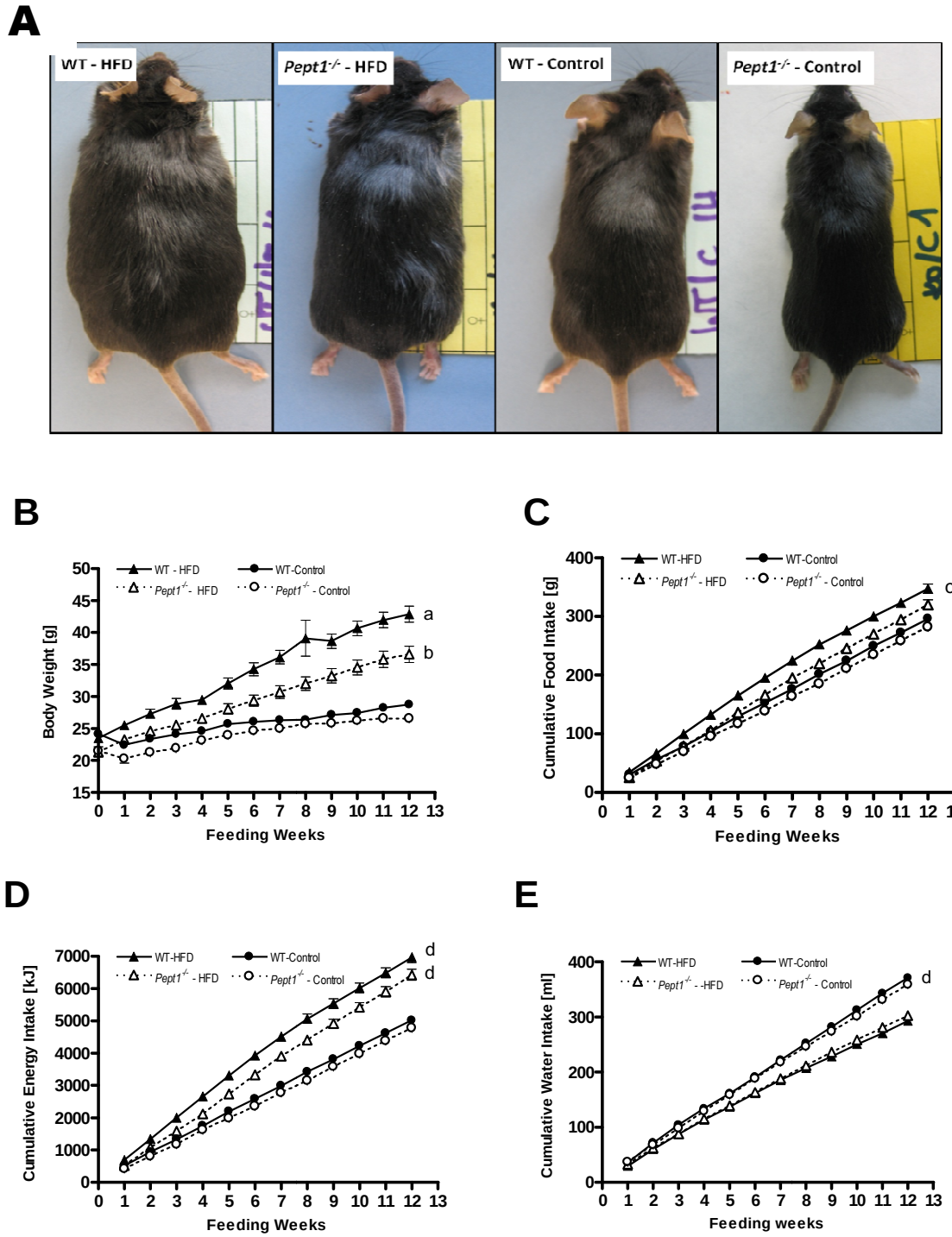

Figure 5: Mean body weight, food, energy and water intake of *Pept1*$^{-/-}$ and WT mice on CD and HFD. (A) Images from sacrificed WT and *Pept1*$^{-/-}$ mice on HFD and CD. Genotypic differences are seen between the mice on a HFD (B) Mean body weight. (C) Cumulative food intake. (D) Cumulative energy intake. (E) Cumulative water intake. During 12 weeks of the feeding study, mice (n=15 per group) had access to food pellets and drinking water *ad libitum*. Data are expressed as mean ± SEM. Significances are given in: (i) a = WT mice on HFD different to all others ($p<0.001$), (ii) b = *Pept1*$^{-/-}$ mice on HFD different to mice on CD ($p<0.001$), (iii) c = WT mice on HFD are different to mice on CD ($p<0.001$), (iv) d = mice on HFD are different to mice on CD ($p<0.001$)

1.2 Body composition

Fat and lean mass was measured every four weeks during the whole study (t=0, t=4, t=8 and t=12 weeks). After four weeks on a HFD, WT mice more than double their fat mass from 9.08 ± 0.81 % to 27.31 ± 4.94 % ($p<0.001$). Interestingly, this effect was not seen in *Pept1*$^{-/-}$ mice on HFD. From the 8th week on *Pept1*$^{-/-}$ mice on HFD had also significantly increased fat mass (24.86 ± 2.40 %) when compared to *Pept1*$^{-/-}$ and WT mice on CD (Figure 6A). A continuous increase of the fat mass was observed for mice on HFD while animals on CD had only a slight increase in their fat mass (Table 4). Consequently, both groups on CD had a significant greater amount of lean mass than *Pept1*$^{-/-}$ and WT mice on HFD (Figure 6B) while both groups fed with the HFD showed a decrease in lean mass over the feeding period (Table 5). Finally, we saw diet-specific differences showing animals on CD having lower fat mass but increased lean mass compared to mice on HFD. But there were also differences between *Pept1*$^{-/-}$ and WT mice on HFD. *Pept1*$^{-/-}$ mice had a lower fat mass but a similar lean mass when compared to WT mice on HFD.

Table 5: Body composition of *Pept1*$^{-/-}$ and WT mice (n=5). Data are expressed as mean ± SEM. WT mice on HFD had a significantly increased fat mass compared to all other groups (from week 4 on). *Pept1*$^{-/-}$ mice on HFD showed significantly increased fat mass compared to both groups on CD (from week 8 on).

Weeks	Mass /body weight [%]	Genotype and diet			
		WT-HFD	*Pept1*$^{-/-}$ -HFD	WT-Control	*Pept1*$^{-/-}$ Control
0	Fat mass	9.08 ± 0.81	10. 44 ± 0.69	8.51 ± 0.81	7.45 ± 0.81
	Lean mass	74.02 ± 2.74	63.10 ± 3.04	69.71 ± 3.84	53.45 ± 3.14
4	Fat mass	27.31 ± 4.94	14.62 ± 1.14	12.10 ± 0.40	8.68 ± 0.28
	Lean mass	63.99 ± 2.25	69.08 ± 1.26	75.47 ± 1.08	75.14 ± 1.47
8	Fat mass	36.57 ± 3.58	26.98 ± 2.11	12.34 ± 1.38	10.59 ± 0.58
	Lean mass	57.73 ± 2.36	61.36 ± 1.49	70.71 ± 2.82	75.17 ± 0.78
12	Fat mass	38.20 ± 2.23	28.24 ± 4.32	13.62 ± 0.99	11.43 ± 0.41
	Lean mass	49.69 ± 1.91	57.65 ± 2.59	70.75 ± 1.51	74.45 ± 0.40

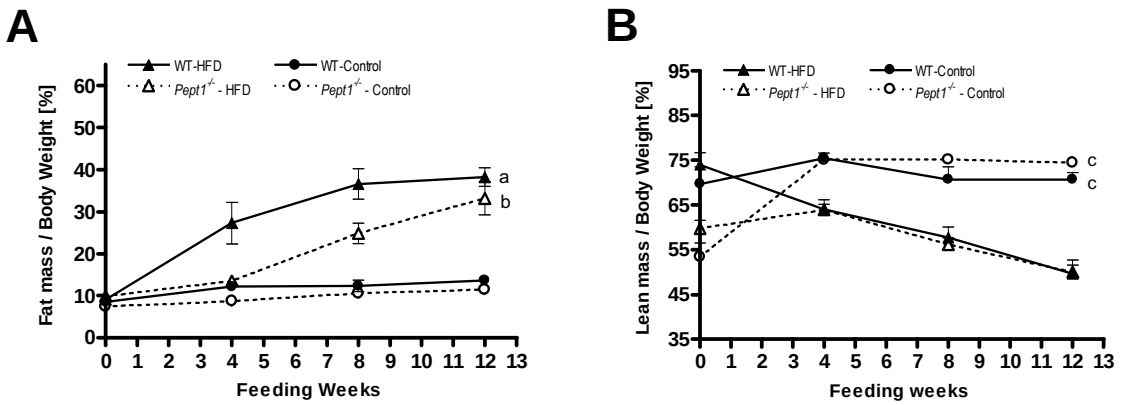

Figure 6: Body composition of *Pept1*$^{-/-}$ and WT mice. Fat and lean mass of *Pept1*-KO and WT animals (n=5 per group) were determined at the beginning of the study (t=0) and after 4, 8 and 12 weeks on HFD. (A) Changes in the percentage of fat mass per body weight. (B) Changes in the percentage of lean mass per body weight. Data are expressed as mean ± SEM. Significances are given in: (i) a = WT mice on HFD different to all others ($p<0.001$), (ii) b = *Pept1*$^{-/-}$ mice on HFD different to mice on CD ($p<0.001$), (iii) c = mice on HFD are different to mice on CD ($p<0.001$)

After 12 weeks, *Pept1*$^{-/-}$ mice on HFD had significantly less perirenal (2.26 ± 0.22 %) and epididymal (4.87 ± 0.46 %) adipose tissue per kg body weight relative to WT mice (3.11 ± 0.18 % and 5.65 ± 0.20 %, respectively). The percentage for inguinal (subcutaneous) (1.33 ± 0.12 %) and brown adipose tissue (0.61 ± 0.06 %) of *Pept1*$^{-/-}$ mice on HFD was comparable to WT animals on HFD (1.54 ± 0.04 % and 0.93 ± 0.03 %, respectively) (Figure 7A). *Pept1*$^{-/-}$ mice on CD had significantly reduced epididymal adipose tissue (1.41 ± 0.07 %) compared to WT mice on CD (2.68 ± 0.14 %). Inguinal, perirenal and brown adipose tissues were comparable between these two groups: *Pept1*$^{-/-}$ mice (0.49 ± 0.03%; 0.46 ± 0.04 %; 0.35 ± 0.03%, respectively) and WT mice (0.67 ± 0.04 %; 0.67 ± 0.08 %; 0.38 ± 0.03%, respectively) (Figure 7B). These diet- and genotype-specific differences were also seen in H&E-staining of epididymal adipose tissue. Epididymal adipocytes of both genotypes fed the HFD were bigger in size relative to those fed the CD (Figure 7C). But *Pept1*$^{-/-}$ mice on HFD had also significantly smaller adipocytes compared to WT animals on HFD.

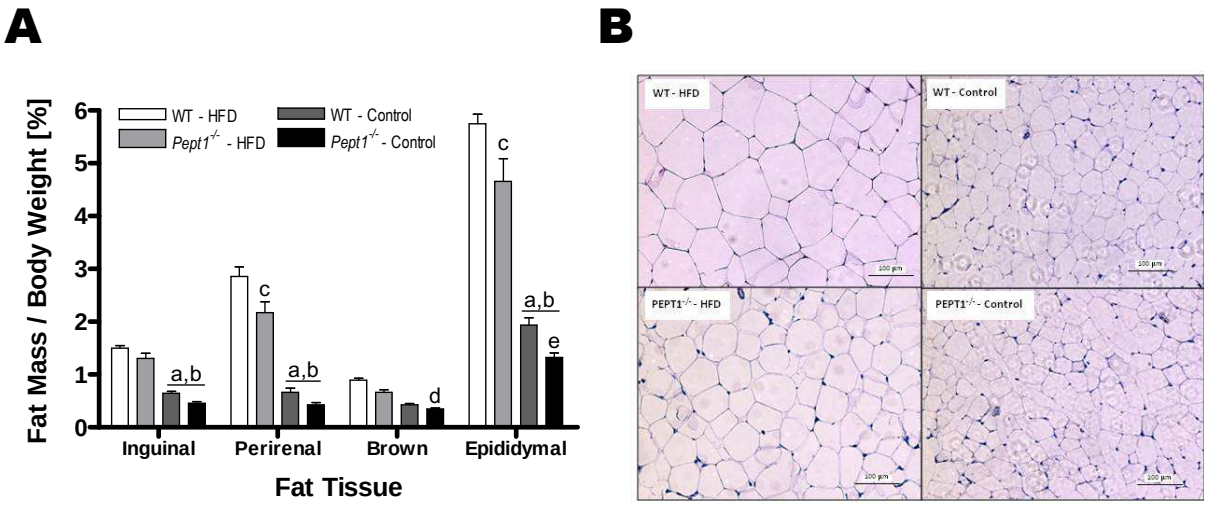

Figure 7: Weight and size of various adipose tissues. Samples (n=15) were collected at the end of 12-weeks HFD. (A) Amount of adipose tissues in relation to total body weight. (B) H&E-staining of epididymal fat tissue. Samples were fixed in 4 % paraformaldehyde and embedded in paraffin. 5 µm thick sections were stained with hemalum and eosyn. Data are expressed as mean ± SEM. Significances are given in: (i) a = WT mice on HFD different to mice on CD ($p<0.001$), (ii) b = *Pept1*$^{-/-}$ mice on HFD different to mice on CD ($p<0.001$), (iii) c = WT mice on HFD different to *Pept1*$^{-/-}$ mice on HFD ($p<0.01$), (iv) d = WT mice on HFD different to *Pept1*$^{-/-}$ mice on CD ($p<0.05$), (v) e = WT mice on CD different to *Pept1*$^{-/-}$ mice on CD ($p<0.01$)

1.3 Locomotor activity, energy expenditure and respiratory quotient

Although not significant, mice on HFD showed reduced locomotor activity during night phases. *Pept1*$^{-/-}$ and WT mice on CD and HFD showed no diet-specific or genotype-specific differences in diurnal patterns and total locomotor activity measured over three continuous days (Figure 8A). WT animals on HFD had in total 11056.31 ± 1835.89 beam breaks and *Pept1*$^{-/-}$ mice on HFD had a total number of 10057.25 ± 239.18 beam breaks. These values were similar to those of mice on the CD: WT mice had 12095.86 ± 839.29 beam breaks and *Pept1*$^{-/-}$ animals had 13125.48 ± 2071.94 beam breaks during the measuring period of three days.

During the measurement on three continuous days, no genotype or diet-specific differences could be determined in overall energy expenditure between the four groups during day periods: *Pept1*$^{-/-}$ and WT animals on CD had an energy expenditure of 0.76 ± 0.06 kJ/h*g and 0.83 ± 0.03 kJ/h*g, respectively, and mice fed the HFD showed values of 0.72 ± 0.10 kJ/h*g (*Pept1*$^{-/-}$) and 0.82 ± 0.04 kJ/h*g (WT) (Figure 9A & 9B). *Pept1*$^{-/-}$ and WT mice on CD tend to have higher energy expenditure during night periods (1.09 ± 0.02 kJ/h*g and 1.13 ± 0.02 kJ/h*g,

respectively) when compared to *Pept1*$^{-/-}$ and WT mice on HFD (0.86 ± 0.12 kJ/h*g and 0.89 ± 0.05 kJ/h*g, respectively), but this is not significant.

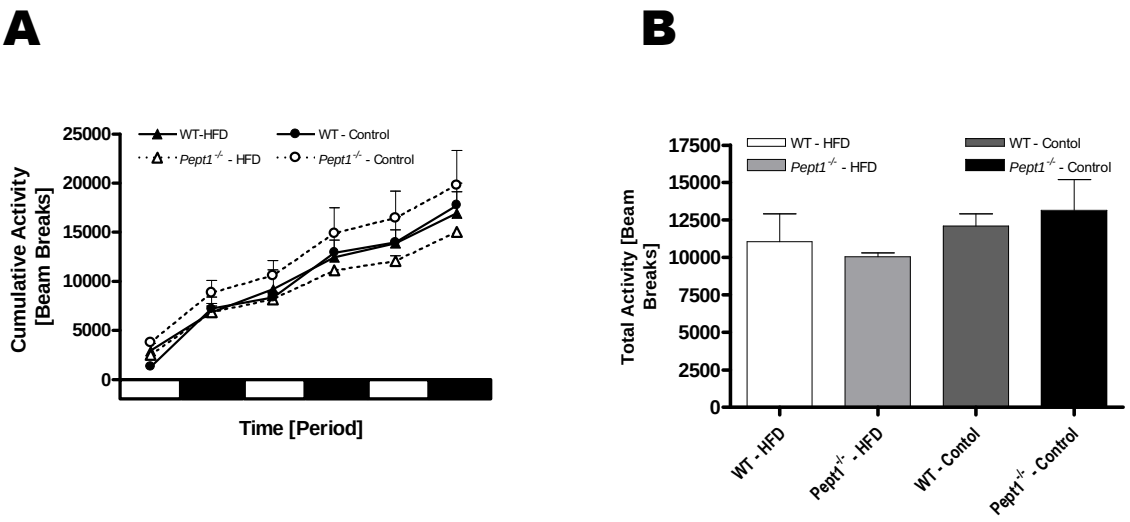

Figure 8: Cumulative locomotor activity in *Pept1*$^{-/-}$ and WT mice. After 4 weeks on HFD and CD, mice (n=5) were placed individually in special feeding-drinking-activity cages that were placed in a TSE-system for three continuous days. (A) Cumulative locomotor activity over the total period of three days. (B) Total locomotor activity of *Pept1*$^{-/-}$ and WT mice. Data are expressed as mean ± SEM.

Both genotypes on CD showed also a significantly higher respiratory quotient (RQ) during day and night phases than mice fed with HFD (Figure 9C & 9D). Mice on CD showed RQ values of 0.82 ± 0.01 (WT) and 0.82 ± 0.01 (*Pept1*$^{-/-}$) during day and 0.94 ± 0.01(WT) and 0.94 ± 0.01(*Pept1*$^{-/-}$) during night. This indicates that these mice used proteins as source for energy production during day and carbohydrates as energy source during their activity phases at night. WT mice on HFD showed a RQ of 0.76 ± 0.01 during day and 0.79 ± 0.01 during night. This indicates that these mice used fat as source for energy production. *Pept1*$^{-/-}$ animals on HFD had RQ values of 0.78 ± 0.01 (day) and 0.81 ± 0.01 (night). For both parameters, energy expenditure and RQ, a strong increase was measurable for mice on CD during activity phases at night while it decreased during resting periods at day. For mice on HFD these changes during day-night-cycles were not as pronounced as for mice on CD.

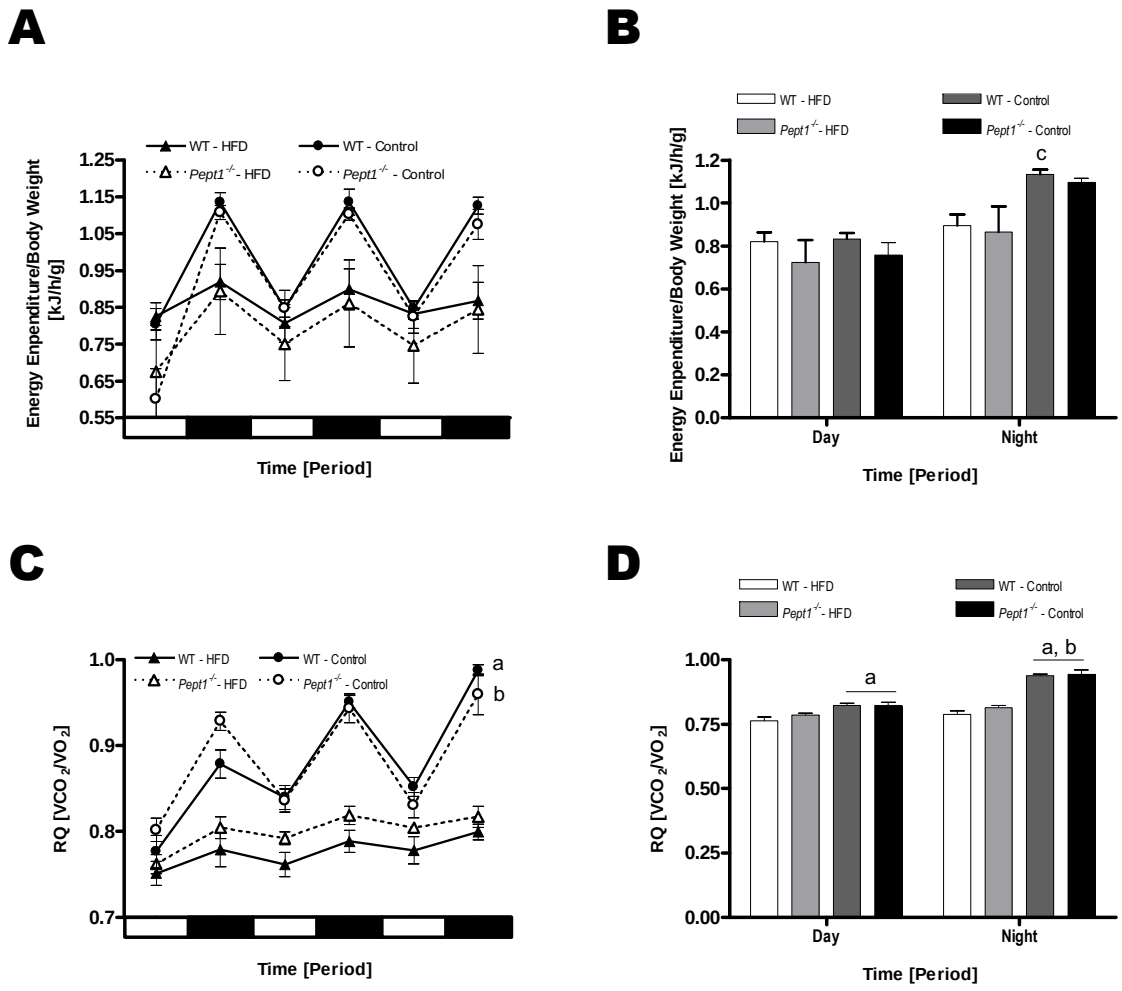

Figure 9: Energy expenditure, O_2 consumption and CO_2 production in *Pept1*$^{-/-}$ and WT mice. Mice (n=5) were placed individually in special calorimetric cages for three continuous days. (A) Median energy expenditure during day and night cycles. B) Total energy expenditure during day and night cycles (C) Median metabolic data (RQ) during day and night cycles. D) Total RQ values during day and night phases. Data are expressed as mean ± SEM. Significances are given in: (i) a = WT mice on HFD different to mice on CD ($p<0.001$), (ii) b = *Pept1*$^{-/-}$ mice on HFD different to mice on CD ($p<0.001$), (iii) c = *Pept1*$^{-/-}$ mice on HFD different to WT mice on CD ($p<0.01$)

1.4 Organ parameters

After 12 weeks of feeding CD or HFD, mice were dissected and organs were collected and weighted. Only WT mice on HFD developed a fatty liver and had much bigger fat depots (Figure 10A). Generally, we found mice on HFD having smaller caeca when compared to animals on CD. Regardless the diets, *Pept1*$^{-/-}$ mice always had significantly larger caeca than WT mice: *Pept1*$^{-/-}$ mice on HFD showed a significantly increased caecum (1.08 ± 0.11 % of body weight) when compared to WT mice on HFD (0.54 ± 0.02 % of body weight). Animals on CD had generally a bigger

caecum: 1.18 ± 0.08 % of body weight (WT mice on CD) while *Pept1*$^{-/-}$ mice on CD had the biggest caecum of all groups (2.30 ± 0.15 % of body weight). All organs weights are summarized in Table 6 and Figure 10B.

Table 6: Percentage of organ weight per body weight of *Pept1*$^{-/-}$ and WT mice. Samples (n=15) were collected at the end of 12-weeks HFD. WT mice on HFD have significantly more epididymal and perirenal adipose tissue compared to all other groups (A). Regardless the diet, *Pept1*$^{-/-}$ mice have a significantly enlarged caecum compared to WT animals. *Pept1*$^{-/-}$ mice on CD have the significantly biggest caecum of all four groups (B). Additionally, *Pept1*$^{-/-}$ mice on CD have significantly longer small intestines when compared to all other groups (C). Data are expressed as mean ± SEM. Values with asterisks represent significant differences: (i) ** = p<0.01 and (ii) *** = p<0.001

Organ weight / body weight [%]	WT – HFD	*Pept1*$^{-/-}$ - HFD	WT – CD	*Pept1*$^{-/-}$ - CD
Body weight [g]	43.22 ± 1.15	35.86 ± 1.15	28.72 ± 0.51	26.52 ± 0.55
Pancreas [%]	0.70 ± 0.04	0.73 ± 0.06	0.94 ± 0.07	1.05 ± 0.18
Spleen [%]	0.21 ± 0.01	0.20 ± 0.02	0.29 ± 0.02	0.34 ± 0.02
Heart [%]	0.39 ± 0.02	0.44 ± 0.04	0.63 ± 0.03	0.64 ± 0.05
Kidney right [%]	0.54 ± 0.02	0.55 ± 0.05	0.73 ± 0.03	0.65 ± 0.01
Kidney left [%]	0.53 ± 0.01	0.51 ± 0.04	0.66 ± 0.03	0.60 ± 0.01
Liver Caudate lobe [%]	0.32 ± 0.03	0.32 ± 0.03	0.31 ± 0.02	0.40 ± 0.02
Liver Right lobe [%]	1.43 ± 0.11	1.23 ± 0.12	1.20 ± 0.06	1.40 ± 0.05
Liver Medial lobe [%]	1.63 ± 0.10	1.37 ±0.13	1.36 ± 0.06	1.56 ±.0.05
Liver Left lobe [%]	1.66 ± 0.10	1.43 ± 0.13	1.39 ± 0.08	1.60 ± 0.05
Caecum [%]	0.55 ± 0.02	1.19 ± 0.11$^{***(B)}$	1.16 ± 0.08	2.38 ± 0.14$^{***(B)}$
Epididymal fat [%]	5.75 ± 0.18$^{***(A)}$	4.18 ± 0.51	1.94 ± 0.14	1.28 ± 0.09
Inguinal fat [%]	1.50 ±0.04	1.19 ± 0.51	0.64 ± 0.04	0.45 ± 0.03
Perirenal fat [%]	2.86 ± 0.18$^{**(A)}$	1.99 ± 0.51	0.67 ± 0.08	0.41 ± 0.04
Brown fat [%]	0.90 ± 0.04	0.61 ±0.07	0.43 ± 0.03	0.34 ±.0.02
Small intestine [cm]	32.47 ± 0.76	36.46 ± 0.61	33.55 ± 0.64	39.72 ± 0.71$^{***(C)}$
Large intestine [cm]	6.19 ± 0.22	6.86 ± 0.17	6.35 ± 0.34	7.21 ± 0.19

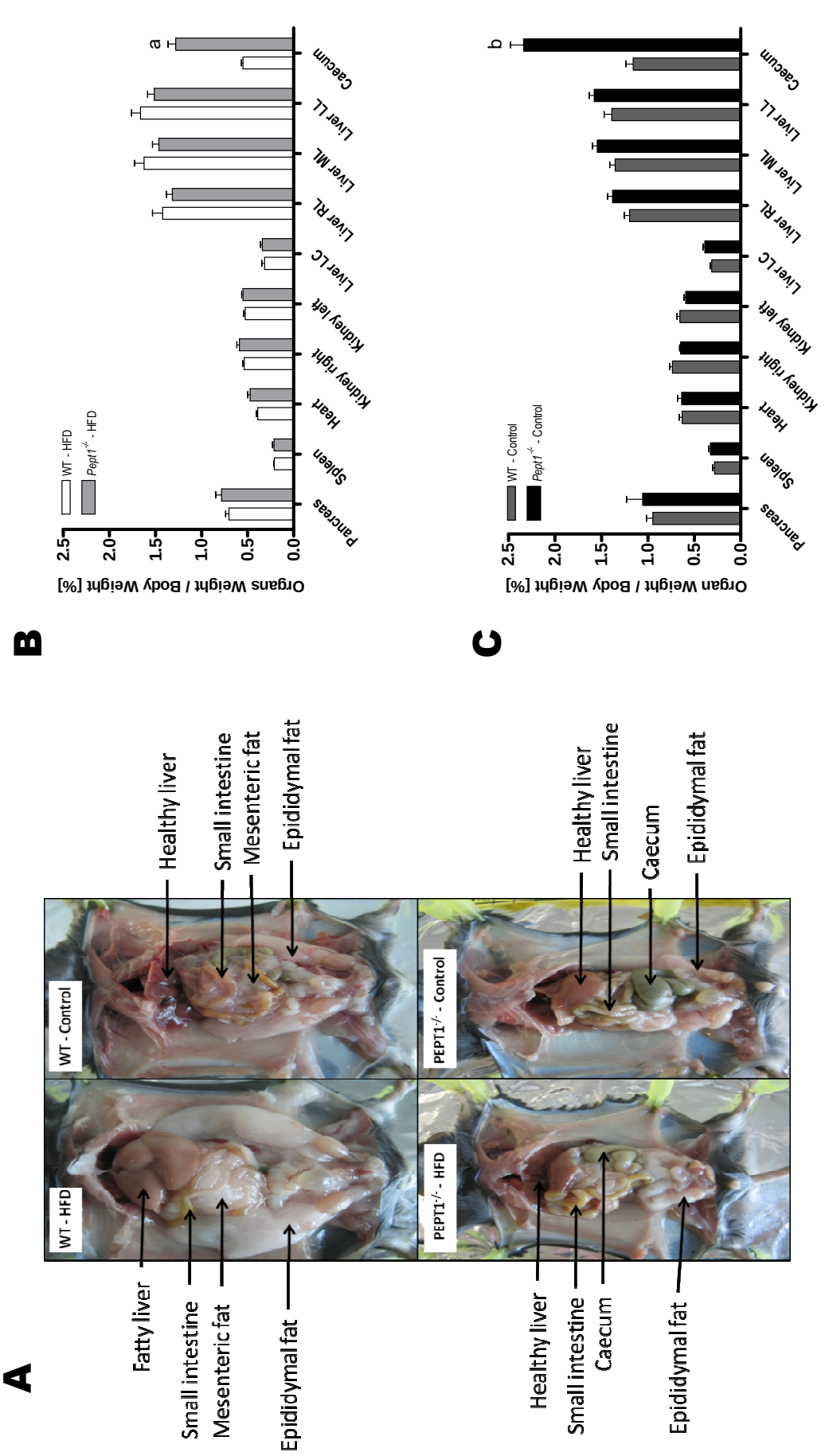

Figure 10: Percentage of various tissues per body weight of *Pept1*$^{-/-}$ and WT mice. Samples (n=15) were collected at the end of 12-weeks HFD. (A) Pictures of various organs in *Pept1*$^{-/-}$ and WT mice on CD and HFD. WT mice on HFD developed a fatty liver. (B) Amount of organs in relation to total body weight measured in mice on HFD. (C) Amount of organs in relation to total body weight measured in mice on CD. Data are expressed as mean ± SEM. Significances are given in: (i) a = WT mice on HFD different to *Pept1*$^{-/-}$ mice on HFD ($p<0.001$), (ii) b = WT mice on CD different to *Pept1*$^{-/-}$ mice on CD ($p<0.001$)

Regardless of the diet, genotype-specific differences in length of small intestines were determined. *Pept1*$^{-/-}$ mice had significantly longer small intestines: 36.46 ± 0.61 cm (HFD) and 39.72 ± 0.71 cm (CD), respectively, than WT animals with 32.47 ± 0.76 cm (HFD) and 33.55 ± 0.64 cm (CD) in length (Figure 11). *Pept1*$^{-/-}$ mice also had shorter villi in the proximal part of the small intestine when compared to WT animals: (i) 547.48 ± 5.46 µm (WT-HFD), (ii) 318.42 ± 9.50 µm (*Pept1*$^{-/-}$-HFD), (iii) 434.72 ± 10.07 µm (WT-Control), and (iv) 303.26 ± 9.09 µm (*Pept1*$^{-/-}$-Control) (Figure 12A). Contrary to the proximal small intestine, villi lengths were comparable between all four groups in the distal part: (i) 209.32 ± 2.64 µm (WT-HFD), (ii) 199.58 ± 3.61 µm (*Pept1*$^{-/-}$-HFD), (iii) 182.12 ± 3.14 µm (WT-Control), and (iv) 182.76 ± 4.43 µm (*Pept1*$^{-/-}$-Control) (Figure 12B).

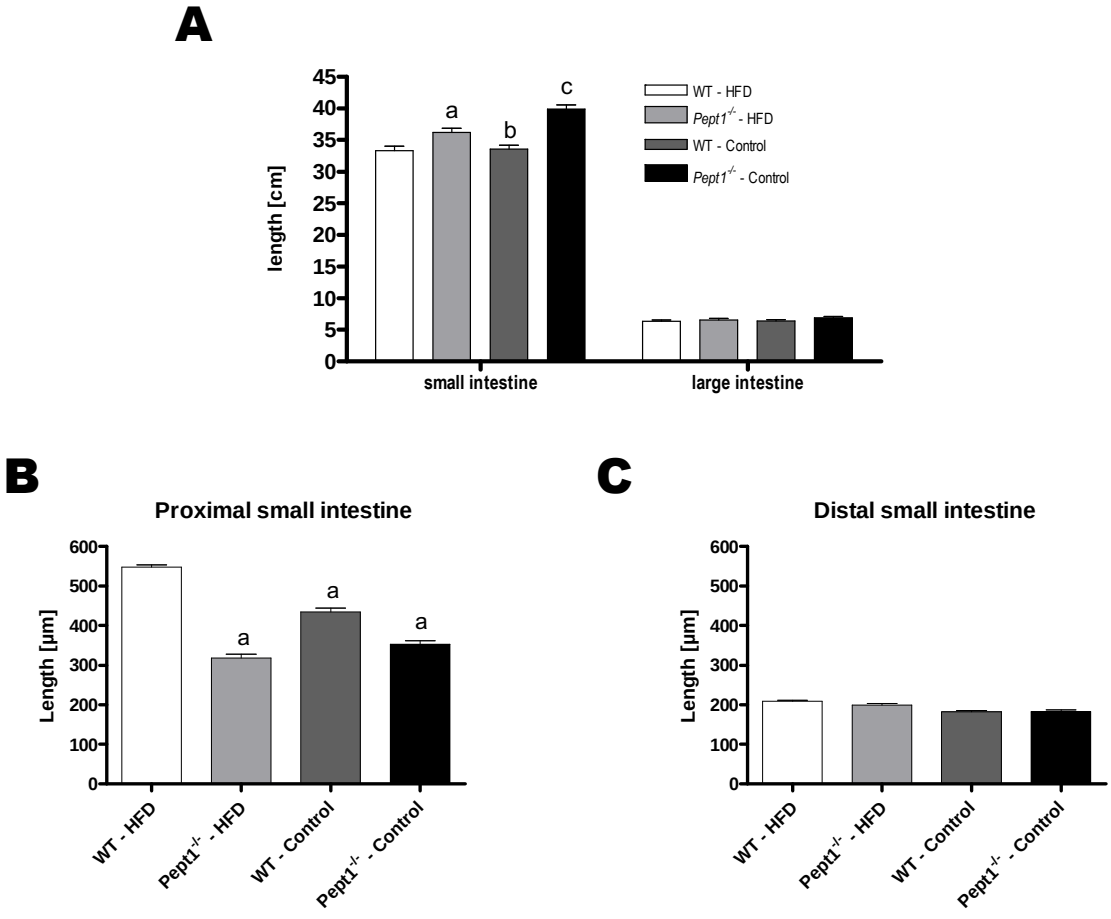

Figure 11: Villi length and length of small and large intestine of *Pept1*$^{-/-}$ and WT mice. Samples (n=15) were collected at the end of 12-weeks HFD. (A) Regardless the diet, *Pept1* knockout animals have significantly longer small intestines while there are no differences in the large intestine. (B) Villi length in the proximal small intestine: *Pept1*$^{-/-}$ mice have shorter villi. (C) Villi length in distal small intestine shows no differences between the four groups. Data are expressed as mean ± SEM. Significances are given in: (i) a = WT mice on HFD different to *Pept1*$^{-/-}$ mice on HFD ($p<0.001$), (ii) b = *Pept1*$^{-/-}$ mice on HFD different to WT mice on CD ($p < 0.001$), (ii) c = *Pept1*$^{-/-}$ mice on HFD different to all other groups ($p < 0.001$)

2 Feces and caecum analyzes

In order to analyze possible changes in the metabolism of *Pept1*$^{-/-}$ and WT mice, feces samples were analyzed for excreted energy and nutrients.

2.1 Feces excretion and transit time

Fecal samples were collected after 4, 8 and 12 weeks of feeding. At all time points *Pept1*$^{-/-}$ mice on HFD showed a significantly reduced feces excretion (1.73 ± 0.15 g feces dry weight). WT animals fed the HFD excreted 2.07 ± 0.09 g dry weight of feces. Both groups fed the CD tend to have a slightly higher feces excretion: 2.45 ± 0.03 g feces dry weight for WT mice and 2.49 ± 0.08 g feces dry weight for the *Pept1*$^{-/-}$ animals (Figure 12). When measuring the gastrointestinal transit time no differences could be detected between both genotypes (WT: 6.00 ± 1.19 h and KO: 6.37 ± 1.63 h) although *Pept1*$^{-/-}$ animals had longer small intestines.

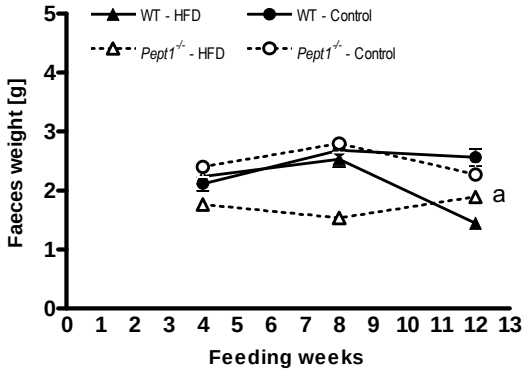

Figure 12: Weekly feces excreted by *Pept1*$^{-/-}$ and WT mice. *Pept1*$^{-/-}$ mice on HFD showed significantly reduced fecal excretion during the whole study. Data are expressed as mean ± SEM. Significances are given in: a = *Pept1*$^{-/-}$ mice on HFD different to all other groups ($p < 0.001$)

2.2 Fecal energy excretion

Fecal energy excretion was measured at 4, 8 and 12 weeks of feeding the selected diets using bomb calorimetry. *Pept1*$^{-/-}$ mice showed significantly higher energy excretion already after 4 weeks on the HFD when compared to the other groups. When calculating the mean energy excretion over the total time of 12 weeks *Pept1*$^{-/-}$ mice on HFD had 15.47 ± 0.26 kJ/g energy in their feces while WT animals on HFD

excreted 13.37 ± 0.20 kJ/g. That was comparable to animals on CD. *Pept1*$^{-/-}$ and WT animals on CD had an energy excretion of 13.21 ± 0.26 kJ/g and 12.69 ± 0.18 kJ/g, respectively (Figure 13A). When calculating the overall fecal energy excretion per week, we did not see any genotype-specific differences but mice fed the CD excreted slightly more energy in their feces. WT and *Pept1*$^{-/-}$ mice on HFD had a mean weekly fecal energy excretion of 27.91 ± 1.59 kJ and 28.10 ± 1.30 kJ, respectively, while WT and *Pept1*$^{-/-}$ animals on CD excreted 31.07 ± 0.39 kJ and 32.91 ± 1.53 kJ, respectively (Figure 13B). Although *Pept1*$^{-/-}$ mice on HFD have increased fecal energy content, the mean weekly fecal energy excretion is similar to the other groups. This results from a slightly lower feces excretion (g).

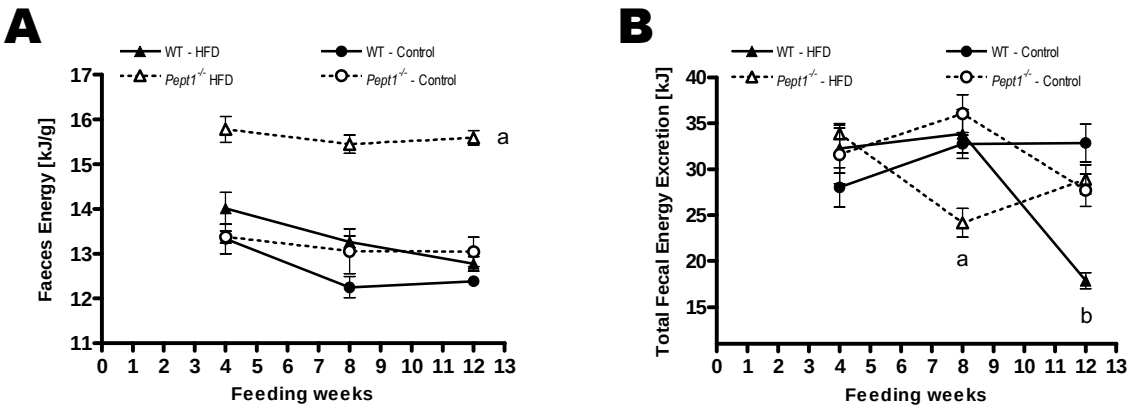

Figure 13: Fecal energy content and total fecal energy excretion of *Pept1*$^{-/-}$ and WT mice. (A) Fecal energy content. *Pept1*$^{-/-}$ mice on HFD have a significantly higher fecal energy content compared to all other groups. (B) Total fecal energy excretion of WT and *Pept1*$^{-/-}$ mice. Data are expressed as mean ± SEM. Significances are given in: (i) a = *Pept1*$^{-/-}$ mice on HFD different to *Pept1*$^{-/-}$ mice on HFD ($p<0.001$), (ii) b = WT mice on HFD different to all other groups ($p < 0.001$)

2.3 Fourier-Transform Infrared spectroscopy (FT-IR) analysis of feces and caecal content

Caecal content was s collected and measured after 12 weeks of feeding the selected diets using the FT-IR technique. Fecal nutrient content was analyzed at 4, 8 and 12 weeks. While slight differences were found in feces samples (Figure 14A) there were no differences in the caecal content between the groups (Figure 14B) which did not change during the feeding period of 12 weeks. Lipids (~2700 cm^{-1}), proteins (~1500 cm^{-1}) and carbohydrates (~1000 cm^{-1}) are presented as peaks in the spectra (see arrows).

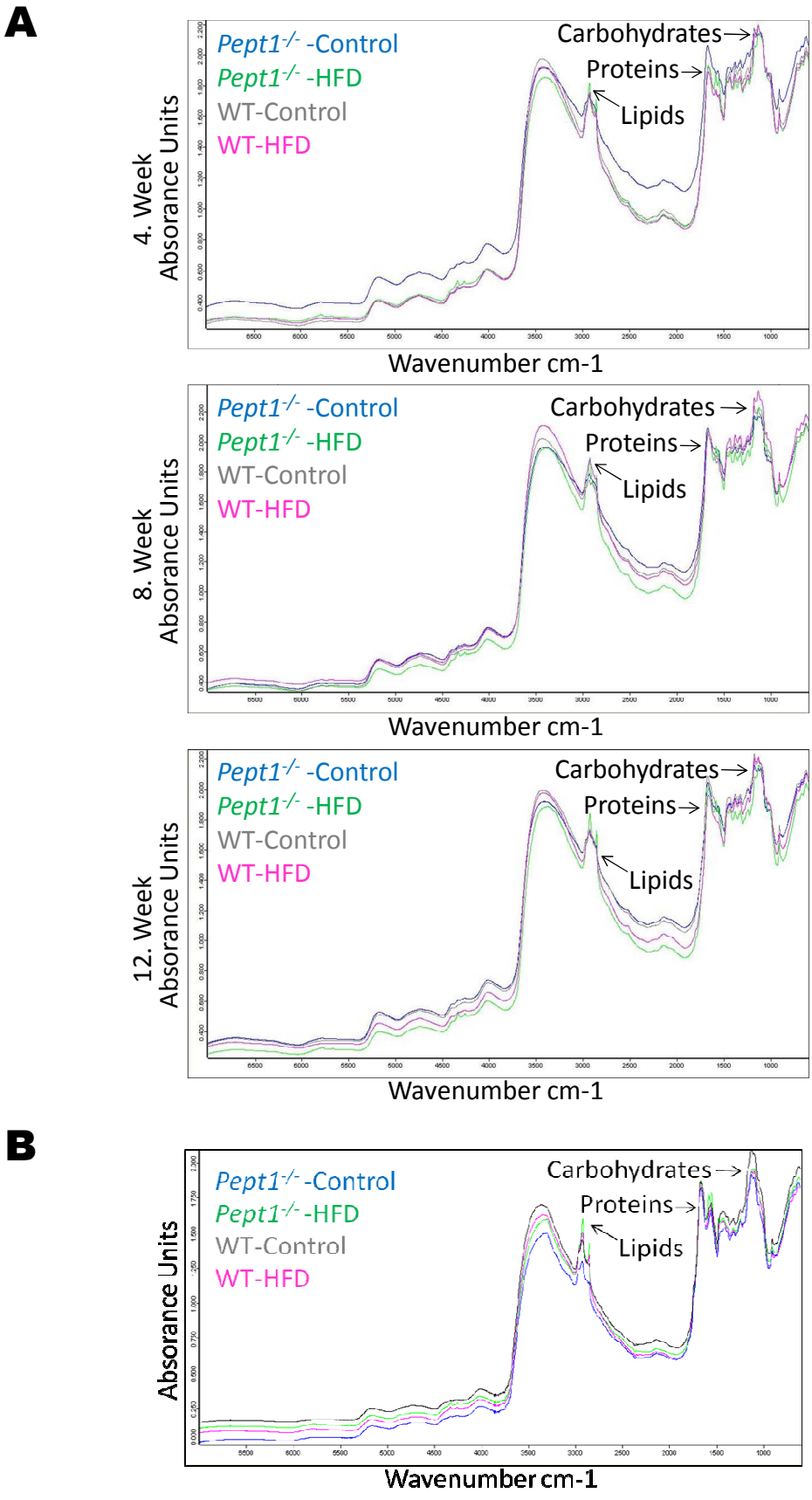

Figure 14: Caecum and feces analysis of *Pept1*$^{-/-}$ and WT mice on CD and HFD. (A) Fecal content analysis after 4, 8, and 12 weeks on the specific diets (n=5). (B) Caecal content analysis after 12 weeks on the selected diets (n=10-15). Lipids (~2700 cm^{-1}), proteins (~1500 cm^{-1}) and carbohydrates (~1000 cm^{-1}) are presented as peaks in the spectra (see arrows).

Regarding the caecal content, mice fed the control diet can be separated from mice that received the HFD (Figure 15A). Also WT and PEPT1-deficient animals are separated. Although the differences between the four groups are only small in fecal samples, the groups can be separated by a cluster analysis (Figure 15B).

A

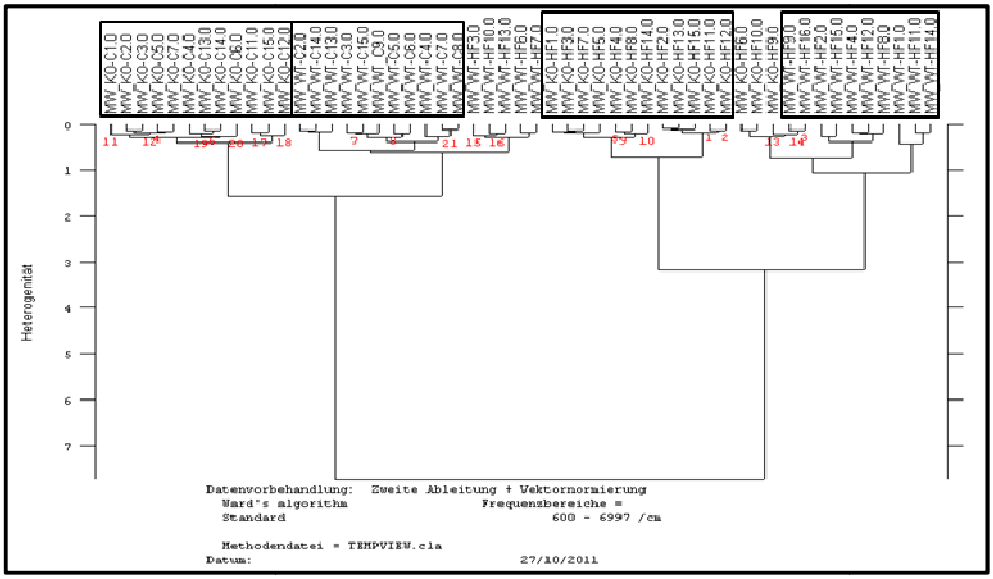

B

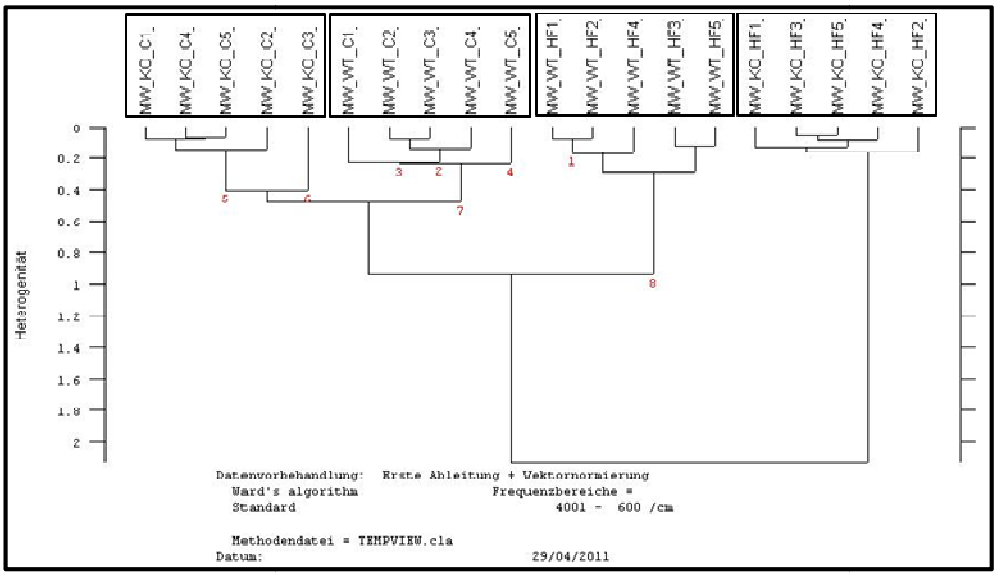

Figure 15: Cluster analysis of fecal and caecal nutrient content of *Pept1*$^{-/-}$ and WT mice. (A) After calculating the secondary derivative, still caecum samples of the groups could not be clustered. (B) Calculating the primary derivative within the feces samples the four groups can be separated.

2.4 Caecal lipid analysis

Lyophilized caecal content was used for triglyceride (TG) and phospholipid (PL) analysis. Among all four groups, highest TG concentrations were measured in WT mice on HFD (137.93 ± 28.90 mg/g dry matter) while *Pept1*$^{-/-}$ mice on HFD had TG concentrations of 74.15 ± 13.37 mg/g dry matter. Both genotypes on CD showed slightly differences in TG concentrations: 34.77 ± 5.29 mg/g dry matter (WT mice on CD) and 18.92 ± 3.45 mg/g dry matter (*Pept1*$^{-/-}$ mice on CD) (Figure 16A). Contrary to this, there were no alterations observed in caecal concentrations (Figure 16B).

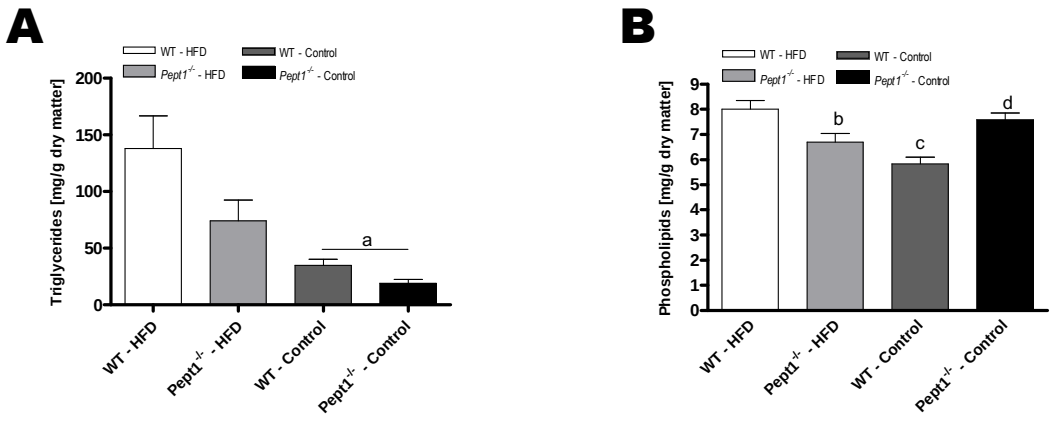

Figure 16: Lipid analysis of caecal content of *Pept1*$^{-/-}$ and WT mice. (A) Caecal triglyceride concentrations. (B) Caecal phospholipid concentrations. Data are expressed as mean ± SEM. Significances are given in: (i) a = WT and *Pept1*$^{-/-}$ mice on CD are significantly reduced compared to WT mice on HFD ($p<0.01$), (ii) b = *Pept1*$^{-/-}$ mice on HFD different to WT mice on HFD ($p < 0.05$), (iii) c = WT mice on CD are different to WT mice on HFD ($p < 0.001$), (iv) d = *Pept1*$^{-/-}$ mice on CD are different to WT mice on CD ($p < 0.01$)

2.5 Free fatty acids in caecal content – GC/MS analysis.

GC/MS analysis revealed *Pept1*$^{-/-}$ mice on HFD having an increased concentration of fatty acids but a decreased concentration of carbohydrates in their caecal content while there are no distinct clusters observed within the WT mice (Figure 17A&B). Test on significant differences among the groups of samples resulting from cluster analysis were performed with Kruskal-Wallis tests (selected FDR limit = 0.05; Bonferroni adjustment); clustering was based on Euclidean distance and average linkage. PCA blot with normalized metabolite data [x = (value-average)/SD] revealed a clear separation caused by different metabolite abundances for *Pept1*$^{-/-}$ animals while WT mice on both diets seem to have comparable metabolites (Figure 17C).

A

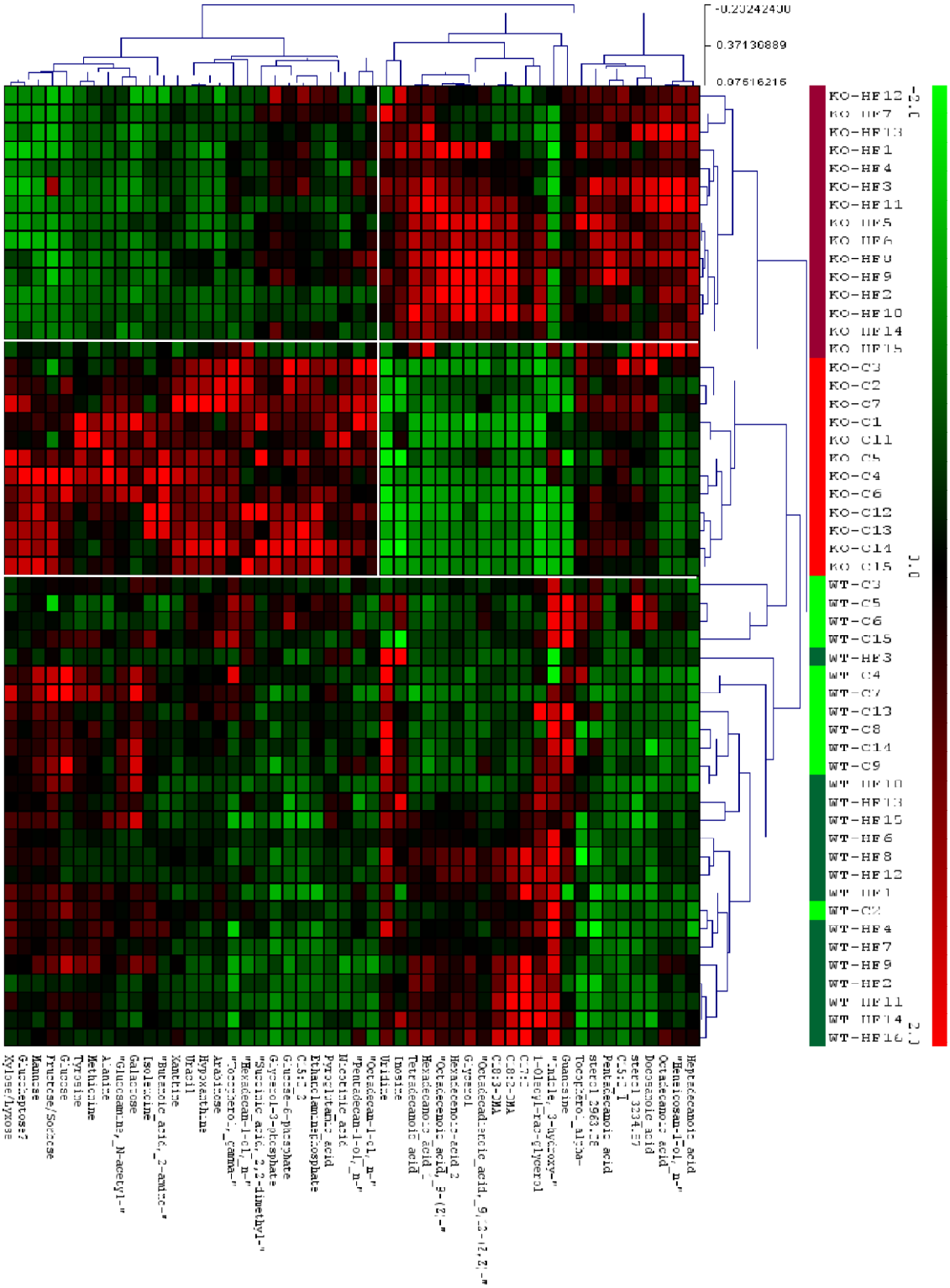
-0.20242430
0.37130889
0.97616216
KO-HF12
KO-HF7
KO-HF13
KO-HF1
KO-HF4
KO-HF3
KO-HF11
KO-HF5
KO-HF6
KO-HF8
KO-HF9
KO-HF2
KO-HF10
KO-HF14
KO-HF15
KO-C3
KO-C2
KO-C7
KO-C1
KO-C11
KO-C5
KO-C4
KO-C6
KO-C12
KO-C13
KO-C14
KO-C15
WT-C3
WT-C5
WT-C6
WT-C15
WT-HF3
WT-C4
WT-C7
WT-C13
WT-C8
WT-C14
WT-C9
WT-HF10
WT-HF13
WT-HF15
WT-HF6
WT-HF8
WT-HF12
WT-HF1
WT-C2
WT-HF4
WT-HF7
WT-HF9
WT-HF2
WT-HF11
WT-HF14
WT-HF16
Heptadecanoic_acid
"Octadecan-1-ol,_n-"
Octadecanoic_acid
Docosanoic_acid
sterol_3234.57
C-5:-_1
Pentadecanoic_acid
sterol_2963.8
Tocophero_alpha-
Guanosine_
"Indole-3-glycerol
1-Oleoyl-rac-glycerol
C-1:-
C-18:3-DMA
"Octadecadienoic_acid,_9,12-
Glycerol
Hexadecenoic_acid_2
"Octadecenoic_acid_9-(Z)-"
Hexadecanoic_acid_
Tetradecanoic_acid
Inosine
Uridine
"Octadecan-1-ol,_n-"
"Pentadecan-1-ol,_n-"
N-octimic_acid
Pyroglutam_c_acid
Ethanolamine_phosphate
C-5:-_2
Glucose-6-phosphate
Glycerol-3-phosphate
"Succinic_acid,_2,3-dimethyl-"
"Hexadecan-1-ol,_n-"
"Tocophero-_gamma-"
Arabitose
Hypoxanthine
Uracil
Xanthine
"Butanoic_acid,_2-amino-"
Isoleucine
Galactose
"Glucosamine,_N-acetyl-"
Alanine
Methionine
Tyrosine
Glucose
Fructose/Sorbose
Mannose
Glucoseptose?
Xylose/lyxose

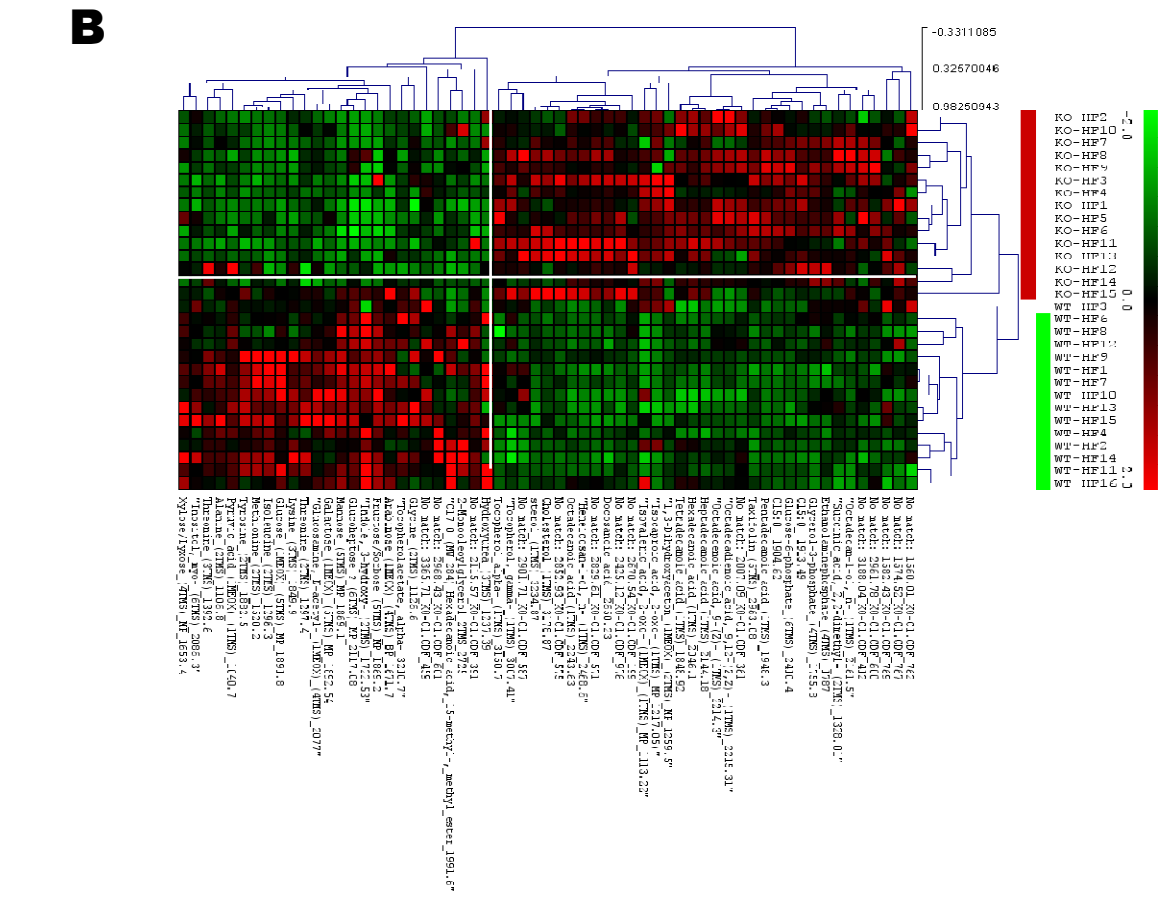

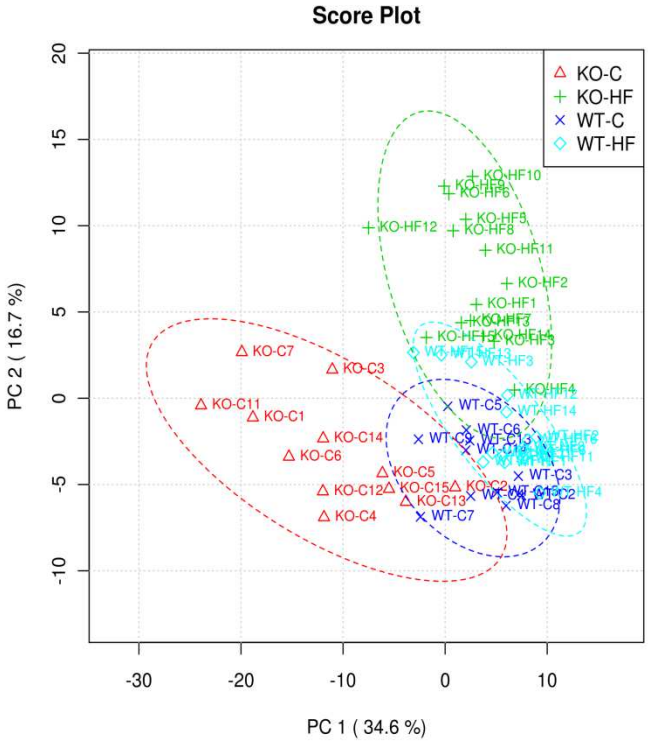

Figure 17: Analysis of free fatty acids in caecal content of *Pept1*$^{-/-}$ and WT mice. (A) Heatmap of all four groups (n=11-15) showing clear diet-specific clustering in *Pept1*$^{-/-}$ mice while there are no distinct clusters observed within the WT mice. (B) Heatmap of WT and *Pept1*$^{-/-}$ mice on HFD showing diet-specific alterations between both genotypes. A color-coded display of significant changes in the metabolite level (relative changes; data are standardized) is given where green indicates a down-regulation and red indicates an up-regulation; metabolites are shown on the right side. Test on significant differences among the groups of samples resulting from cluster analysis were performed with Kruskal-Wallis tests (selected FDR limit = 0.05; Bonferroni adjustment); clustering was based on Euclidean distance and average linkage. (C) PCA blot with normalized metabolite data [x = (value-average)/SD] revealed a clear separation caused by different metabolite abundances for *Pept1*$^{-/-}$ animals while WT mice seem to have comparable metabolites (n=11-15).

3 Liver lipids

Since WT mice on HFD developed a fatty liver, they showed the highest concentrations of TG (488.92 ± 58.34 mg/g protein), PL (1302.84 ± 286.14 mg/g protein) and non-esterified fatty acids (NEFAs) (1509.04 ± 242.26 mmol/g protein). Knock-out mice on HFD showed concentrations of 404.19 ± 66.62 mg/g protein TG, 820.13 ± 114.56 mg/g protein PL and 428.11 ± 116.64 mmol/g protein NEFAs. Regardless of the diet, *Pept1*$^{-/-}$ animals had always lower concentrations in all three parameters when compared to WT mice (Figure18). On CD, lipid concentrations in WT mice were measured to be 243.15 ± 58.46 mg/g protein TG, 686.31 ± 77.97 mg/g protein PL and 402.31 ± 69.43 mmol/g protein NEFAs. Concentrations determined in *Pept1*$^{-/-}$ mice were 184.54 mg/g protein TG, 569.74 ± 74 mg/g protein PL and 164.37 ± 19.27 mmol/g protein NEFAs. NEFA concentrations determined a genotype-specific difference for mice on HFD, whereas triglycerides and phospholipids showed only diet-specific alterations.

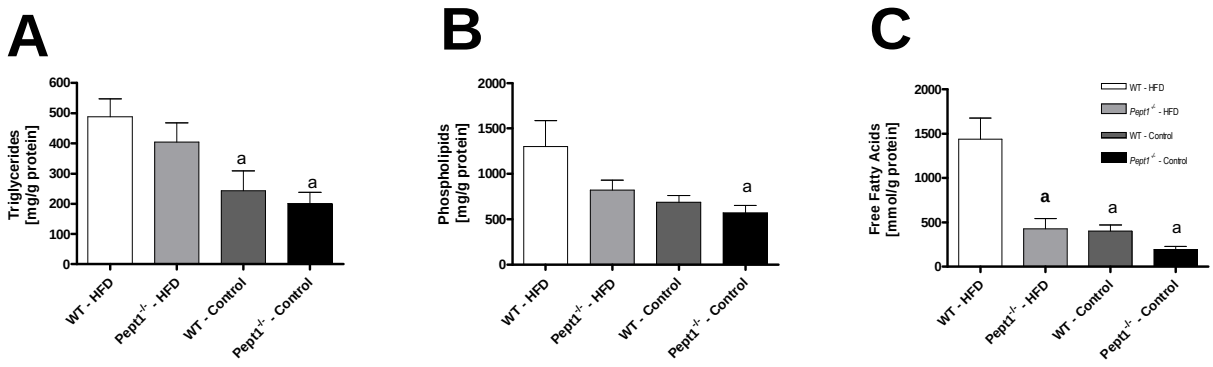

Figure 18: Triglyceride, phospholipid and non-esterified free fatty-acid concentrations in livers of *Pept1*$^{-/-}$ and WT mice. Samples (n=10) were collected at the end of 12-weeks HFD. (A) Triglyceride concentrations. Mice on CD showed significantly decreased TG concentrations compared to WT animals o HFD. (B) Phospholipid concentrations. Knockout mice tend to have lower PL concentrations. Only *Pept1*$^{-/-}$ mice on CD had significantly reduced PL content. (C) NEFA concentrations showed diet- and genotype-specific differences. WT mice on HFD had significantly increased NEFA concentrations compared to all other groups. Data are expressed as mean ± SEM. Significances are given in: a = all labeled groups are significantly reduced compared to WT mice on HFD ($p<0.01$)

4 Blood parameters

4.1 Lipid parameters

After 12 weeks of feeding a HFD, *Pept1*$^{-/-}$ mice were not as obese as WT animals on HFD - but they had comparable lipid concentrations for cholesterol, HDL and triglycerides (Table 7). In contrast, *Pept1*$^{-/-}$ on HFD mice had significantly reduced concentrations for LDL, VLDL, alanine-aminotransferase (ALT), and glucose: 32.67 ± 7.06 U/L, 62.00 ± 4.10 U/L and 263.33 ± 16.29 mg/dL, respectively, when compared to WT animals on HFD: 105.67 ± 25.76 U/L (ALT), 121.33 ± 18.82 U/L (AST) and 366.00 ± 28.45 mg/dL (glucose). Animals on CD generally had reduced amounts of all parameters when compared to mice on HFD. *Pept1*$^{-/-}$ and WT mice on CD had comparable blood concentrations of cholesterol, HDL and triglycerides. But *Pept1*$^{-/-}$ mice on CD had significantly reduced amounts of ALT and glucose (18.67 ± 1.65 U/L, 53.00 ± 3.19 U/L and 177.50 ± 6.35 mg/dL, respectively) compared to WT mice on CD or HFD. All data is summarized in Figure 19 and Table 7.

Table 7: Plasma lipid parameters of *Pept1*$^{-/-}$ and WT mice on CD and HFD (n=6). Data are expressed as mean ± SEM. Values with asterisks represent significant differences: (i) * = p<0.05, ** = p<0.01 and (iii) *** = p<0.001

	WT - HFD	*Pept1*$^{-/-}$ - HFD	WT - Control	*Pept1*$^{-/-}$ - Control
Cholesterol [mg/dL]	187.00 ± 6.17	162.67 ± 5.16	89.00 ± 11.32	88.00 ± 3.86
HDL [mg/dL]	109.00 ± 4.12	95.67 ± 4.94	65.50 ± 8.52	61.50 ± 2.86
Triglycerides [mg/dL]	78.67 ± 5.77	80.33 ± 6.99	58.33 ± 4.79	52.00 ± 5.27
Glucose [mg/dL]	366.00 ± 28.45***	263.33 ± 16.29	244.83 ± 44.71**	177.50 ± 6.35
Total Cholesterol/HDL	3.47 ± 0.08	3.43 ± 0.20	1.35 ± 0.02	1.43 ± 0.02
LDL [mg/dL]	63.00 ± 3.92	51.33 ± 6.59	12.00 ± 2.68	15.83 ± 1.82
VLDL [mg/dL]	15.67 ± 1.20	16.00 ± 1.26	11.67 ± 1.02	10.50 ± 0.96

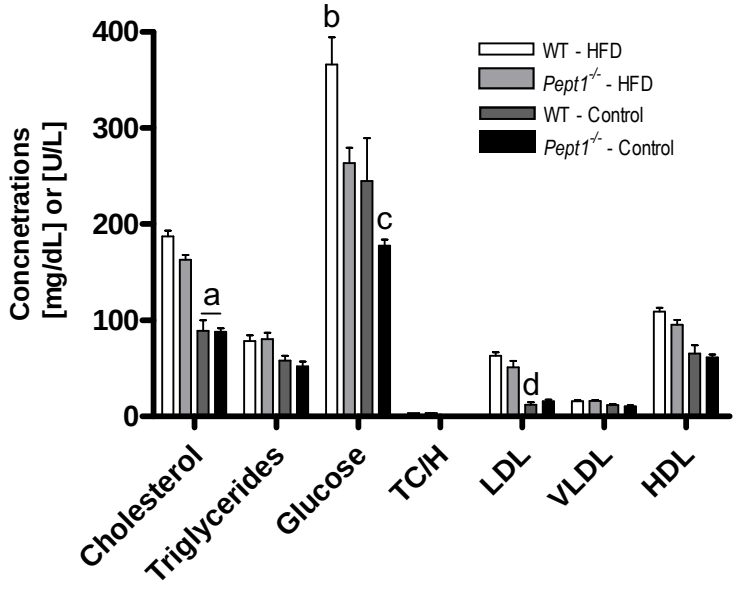

Figure 19: Plasma lipid parameters in *Pept1*$^{-/-}$ and WT mice. Diet-specific differences are detected for all parameters. Data are expressed as mean ± SEM of n=8 mice per group. Significances are given in: (i) a = mice on CD have lower cholesterol concentrations than groups on HFD ($p<0.001$), (ii) b = WT mice on HFD have highest glucose concentrations compared to all other groups ($p<0.001$), (iii) c = *Pept1*$^{-/-}$ mice on CD have lower levels than WT mice on CD and *Pept1*$^{-/-}$ mice on HFD ($p<0.01$), (iv) d = WT mice on CD have lower LDL levels compared to WT mice on HFD ($p<0.05$).

Highest plasma levels of non-esterified free fatty-acids (NEFAs) were detected in WT mice on HFD (0.91 ± 0.03 mmol/L) while *Pept1*$^{-/-}$ mice on HFD had 0.82 ± 0.05 mmol/L circulating in plasma. Concentrations measured in mice on CD were significantly lower compared to those on HFD showing a diet-specific change in this parameter. *Pept1*$^{-/-}$ animals on CD had lower NEFA levels compared to WT mice (0.43 ± 0.03 mmol/L and 0.59 ± 0.05 mmol/L, respectively) (Figure 20A).

Also phospholipid concentrations displayed diet-specific changes with mice on CD having lower levels compared to WT mice on HFD (320.72 ± 35.22 mg/dL): 221.37 ± 12.86 mg/dL (KO-C) and 184.29 ± 68.72 mg/dL (WT-C). Surprisingly, phospholipid concentrations in *Pept1*$^{-/-}$ mice on HFD were significantly reduced compared to WT mice on HFD: 258.60 ± 42.95 mg/dL (Figure 20B).

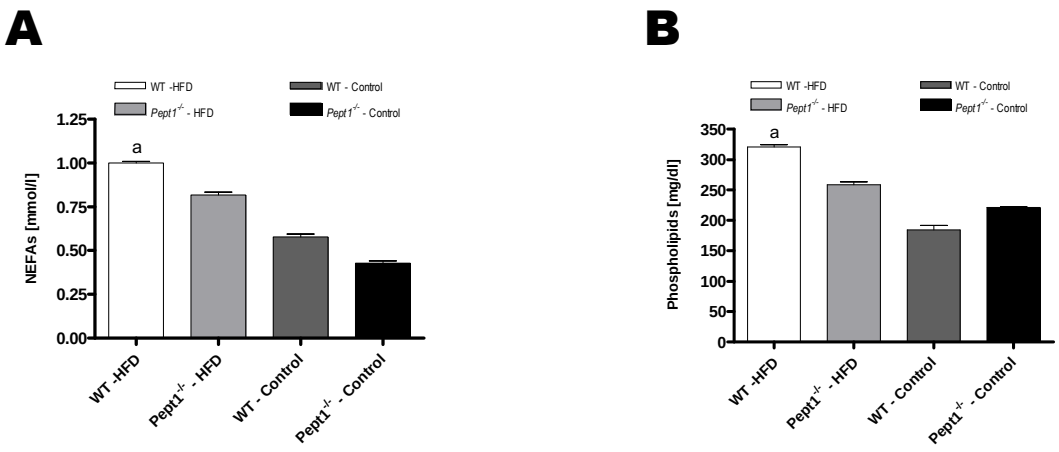

Figure 20: Non-esterified free fatty-acid (NEFAs) and phospholipid concentrations in plasma of *Pept1*$^{-/-}$ and WT mice. Samples (n=10) were collected at the end of 12-weeks HFD. (A) NEFA concentrations showed diet- and genotype-specific differences. Mice on CD had lower levels compared to animals on HFD. Knockout animals also showed lower concentrations compared to WT mice. (B) Phospholipid concentrations showed diet- and genotype-specific differences. Mice on CD had lower levels compared to animals on HFD. Knockout animals also showed lower concentrations compared to WT mice. Data are expressed as mean ± SEM. Significances are given in: (i) a = WT mice on HFD have higher concentrations compared to all other groups ($p<0.001$)

4.2 General chemistry

After 12 weeks of feeding a HFD, *Pept1*$^{-/-}$ mice and WT animals on HFD and CD had comparable concentrations for albumin, calcium, creatinine, γ-glutamyltransferase (GGT), total bilirubin, total protein, blood urea nitrogen (BUN) and ureic acid in blood (Table 11). In contrast, *Pept1*$^{-/-}$ mice on HFD and CD had significantly increased concentrations for alkaline phosphatase (87.00 ± 13.64 U/L and 76.33 ± 4.06 U/L, respectively) when compared to WT animals: 71.67 ± 7.01 U/L (HFD) and 57.33 ± 4.94 U/L (CD). Additionally, liver parameters for ALT and AST showed diet-specific and genotype-specific differences. For both enzymes levels were significantly decreased in mice on CD and knockout animals on both diets had lower levels to WT mice on the same diet. *Pept1*$^{-/-}$ mice on HFD had plasma concentrations of 31.67 ± 6.64 U/L (ALT) and 65.67 ± 4.57 U/L (AST). WT mice on the same diet had levels of 105.33 ± 25.54 U/L (ALT) and 129.67 ± 21.28 U/L (AST) while WT mice on CD had 36.67 ± 9.53 U/L (ALT) and 100.50 ± 16.89 U/L (AST). *Pept1*$^{-/-}$ mice on CD had the lowest levels measured for both parameters: 19.83 ± 2.12 U/L (ALT) and 57.67 ± 2.64 U/L (AST) (Table 8 and Figure 21).

Table 8: General organ parameters measured in plasma of *Pept1*$^{-/-}$ and WT mice on CD and HFD. Data are expressed as mean ± SEM of n=8 mice per group. Values with asterisks represent significant differences: (i) ** = p<0.01 and (ii) *** = p<0.001

	WT - HFD	*Pept1*$^{-/-}$ - HFD	WT - Control	*Pept1*$^{-/-}$ - Control
Albumin [mg/dL]	2.23 ± 0.08	1.90 ± 0.04	2.03 ± 0.21	2.13 ± 0.02
Alkaline Phosphatase [U/L]	71.67 ± 7.01**	87.00 ± 13.64	57.33 ± 4.94***	76.33 ± 4.06
ALT [U/L]	105.33 ± 25.54	31.67 ± 6.64	36.67 ± 9.53	19.83 ± 2.12
AST [U/L]	129.67 ± 21.28	65.67 ± 4.57	100.50 ± 16.89	57.67 ± 2.64
Calcium [mg/dL]	10.30 ± 0.24	9.60 ± 0.18	10.07 ± 0.15	9.85 ± 0.13
Creatinine [mg/dL]	0.27 ± 0.04	0.20 ± 0.00	0.20 ± 0.00	0.20 ± 0.00
GGT [U/L]	5.00 ± 0.00	5.00 ± 0.00	5.00 ± 0.00	5.00 ± 0.00
Total Bilirubin [mg/dL]	0.70 ± 0.07	0.40 ± 0.06	0.67 ± 0.04	0.40 ± 0.00
Total Protein [mg/dL]	5.80 ± 0.16	5.05 ± 0.11	5.47 ± 0.11	5.15 ± 0.04
BUN [mg/dL]	20.00 ± 1.15	24.17 ± 1.92	21.33 ± 1.43	27.50 ± 1.84
Ureic Acid [mg/dL]	1.85 ± 0.63	0.95 ± 0.38	0.92 ± 0.17	0.80 ± 0.11

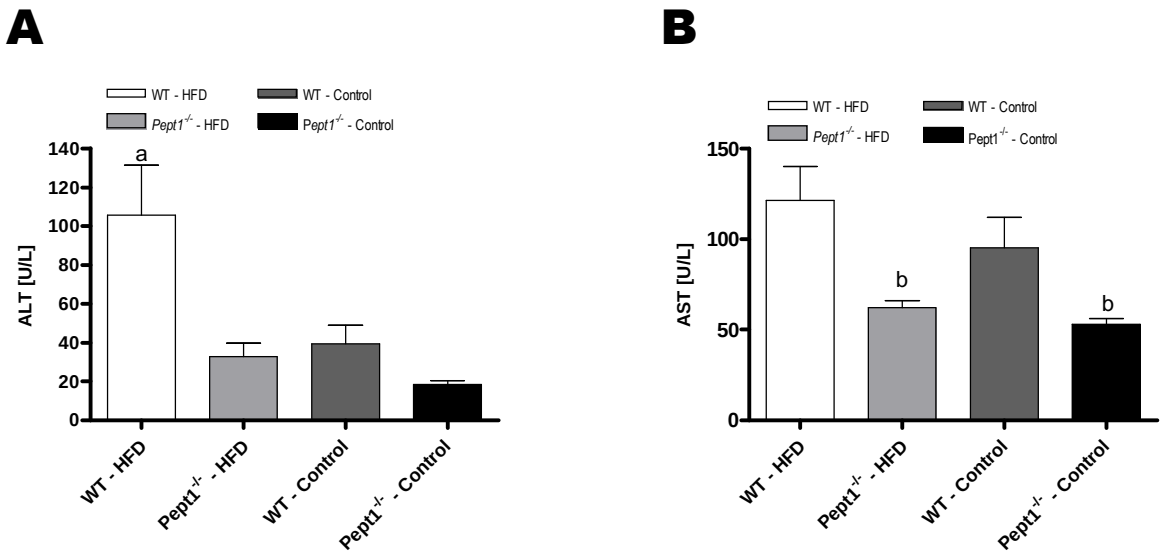

Figure 21: ALT and AST concentrations in plasma of *Pept1*$^{-/-}$ and WT mice. Samples (n=6) were collected at the end of 12-weeks HFD. (A) ALT concentrations showed diet-specific differences. Also genotype-specific differences were observed in animals on HFD showing *Pept1*$^{-/-}$ mice to have significantly lowered levels of ALT. (B) AST concentrations showed diet- and genotype-specific differences. *Pept1*$^{-/-}$ mice on both diets had significantly decreased AST levels compared to WT mice on HFD. Data are expressed as mean ± SEM. Significances are given in: (i) a = WT mice on HFD have higher concentrations compared to all other groups (p<0.001), (ii) b = *Pept1*$^{-/-}$ mice on both diets have lower concentrations compared to WT mice on HFD (p<0.01)

4.3 Insulin concentration

After 12 weeks on the specific diets, a general diet-specific decrease in plasma insulin levels was observed. On the HFD, *Pept1*$^{-/-}$ mice showed reduced plasma insulin concentrations (1.86 ± 0.39 ng/ml) when compared to WT mice on HFD (3.49 ± 0.67 ng/ml). Animals fed the CD showed significantly decreased insulin concentrations: *Pept1*$^{-/-}$ mice had a final concentration of 0.60 ± 0.16 ng/ml and WT mice 0.74 ± 0.09 ng/ml (Figure 22). Although there were no genotype-specific differences observed, knockout animals on HFD tend to have lower insulin concentrations.

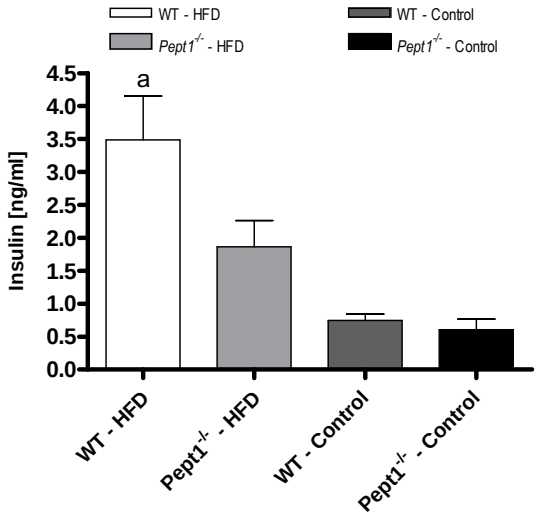

Figure 22: Plasma insulin concentrations of *Pept1*$^{-/-}$ and WT mice. Diet-specific effects showed mice on CD having plasma insulin concentrations. Samples (n=5) were collected at the end of 12-weeks HFD. Data are expressed as mean ± SEM. Significances are given in: a = WT mice on HFD have higher concentrations compared to all other groups ($p<0.001$)

4.4 Leptin concentration

Plasma leptin concentrations showed diet- and genotype-specific differences. In general, mice on CD had lower leptin level compared to both genotypes on HFD, but *Pept1*$^{-/-}$ animals on HFD showed reduced leptin concentrations (38.17 ± 5.20 ng/ml) when compared to WT mice on HFD (68.06 ± 7.95 ng/ml). There were no differences detected between WT and knockout animals on CD: *Pept1*$^{-/-}$ mice had final levels of 1.53 ± 0.42 ng/ml and WT on CD showed concentrations of 2.56 ± 0.35 ng/ml (Figure 23).

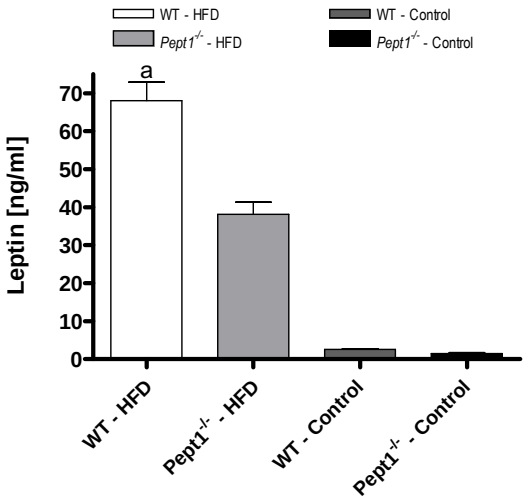

Figure 23: Plasma leptin concentrations of *Pept1*$^{-/-}$ and WT mice. In a diet-specific manner, mice on CD showed significantly reduced leptin levels compared to animals on HFD. On HFD, *Pept1*$^{-/-}$ mice have significantly reduced leptin concentrations compared to WT mice. Samples (n=8) were collected at the end of 12-weeks HFD. Data are expressed as mean ± SEM. Significances are given in: a = WT mice on HFD have higher concentrations compared to all other groups ($p<0.001$)

4.5 Pancreatic lipase and amylase activity

The activity of pancreatic lipase was comparable for all groups after 12 weeks of feeding either a HFD or a CD (Table 9, Figure 24A).

Table 9: Activities of pancreatic enzymes of *Pept1*$^{-/-}$ and WT mice on CD and HFD. Data are expressed as mean ± SEM of n=8 mice per group.

	WT – HFD	*Pept1*$^{-/-}$ - HFD	WT – Control	*Pept1*$^{-/-}$ - Control
Lipase [U/l]	36.09 ± 2.45	35.07 ± 1.86	28.51 ± 4.82	36.50 ± 4.60
Amylase [U/l]	1102.67 ± 86.59	982.33 ± 23.73	757.17 ± 29.52	694.50 ± 44.71

Pancreatic amylase displayed diet- and genotype-specific differences. The activity was generally reduced in mice on CD when compared to animals on HFD (Figure 24B). Regardless the diet, amylase activity was significantly reduced for *Pept1*$^{-/-}$ mice: 982.33 ± 23.73 U/L (HFD) and 694.50 ± 44.71 U/L (CD). WT mice displayed an activity of 1102.67 ± 86.59 U/L (HFD) and 757.17 ± 29.52 U/L (CD), respectively.

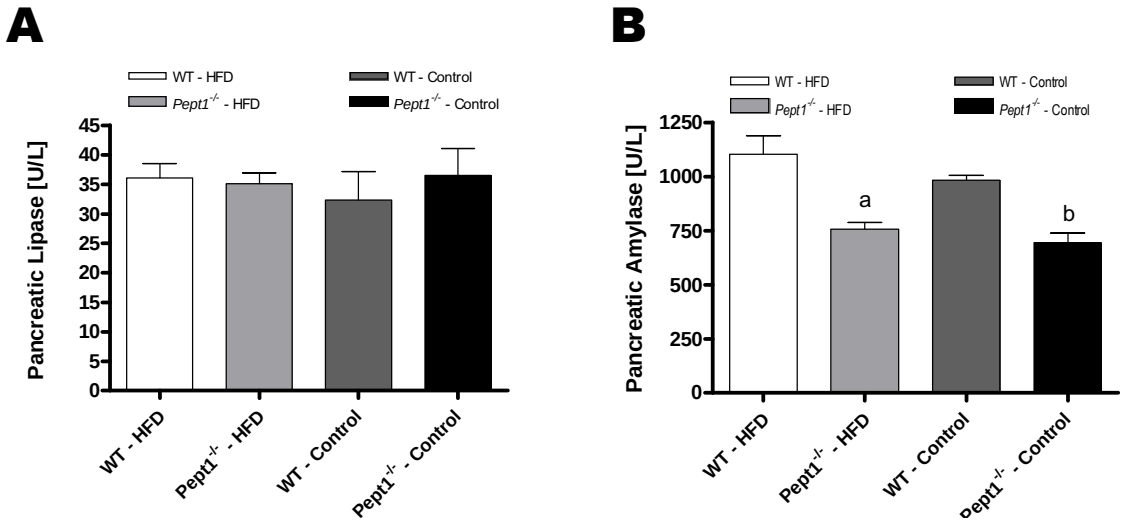

Figure 24: Enzymatic activity of pancreatic lipase and amylase in *Pept1*$^{-/-}$ and WT mice. Samples (n=8) were collected at the end of 12-weeks HFD. (A) Enzymatic activity of pancreatic lipase is similar between all four groups. (B) Enzymatic activity of pancreatic amylase. *Pept1*$^{-/-}$ mice show a significant genotype specific reduction on both diets. Data are expressed as mean ± SEM. Significances are given in: (i) a = *Pept1*$^{-/-}$ mice on HFD have lower concentrations compared to WT mice on HFD ($p<0.001$), (ii) b = *Pept1*$^{-/-}$ mice on CD have lower concentrations compared to WT mice on CD ($p<0.01$)

4.6 Amino acid analysis

Plasma samples were collected after 12 weeks on CD or HFD and analyzed for its free amino acid (aa) concentration. Most of the aa analyzed had comparable concentrations between all four groups. Although there are no obvious diet- or genotype-specific changes, four aa, taurine, proline, arginine and lysine, showed differences in concentrations. WT mice on HFD had significantly increased taurine concentrations (767.92 ± 105.42 µM) when compared to all other groups: 499.46 ± 39.67 µM (KO-HFD), 442.10 ± 40.29 µM (KO-Control) and 450.03 ± 47.40 µM (WT-Control), respectively. Regardless the diet, proline concentrations tend to be slightly lower in WT mice compared to *Pept1*$^{-/-}$ mice. There was a diet-specific difference for proline in *Pept1*$^{-/-}$ mice with a 25 % reduced proline content on a HFD: 191.83 ± 23.42 µM (KO-CD) and 147.75 ± 20.02 µM (KO-HFD). Lysine levels were significantly increased in *Pept1*$^{-/-}$ mice on CD (420.14 ± 42.87 µM) when compared to all other groups: 353.15 ± 24.82 µM (KO-HFD), 311.15 ± 19.67 µM (WT-HFD) and 313.15 ± 33.42 µM (WT-Control). Plasmic arginine concentrations were also significantly higher in *Pept1*$^{-/-}$ mice on CD (118.48 ±14.65 µM) than in both WT

groups: 47.84 ± 7.89 µM (WT-HFD) and 74.85 ± 13.96 µM (WT-Control). Additionally, arginine levels tend to be decreased in *Pept1*$^{-/-}$ mice on HFD (97.17 ± 9.29 µM) when compared to *Pept1*$^{-/-}$ animals on CD. All data is summarized in Table 10 and Figure 25.

Table 10: Concentrations of plasmic free amino acid in *Pept1*$^{-/-}$ and WT mice. There are no differences observed except for taurine, proline, argininge and lysine (indicated by asterisks). Taurine levels are significantly increased in WT mice on HFD compared to the other groups. Contrary to this, proline, arginine and lysine concentrations in plasma are increased significantly in WT mice on CD when compared to the other groups. Data are expressed as mean ± SEM of n=9 mice per group. Asterisks represent aa that show significant changes.

Amino acids [µM]	WT – HFD	*Pept1*$^{-/-}$ - HFD	WT – Control	*Pept1*$^{-/-}$ - Control
PEtN	6.57 ± 0.87	5.86 ± 0.15	3.76 ± 0.53	4.07 ± 0.51
Tau	767.92 ± 105.42***	499.46 ± 39.67	450.03 ± 47.40	442.10 ± 40.29
Asn	92.18 ± 9.53	94.82 ± 6.72	89.02 ± 16.38	72.96 ± 8.64
Ser	180.00 ± 15.97	166.15 ± 6.38	167.41 ± 26.49	141.14 ± 13.54
Hyp	14.85 ± 0.66	18.10 ± 1.28	16.97 ± 1.52	21.99 ± 2.12
Gly	253.85 ± 12.26	207.62 ± 9.80	266.66 ± 27.74	178.32 ± 18.29
Gln	1070.46 ± 86.04	944.00 ± 38.90	868.49 ± 85.33	897.73 ± 74.60
Asp	10.76 ± 1.27	9.51 ± 1.62	11.77 ± 3.93	8.78 ± 0.90
Cit	53.63 ± 3.08	67.80 ± 5.69	55.83 ± 6.22	76.15 ± 8.55
bAla	17.44 ± 1.99	21.33 ± 2.36	11.64 ± 1.40	12.19 ± 2.06
Ala	706.69 ± 66.33	676.00 ± 39.10	588.67 ± 99.82	583.00 ± 66.74
Thr	238.69 ± 23.72	201.23 ± 16.09	184.00 ± 23.54	155.72 ± 15.90
Glu	67.24 ± 7.85	62.42 ± 5.29	61.18 ± 11.94	52.00 ± 4.36
His	95.39 ± 5.18	85.84 ± 4.94	95.24 ± 16.18	79.89 ± 9.38
Abu	6.27 ± 0.48	6.35 ± 0.51	9.13 ± 1.35	10.67 ± 1.31
Aad	9.15 ± 0.66	10.77 ± 0.84	12.21 ± 1.66	16.54 ± 1.72
Pro	128.02 ± 19.73	147.75 ± 20.02	157.44 ± 35.87	191.83 ± 23.42
Arg	47.84 ± 7.89**	97.17 ± 9.29	74.85 ± 13.96	118.48 ± 14.65
Orn	107.83 ± 7.58	80.23 ± 9.32	88.04 ± 21.23	60.40 ± 6.38
Lys	311.15 ± 19.67	353.15 ± 24.82	313.12 ± 33.42***	420.14 ± 42.87
Val	300.23 ± 20.47	281.62 ± 22.40	269.22 ± 34.11	251.52 ± 26.74
Met	37.17 ± 5.15	48.95 ± 3.63	38.72 ± 5.55	41.38 ± 6.23
Tyr	102.65 ± 9.44	112.38 ± 11.74	123.20 ± 23.04	109.55 ± 11.51
Ile	124.38 ± 10.26	109.58 ± 8.37	107.53 ± 13.22	95.93 ± 8.78
Leu	208.77 ± 16.88	185.77 ± 14.76	178.34 ± 22.69	170.90 ± 17.38
Phe	88.80 ± 5.50	82.35 ± 5.99	85.21 ± 13.38	73.27 ± 7.36
Trp	85.28 ± 2.29	75.04 ± 3.12	79.57 ± 8.19	65.52 ± 6.54

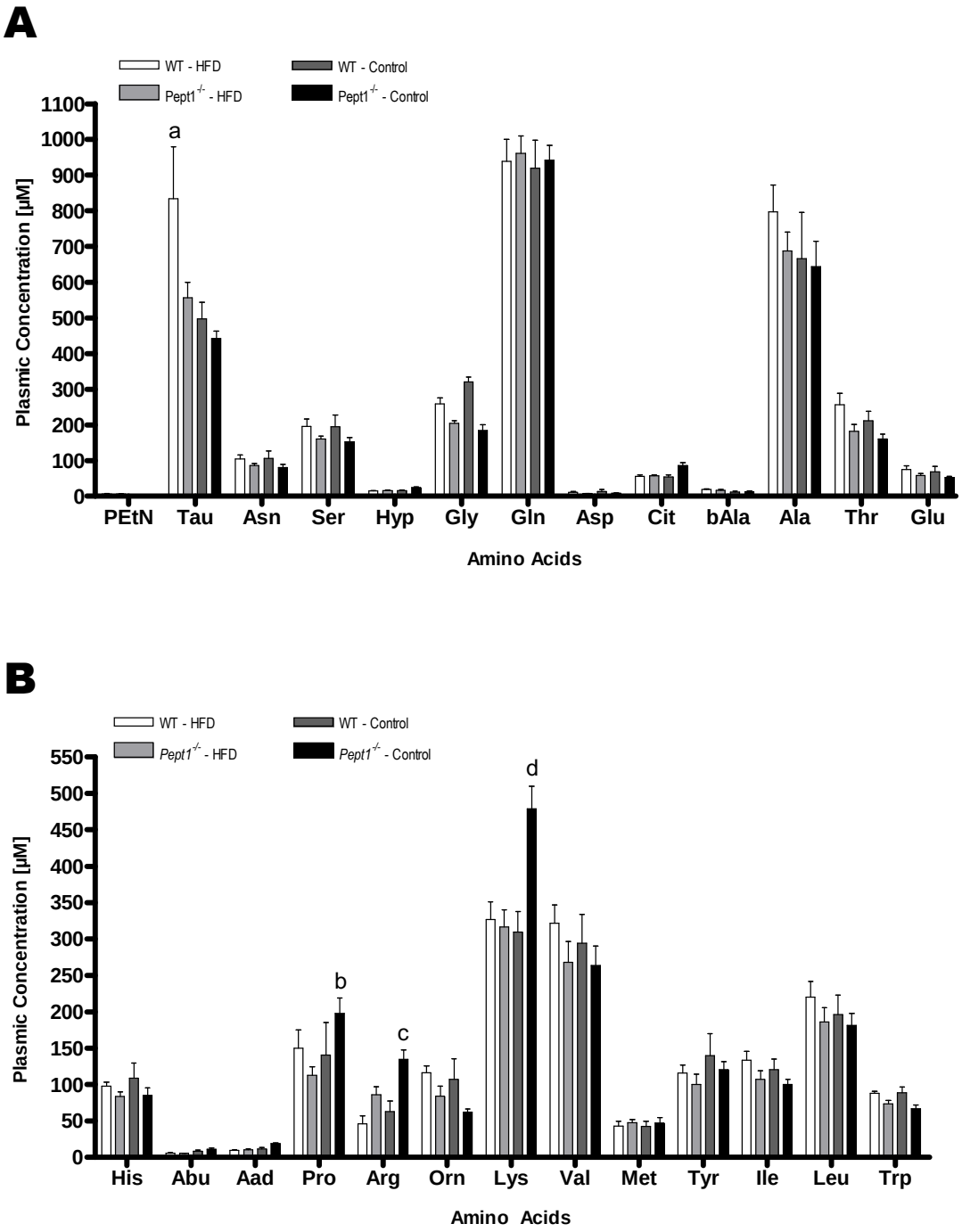

Figure 25: C**oncentrations of free amino acids in plasma of *Pept1*$^{-/-}$ and WT mice**. Samples (n=9) were collected at the end of 12-weeks HFD. Concentrations of free plasma aa remained unchanged for most aa measured. Taurine was increased in WT mice on HFD compared to all other groups. Proline, arginine and lysine were elevated in *Pept1*$^{-/-}$ mice on CD compared to the other groups. Data are expressed as mean ± SEM. Significances are given in: (i) a = WT mice on HFD have higher taurine concentrations compared to all other groups ($p<0.001$), (ii) b = *Pept1*$^{-/-}$ mice on CD have higher proline concentrations compared to *Pept1*$^{-/-}$ mice on HFD ($p<0.01$), (iii) c = *Pept1*$^{-/-}$ mice on CD have higher arginine concentrations compared to WT mice on both diets ($p<0.05$), (iv) d = *Pept1*$^{-/-}$ mice on CD have higher lysine concentrations compared to all other groups ($p<0.001$).

5 Interaction of PEPT1 and NHE3

5.1 Inhibitory effect of amiloride

WT mice were given amiloride (sodium-channel inhibitor) in different concentrations to find the lowest effective dose for further studies. After 2 weeks of feeding the HFD, 5 or 10 µg/ml of amiloride was added into drinking water of the animals. There was no effect observed. During the second week of treatment with either 20 or 30 µg/mol amiloride in the water, we saw a significant reduction of body weight in the group receiving 30 µg/ml amiloride. Contrary to this, the control animals and those treated with 20 µg/ml amiloride showed higher body weights (Figure 26A). During the whole study all animals showed similar food and water intake: 30.57 g (control group), 29.74 ± 1.76 g (mice treated with 20 µg/ml amiloride) and 30.51 ± 0.91 g (mice treated with 30 µg/ml amiloride) (Figure 26B). There were also no changes in water consumption between all groups. So we conclude the decreased body weight being due to amiloride treatment and not to alterations in food and drinking behavior.

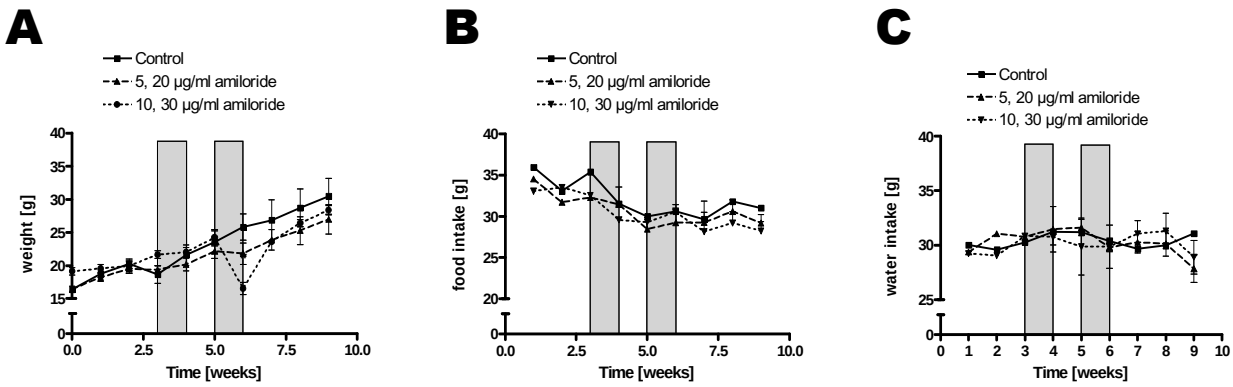

Figure 26: Mean body weight, food and water intake of WT mice treated with amiloride. During the whole study mice (n=5) were fed the HFD. (A) Mean body weight showing a significant decrease after treatment with 30 µg/ml amiloride (grey bar between weeks 5-6), (B) cumulative food intake showing no differences between the groups and (C) cumulative water intake of WT mice. Grey bars in weeks 3-4 and 5-6 represent the weeks when mice received amiloride in drinking water. In weeks 3-4 mice were administered either 5 or 10 µg/ml amiloride while in week 5-6 amiloride concentrations were 20 or 30 µg/ml. Data are expressed as mean ± SEM. Values with asterisks represent significant differences of WT mice on HFD compared to the other groups: * = $p<0.05$

5.2 S1611 treatment does not inhibit NHE3

After 2 weeks of feeding the HFD, 5 or 10 µg/ml of S1611 (specific NHE3 inhibitor) were added into drinking water of the animals. There was no effect (e.g. changes in body weight, eating or drinking behavior) observed. During the second week of treatment with either 20 or 30 µg/mol S1611 in the water, we saw no differences in treated mice compared to control animals. At the end control mice had a weight of 33.22 ± 0.39 g, mice treated with 20 µg/ml of S1611 had 32.60 ± 0.98 g and mice treated with 30 µg/ml of S1611 showed a weight of 31.03 ± 0.82 g (Figure 27A). During the whole study all animals showed similar food intake: 13.36 g (control group), 13.74 g (mice treated with 20 µg/ml of S1611) and 13.07 g (mice treated with 30 µg/ml of S1611) (Figure 27B). There were also no changes in water consumption between all groups: 115.58 g (control group), 15.54 g (mice treated with 20 µg/ml of S1611) and 16.84 g (mice treated with 30 µg/ml of S1611) (Figure 27C). Since S1611 is a highly potent NHE3 inhibitor (IC_{50} = 0.05 µM) we did not further increase the concentrations.

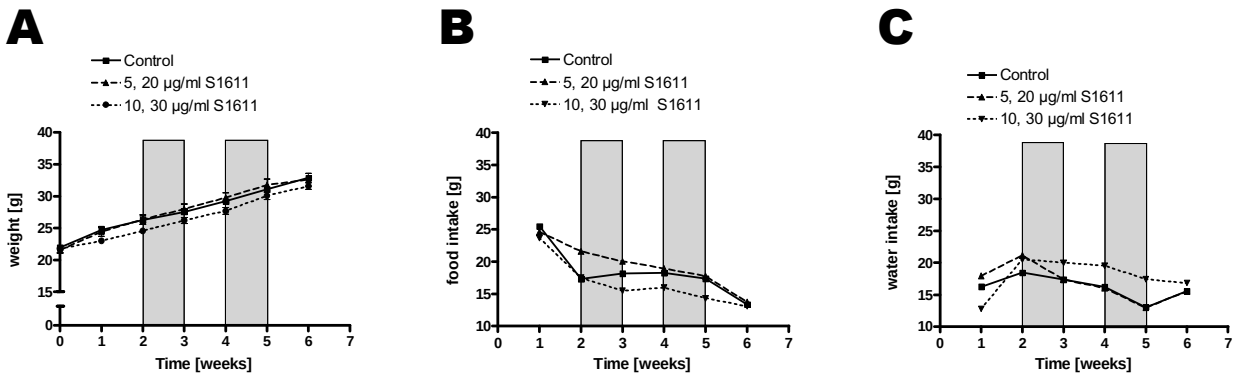

Figure 27: Mean body weight, food and water intake of WT mice treated with S1611. During the whole study mice (n=5) were fed the HFD. (A) Mean body weight, (B) cumulative food intake and (C) cumulative water intake of WT mice. Grey bars in weeks 2-3 and 4-5 represent the weeks when mice received S1611 in drinking water. In week 2-3 mice were administered either 5 or 10 µg/ml S1611 while in week 4-6 S1611 concentrations were 20 or 30 µg/ml. Data are expressed as mean ± SEM.

5.3 Fat mass analysis during amiloride and S1611 treatment

NMR anaylsis of fat and lean mass content in the body was measured weekly. For fat mass analysis, mice showed also no significant difference during the first five weeks. When mice were treated with 30 µg/ml of amiloride for a period of one week, these mice had significantly reduced fat mass in their body compared to the other groups:

0.54 ± 0.12 g (mice treated with 30 µg/ml amiloride), 4.20 ± 0.63 g (mice treated with 20 µg/ml amiloride) and 8.57 ± 1.88 g (control group) (Figure 28A). When measuring body lean mass, there were no differences between the three groups during the whole study: 14.75 ± 1.16 g (mice treated with 30 µg/ml amiloride), 15.85 ± 0.48 g (mice treated with 20 µg/ml amiloride) and 15.84 ± 0.24 g (control group) (Figure 28B).

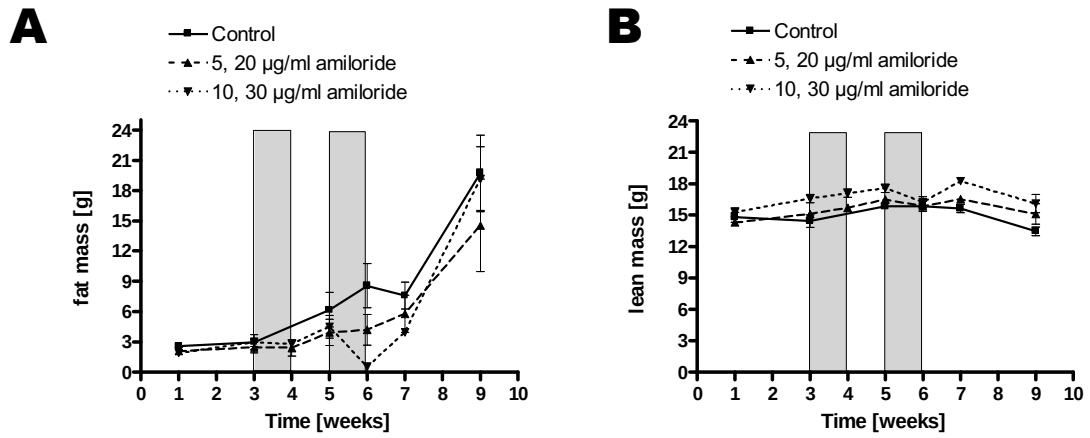

Figure 28: NMR analysis of fat and lean mass of WT mice (n=5) treated with amiloride. During the whole study mice were fed the HFD. (A) Fat mass content was significantly reduced after treatment with 30 µg/ml amiloride (grey bar between weeks 5-6), (B) Lean mass content remained unchanged during the total study between all groups. Grey bars in weeks 3-4 and 5-6 represent the weeks when mice received amiloride in drinking water. In weeks 3-4, mice were administered either 5 or 10 µg/ml amiloride while in week 5-6 amiloride concentrations were 20 or 30 µg/ml. Data are expressed as mean ± SEM. Values with asterisks represent significant differences of WT mice on HFD compared to the other groups: (i) * = $p<0.05$, (ii) ** = $p<0.01$

Mice treated with S1611 showed increasing fat mass during 6 weeks of feeding the HFD which is due to the high calorie feeding. Regardless the administered S1611 concentration, there were no differences observed in fat mass between all groups: 11.62 ± 0.56 g (control group), 10.74 ± 0.76 g(mice treated with 20 µg/ml of S1611) and 8.15 ± 0.53 g (mice treated with 30 µg/ml of S1611) (Figure 29A). The amount of leans mass remained the same during the whole period of 6 weeks and displayed no differences between the groups: 17.14 ± 0.18 g (control group), 17.90 ± 0.31 g (mice treated with 20 µg/ml of S1611) and 18.88 ± 0.40 g (mice treated with 30 µg/ml of S1611) (Figure 29B).

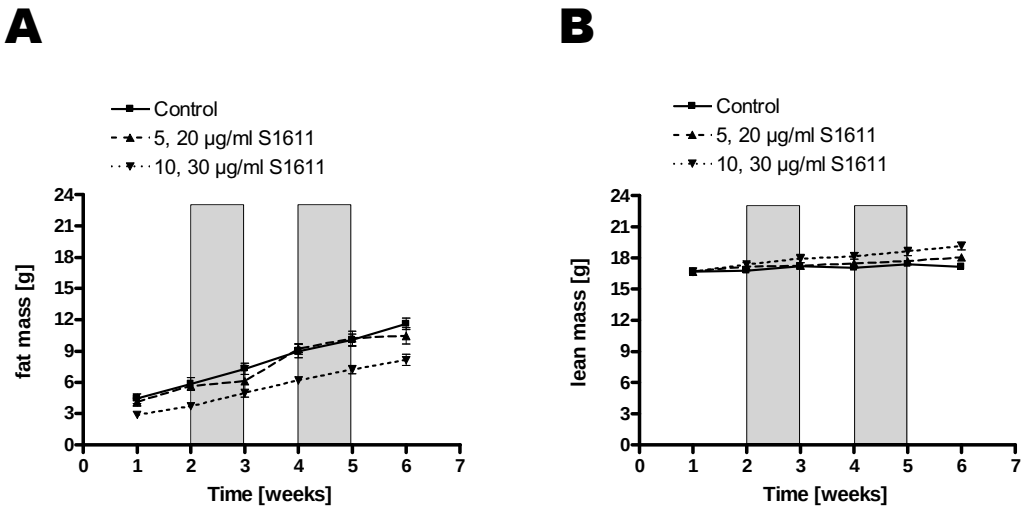

Figure 29: NMR analysis of fat and lean mass of WT mice (n=5) treated with S1611. During the whole study mice were fed the HFD. (A) Fat mass content and (B) Lean mass content remained unchanged during the total study between all groups. Grey bars in weeks 3-4 and 5-6 represent the weeks when mice received S1611in drinking water. In weeks 3-4, mice were administered either 5 or 10 µg/ml S1611 while in week 5-6 S1611 concentrations were 20 or 30 µg/ml. Data are expressed as mean ± SEM.

Discussion

1 Metabolic syndrome

In 1988, Reaven described the Syndrome X that was defined as hyperinsulinemia, hyperlipidemia and hypertension in non-diabetic individuals [110]. Today Syndrome X is known as the “metabolic syndrome” and seems to be associated with life style changes in the westernized countries: (i) increased mechanization of work that was formerly done by human physical activity, (ii) increasing automobile use, and (iii) increased accessibility of dense, high-caloric foods. Additionally, there is evidence that the development of insulin resistance and Type II diabetes is related to fat consumption [111]. Besides fat and carbohydrates, diets include proteins. Dietary proteins are first digested by several linguinal, gastric and pancreatic proteases and further degraded by peptidases in the intestinal brush-border membrane [112] resulting mainly in di- and tripeptides. These are then transported into enterocytes mainly by the intestinal low-affinity, high-capacity peptide transporter PEPT1 that is energized by an inwardly-driven proton gradient. This gradient is maintained by the sodium-proton exchanger 3 (NHE3). The role of PEPT1 *in vivo* was initially investigated using the nematode *Caenorhabditis elegans*. Deleting PEPT1 in the worm resulted in drastic changes, i.e. amino acid deficiency, a reduced growth and a reduction of progeny by 60 % [113], a 2-fold increased amount of body fat and also larger fat granules in intestinal cells when compared to wild-type worms [1]. Silencing the *nhx*-2 in worms (homologue of NHE3) by RNAi lead to a reduced fat content and smaller fat granules in wild-type and *pept-1(lg601)* worms. These results indicate (i) peptide absorption as a key process in body protein homeostasis and (ii) a link between PEPT1, NHE3 and the lipid metabolism. In the present study, it was determined whether or not the results from *C. elegans* hold true in mice.

2 The *Pept1*$^{-/-}$ mouse – phenotypes on standard chow and high-protein diet

Wild-type (*Pept1*$^{+/+}$) and knockout (*Pept1*$^{-/-}$) mice with a C57BL/6 genetic background showed no pathological phenotype when fed a standard diet. Hu and colleagues demonstrated *Pept1*$^{-/-}$ mice to grow to normal size, body and organ weight.

Furthermore, these mice showed no differences in serum clinical parameters, e.g. glucose, bilirubin, urea nitrogen, alkaline phosphatase, ALT, AST or albumin. Histological analyzes of major organs also excluded any genotype-related abnormalities [114].

When fed a 45 energy% high-protein diet (HPD), *Pept1*$^{-/-}$ mice showed a significantly reduced food intake during the first three days when compared to WT mice on the same diet. After four days, *Pept1*$^{-/-}$ mice recovered and had a similar food intake to WT mice on HPD until the end of the experiment. Going along with the reduced food intake, *Pept1*$^{-/-}$ mice lost weight during the first three days on the HPD. Regardless the recovery in food intake, *Pept1*$^{-/-}$ mice did not recover in body weight and stayed significantly leaner than WT mice [115] during the whole study. Analysis of the basal levels of 40 plasma amino acids and derivatives showed that 24 were increased in *Pept1*$^{-/-}$ mice compared to WT animals [116]. Also in urine, basal amino acid concentrations, osmolarity and creatinine levels displayed no differences between both genotypes. Liver analysis revealed no differences in enzyme activities (glutamate dehydrogenase, AST, ALT, arginase) and the sum of all amino acids. Only citrulline, phosphoethanolamine and ethanolamine were significantly increased but urea was decreased in *Pept1*$^{-/-}$ mice. Additionally, 60 min. after an oral protein load (178 mg protein), WT mice have significantly higher plasma level in a total of 15 amino acids, including the branched-chain amino acids valine and isoleucine, with the biggest changes in proline. In liver, concentrations were increased for a total of 12 amino acids with the most pronounced found for proline. But enzyme activities and urea concentrations showed no differences [116]. Regarding plasma hormone concentrations, *Pept1*$^{-/-}$ mice showed no GLP-1 secretion after an oral protein load while GIP and CCK concentrations were similar to WT mice (Laure Fourchaud, personal communication). PEPT1-deficiency goes along with amino acid imbalance showing amino acids directly or indirectly linked to the urea cycle being over-expressed. This may indicate an altered hepatic detoxification capacity. Based on these findings it can be said that under normal conditions PEPT1 contributes only marginally to amino acid homeostasis while its role increases under high-protein conditions.

3 C57BL/6 mice – an obesity prone model for diabetes and metabolic syndrome

It was already demonstrated that increasing the dietary fat content leads to obesity and diabetes in different strains of mice, including C57BL/6 [117, 118], and rats [119]. When fed a HFD *ad libitum*, BL6 mice develop obesity that is accompanied by several metabolic abnormalities, e.g. hyperglycemia, hyperinsulinemia, hypertension and hypertrophy [117]. All this parallels the abdominal obesity in humans which is an independent risk factor for the development of diabetes [111, 120]. Furthermore, obese humans suffering from the metabolic syndrome have hypertension and increased sympathetic nervous system activity [121]. This makes BL6 mice a very good model to study the human metabolic syndrome.

4 *Pept1*$^{-/-}$ mice are partially resistant to high-fat diet-induced obesity

4.1 *Pept1*$^{-/-}$ mice showed lower weight gain despite similar energy intake

In the present study, we challenged WT and *Pept1*$^{-/-}$ mice with a high-carbohydrate control diet (CD) or an isocaloric replaced 48 energy% high-fat diet (HFD) (fat source: palm oil) for 12 weeks. All mice grew to normal size and did not show altered body temperatures. Contrary to our findings, Bjursell and colleagues reported increased rectal core temperatures in mice fed a western diet with 40.3 energy% from fat. Body temperatures remained increased after 14 days but normalized after 21 days on the western diet [122]. Since we measured rectal body temperatures only after 12 weeks of feeding the specific diets, possible changes may be already normalized again.

The HFD fed mice had increased body weight, food intake, energy intake, and energy absorption. It is known that, satiety and food intake are correlated with gastrointestinal (GI) transit and gastric emptying. High-fat meals slow down gastric emptying from the stomach and are less satiating than isoenergic low-fat meals [123]. We did not see any difference of GI transit time between both genotypes, concluding that the knockout of the peptide transporter does not influence gastric emptying or transit of HFD. Human studies showed that a single HF meal delayed gastric emptying (GE) and increased hunger 7 h later [123]. While volunteers had shortened mouth-to-caecum transit time (MCTT) and GE, there were no differences in satiety

after a 3 days administration of a high-fat meal [124]. A long-time study over 4 weeks revealed that after 1 week of high-fat intervention (i) GE latency time and MCTT were decreased and (ii) hunger was increased. GE and MCTT showed no changes after 4 weeks whereas hunger remained increased [125]. This indicates that (i) mass and energy content of a meal regulate hunger/satiety, (ii) a single HF meal has a hyperphagic effect and (iii) a GI adaptation to HF diet occurs within 1 week but returns to pre-diet levels after longer periods.

4.2 Lower body weight are not due to changes in locomotor activity

Surprisingly, after four weeks on the specific diets, mice fed the HFD had lower energy expenditure (EE) and respiratory quotient (RQ) than mice on CD. But there were no significant differences in locomotor activity although HFD fed mice tend to show reduced activity during night phases. In former studies it was shown diet-induced obesity is not simply explained by an increased food intake. C57BL/6 mice on HFD develop severe obesity, hyperglycemia and hyperinsulinemia when compared to the obesity-resistant A/J strain. Although both mouse strains had the same caloric intake, BL6 mice exhibited a higher feed efficiency, i.e. gained more weight per calories consumed [126-128]. Additionally, Brownlow and colleagues compared the role of motor activity in diet-induced obesity in C57BL/6 and A/J mice. They showed that spontaneous motor activity was increased in C57BL/6 mice when compared to A/J animals [126]. Contrary to Brownlow, Bjursell and colleagues reported a diet-induced reduction in locomotor activity for male C57BL/6 mice 3-5 hours after changing the standard chow to a western diet. When correlating EE and locomotor activity, they could explain ~ 62 % of the weight gain being due to reduced locomotor activity.

Body composition analysis via nuclear magnetic resonance (NMR) revealed WT and *Pept1*$^{-/-}$ mice on HFD having bigger fat depots (epidiymal, perirenal, inguinal, mesenteric and brown adipose tissue) compared to mice on CD. We observed genotype-specific differences in visceral fat depots (perirenal, mesenteric and epididymal fat): (i) *Pept1*$^{-/-}$ mice on CD had smaller amount of epididymal fat compared to WT mice on CD and (ii) *Pept1*$^{-/-}$ animals on HFD had significantly smaller fad pads of perirenal/retroperitoneal and epididymal adipose tissue than WT mice on HFD. Mice fed the CD had smaller adipocytes compared to mice on HFD.

This indicates a role of PEPT1 in the uptake and storage of fatty acids. Supporting our data, Rebuffe-Scrive and colleagues demonstrated that C57BL/6 and A/J mice on HFD have more subcutaneous (inguinal) and visceral (mesenteric) fat compared to mice on a CD. The selective accumulation of mesenteric adipose tissue was shown to be characteristic for diet-induced diabetes and obesity in BL6 mice. Additionally, these mice have enlarged fat cells and higher lipoprotein lipase activities [129]. Some years later, Funkat and colleagues showed C57BL/6, DBA/2 and 129T2 mice on a 60 % HFD have larger epididiymal, subcutaneous and retroperitoneal fat pads than mice of the same strain on a CD [130], supporting our findings.

4.3 WT and *Pept1*$^{-/-}$ mice on HFD – suffering from NAFLD?

We saw enlarged adipocytes within the epididymal fat depots of HFD fed animals while there were no obvious alterations in animals on CD. Within the HFD group, adipocytes of WT mice were significantly increased when compared to *Pept1*$^{-/-}$ animals. It is well known that during obesity adipocytes enlarge and undergo alterations that affect the systemic metabolism, e.g. fasting whole-body free fatty acids (FFA) and glycerol release were shown to be increased in obese women compared to lean women [131-133].

High levels of circulating FFAs may result from (i) increased adipose tissue mass and lipolysis in adipocytes [134], (ii) dietary sources and (iii) *de novo* lipogenesis (DNL) [135]. In obese subjects and individuals with type 2 diabetes (T2D) it was observed that plasma non-esterified free fatty acid (NEFA) concentrations increase in response to a lowered capacity of NEFA uptake of the skeletal muscle [134]. FFAs can either undergo β-oxidation or re-estrification to triglycerides. In this form they are transported in very-low density lipoproteins (VLDL) from adipose tissue to the liver. In the latter case, increased amounts of PLs are needed for package of FFAs and other components. An increased fat synthesis and fat delivery in combination with a decreased fat export and fat oxidation leads to esterification of FFAs and glycerol and hepatic TG accumulation [135] – a characteristic for non-alcoholic fatty liver disease (NAFLD). In patients suffering from NAFLD, it was shown that approx. 60 % of liver TGs result from FFA influx from adipocytes, 26 % from DNL and 15 % are from ingested diets [136]. Contrary to this, in healthy individuals only < 5 % of hepatic TGs derive from DNL [137, 138]. In our study, livers of WT mice on HFD were drastically

increased in size and weight and showed the morphology of a fatty liver. Contrary to these mice, *Pept1*$^{-/-}$ animals on HFD showed a normal liver size and morphology. NAFLD and non-alcoholic steatohepatitis (NASH) is seen as the hepatic manifestation of the metabolic syndrome. Furthermore, it seems to be strongly associated with visceral obesity [139]. Thomas and colleagues used proton magnetic resonance spectroscopy (MRS) and whole body magnetic resonance imaging (MRI) to investigate the interplay between intrahepatocellular lipids (IHCL) and body fat content and distribution. They showed that IHCL was increased in subjects with hepatic steatosis or overweight individuals – suggesting a relationship between hepatic steatosis and central adiposity [140]. Some years later, Park and colleagues demonstrated that NAFLD is closely associated with increased "waist circumference, fat mass, percentage of body fat and abdominal fat" [141]. Additionally, they found that obese subjects with insulin resistance (IR) and central obesity are more prone to NAFLD than individuals with less IR and central adiposity.

WT mice on HFD had highly increased plasma insulin, leptin, ALT and AST level. Elevated plasma glucose and insulin concentrations may indicate for an insulin resistance (IR). Insulin may suppress adipose tissue lipolysis. In the state of IR, e.g. NAFLD, its suppressing action is altered. That leads to an increased efflux of FFAs from adipose tissue [142] and inhibition of β-oxidation of FFAs and by this further increasing hepatic lipid accumulation [135]. Furthermore, several studies showed higher leptin levels in obese patients (usually regarded as leptin resistant) and individuals suffering from NAFLD. Huang and colleagues determined the connection of the leptin system and NAFLD. They reported increased body-mass-index (BMI) and serum leptin level in patients with NAFLD (men and women) compared to controls. Additionally, they saw that the percentage of hepatocyte steatosis correlates to serum leptin levels, i.e. leptin concentrations seem to increase as steatosis develops. These results suggest that NAFLD patients show higher resistance to the action of leptin compared to healthy individuals [143]. Leptin is a small adipocyte-derived hormone (~ 16 kDa). It is involved in the control of energy intake and expenditure [144], the regulation of the immune system [145, 146], but also in the promotion of inflammation and fibrosis [146, 147]. Therefore it is possible that leptin contributes to NAFLD pathogenesis.

Besides that, Doi and colleagues investigated the correlation of liver enzymes and diabetes. During a 9-years follow-up study with 1804 healthy volunteers, 135 subjects developed diabetes. This went along with increased serum levels of γ-glutamyl transferase (GGT), ALT, and AST (only in men – not in women) [148]. ALT and AST are mainly located in liver tissue. Therefore, these enzymes function as indicators for liver inflammation since their concentrations increase during hepatocyte damage. Regarding all these increased parameters it seems most likely that WT mice on HFD suffered from NAFLD while *Pept1*$^{-/-}$ mice on HFD did not. ALT and AST are important enzymes in amino acid metabolism. We demonstrated before that *Pept1*$^{-/-}$ mice have an altered handling of amino acids. Only after a high-protein load most plasma amino acid concentrations were increased in *Pept1*$^{-/-}$ animals. Therefore PEPT1 seems to provide an additional transport mechanism for amino acids when other amino acid transporters are already saturated. These increased amino acid concentrations are most likely due to alterations in the hepatic amino acid metabolism since renal excretion is unchanged [116].

4.4 Adaptation to HFD leads to morphological changes in the small intestine

Our measurements revealed that *Pept1*$^{-/-}$ mice fed a HFD have shorter villi in the small intestine than WT mice on the same diet. This corresponds to an observation in mice lacking the transcriptional co-regulator tetradecanoyl phorbol acetate induced sequence 7 (Tis7). Yu and colleagues fed WT and *Tis7*$^{-/-}$ mice a 42 energy% HFD for 8 weeks. They demonstrated *Tis7*$^{-/-}$ mice having lower villus heights compared to their WT counterpart. Tis7-deficient animals also showed a reduced weight gain and lower hepatic TG and cholesterol concentrations than WT mice. Additionally, Tis7 over-expressing mice showed a higher weight gain and higher TG absorption on a HFD suggesting Tis7 being a regulator of lipid absorption and metabolism [149]. Already Thomson and colleagues demonstrated that rabbits fed a HFD have reduced jejunal villus height and surface area and mucosal surface area indicating the importance of dietary fat on villus morphology [150]. Furthermore it was shown that female Wistar rats fed a high saturated fatty acid diet had decreased ileal villus height, width, thickness, surface area, cell size, villus density and mucosal surface area when compared to animals on a high poly-unsaturated fatty acid diet. While ileal leucine uptake was increased, these rats showed reduced jejunal glucose transport

[151]. Contrary to this, Li et al. demonstrated an intestinal adaptation, i. e. increased villus height with long round villi, in pigs that received a HFD of soybean oil (high percentage of long-chain unsaturated fatty acids) and coconut oil (high percentage of short-chain saturated fatty acids) for 5 weeks [152]. Also Goda and colleagues reported an adaptation of rats to the HFD resulting in increased jejunal villus height, mucosal weight and total protein amount while length of microvilli was decreased [153]. It was shown that an adaptation occurs to high fat feeding for 4 weeks on a 20 % or 45 % HFD, respectively. Besides an increased villus height resulting from stimulated cell proliferation the uptake of oleic acid was elevated upon receipt of a HFD [154-156]. Additionally, dry weight of mucosa is increased in the proximal part of the ileum thus meaning that mucosa responds to HFD by hypertrophy. Taken together, hypertrophy and an enhanced fat digestion could influence the gastrointestinal function and energy intake due to the decreased length of small intestine exposed to dietary fat. Even rats suffering from short bowel syndrome (SBS) that were fed a 50 % HFD for 2 weeks had: (i) increased duodenal and jejunal bowel and mucosa weights and (ii) increased ileal villus height and jejunal crypt depths when compared to SBS-rats on normal chow (10 % fat) [157].

Going along with morphological changes in the gut also functional changes were observed in animals fed a HFD. It was shown that pancreatic lipase adapts to dietary alterations by changes in synthesis, e.g. pancreatic lipase was maximally stimulated in rats that received a 67 % HFD [158]. In our study, we neither did observe any changes in pancreatic lipase activity in plasma with respect to WT and *Pept1*$^{-/-}$ mice (regardless the diet). Nor did we see any alterations when comparing the diets (regardless the genotype). It was also reported that higher fat concentrations in the diet lead to increased secretion of fat-digesting enzymes in the pancreatic juice. Spannagel et al. measured increased release of cholecystokinin (CCK) in rats on a 20 % HFD and an overall increased secretory response when compared to the control group [159]. In an earlier study in our group Laure Fourchaud assessed the question whether PEPT1 contributes to postprandial gastrointestinal hormone secretion by giving these mice a high protein load via an oral gavage. While she did not see any genotype-specific differences in the secretion of CCK and GIP, no GLP-1 secretion was detectable for *Pept1*$^{-/-}$ mice (for further information see PhD thesis of Laure Fourchaud). In this study we could detect a decreased activity of pancreatic amylase in *Pept1*$^{-/-}$ mice regardless the diet. Summarizing, *Pept1*$^{-/-}$ mice have the

same secretion pattern of CCK, GIP and pancreatic lipase as WT mice – but these mice show reduced pancreatic amylase activity and almost no GLP-1 secretion when compared to WT animals. These results suggest a partially altered pancreatic activity in PEPT1-deficient mice.

4.5 Amino acids and impaired bile acid secretion - leading to maldigestion or malabsorption?

Already in the 1960s and 1970s it has been reported that in state of obesity specific amino acids, i.e. valine, leucine, isoleucine, phenylalanine and tyrosine, show elevated plasma concentrations. Proportional with elevated amino acid levels an increase in insulin was observed suggesting IR in obese subjects (for review see [160]). Especially branched-chain amino acids (BCAAs), i.e. leucine, isoleucine and valine, are associated with a lower prevalence of developing obesity [161]. During our study, we observed changes in some plasma amino acids: taurine, tryptophane, phenylalanine, lysine, arginine and proline. Taurine levels were increased during our study in WT mice on HFD that were suffering from fatty liver. The three other groups had comparable lowered taurine plasma concentrations. Additionally, tryptophane and phenylalanine were increased in WT animals on both diets when compared to *Pept1*$^{-/-}$ mice on the same diets. But BCAA concentrations remained unchanged. Besides proteins, the free amino acids tryptophane and phenylalanine have a high impact on enzyme secretion by the pancreas. As both amino acids are reduced in *Pept1*$^{-/-}$ mice, these animals seem to have a reduced pancreatic enzyme secretion. Taurine (2-aminoethanesulphonicacid) is a sulfonic acid that is present in diet (especially seafood and meat), and which can also be synthesized from cysteine and methionine in postnatal life. Taurine plays a role in the lipid metabolism where it is needed for bile acid synthesis. Secreted bile acids enhance cholesterol degradation. Studies in hamsters fed a HFD have shown that taurine seems to have plasma lipid-lowering effects. On the one hand, supplementation with taurine increased the activity of cholesterol 7-α hydroxylase (CYP7A1) resulting in enhanced bile acid synthesis and cholesterol degradation. On the other hand, it inhibited elevation of hepatic acyl-CoA:cholesterol acyltransferase and by this storage of cholesterol [162]. In addition, taurine seems to improve insulin sensitivity in Otsuka Long-Evans Tokushima Fatty (OLETF) rats. These animals are a model for T2D and IR. OLETF

rat on non-purified standard chow show hyperglycemia, IR, increased abdominal fat accumulation and elevated serum and liver TG and cholesterol levels when compared with controls. In contrast, taurine-treated OLETF animals have a significant decrease in all parameters when compared to non-treated OLETF rats. Additionally, taurine-supplemented rats have an elevated nitric oxide production and urinary nitrite excretion – suggesting an improved lipid metabolism by enhanced cholesterol excretion and decreased cholesterol production [163]. A recent study reported that taurine supplementation counteracts liver damage in NZB/W F1 mice fed with a high-cholesterol diet [164]. Huang et al. investigated the effects of taurine on development of hepatic steatosis in hamsters fed a high-fat/cholesterol diet. Supplementing taurine in drinking water resulted in (i) smaller liver size, (ii) decreased hepatic lipids, (iii) up-regulation of the LDL-receptor and CYP7A1 gene expression that leads to elevated fecal cholesterol and bile acid output, (iv) up-regulation of peroxisome proliferator-activated receptor-α (PPAR-α) and uncoupling protein 2 (UCP2) gene expression and by this led to an increased energy excretion, (v) enhanced liver antioxidant capacities and (vi) decreased lipid peroxidation [165].

While it was shown that bile acids could contribute to maintain lipid, glucose and energy homeostasis, the role of CYP7A1 in obesity and diabetes remains unclear. Li and colleagues demonstrated that transgenic mice over expressing CYP7A1 are resistant to high-fat diet-induced obesity and show increased hepatic cholesterol catabolism and bile acid pool [166]. Several studies showed hypercholesterolemia being related to an up-regulation of bile acid synthesis and fecal bile acid excretion [167-169]. Therefore, bile acid homeostasis seems to be important for maintaining lipid, glucose and energy homeostasis.

4.6 The *Pept1*$^{-/-}$ mouse – increased energy excretion due to changes in microbiota?

Different bacterial strains, > 99.9 % of them anaerobes [170], make up the gut microbiota and are essential for converting ingested food into energy [171]. Berg and colleagues demonstrated that microbiota occupy all available niches in healthy humans [172]. The current view is that the human gut flora is composed of 500 – 1,000 different species with a biomass of ≈ 1.5 kg [173]. Shaping of the intestinal microorganisms begins already at birth [174]. Šefčiková and colleagues exposed

Sprague-Dawley rats suckling pups to a high-fat diet. Interestingly, rat mothers with a small litter (SL, n=4) had a higher milk fat concentrations than mothers with normal litter (NL) size (n=10). In the post weaning period, both litter groups received a standard diet. Still SL pups showed faster growth that was accompanied by a higher body weight and bigger epididymal and perirenal fat pads. This went along with a change in the composition and function of intestinal microbiota in jejunum and colon: SL pups had higher numbers of *Lactobacillus/Enterococcus* but lowered amount of *Bacteroides/Prevotella* when compared to the NL controls [175]. It is known that the composition of the gut microbiota is influenced by several factors, e.g. the host development [174, 176, 177], host genotype [178], and the environment [179]. Additionally, it was demonstrated that obesity alters composition and function of the gut flora in humans and mice [171, 180]. An increased energy yield from ingested food resulting from an increased efficiency of bacterial fermentation and increased extraction of energy from dietary fiber may lead to excessive weight gain [181]. Bäckhed et al. showed germ-free (GF) mice being resistant to diet-induced obesity (DIO) while mice with a gut flora are not. Since *Pept1*$^{-/-}$ mice on HFD showed a reduced weight gain compared to WT animals on HFD this might indicate an altered/reduced composition of gut microbiota. Furthermore they observed that GF mice lacking the fasting-induced adipose factor (Fiaf) are no longer protected from DIO. Expression of this circulating lipoprotein lipase inhibitor is normally selectively suppressed by microorganisms in the gut epithelium. The lean GF mice had increased levels of phosphorylated AMP-activated protein kinase (AMPK) and its targets involved in fatty acid oxidation. Moreover, Fiaf was shown to induce peroxisomal proliferator-activated receptor co-activator (Pgc-1alpha) [182]. Therefore intestinal bacteria play a crucial role in energy intake and body weight regulation. Thus, they might be involved in the development of obesity and diabetes that are characterized by insulin resistance, enhanced intestinal permeability, and a low-grade inflammation. In an earlier study performed in our animal facility, we measured higher crude protein and crude fat excretion in the feces of *Pept1*$^{-/-}$ mice on HFD (data not shown) compared to WT animals on the same diet indicating a change in microbial composition. GC-MS analysis of caecal content revealed that *Pept1*$^{-/-}$ mice on HFD have a higher amount of free fatty acids compared to WT animals on HFD. Comparable results were observed in mice with inhibited Hedgehog (Hh) signaling. Since a knockout of Sonic-Hh and Indian-Hh is lethal, Buhman and colleagues

inhibited this signaling cascade by administration of an anti-Hh monoclonal antibody (moAb) to Balb/c mice. Although these mice had a normal lipid absorption on a 21 energy% HFD, they had a lower TG absorption and an increased fecal excretion of FFA compared to mice treated with a control moAb [183]. This may indicate a role of Hh signaling in diet-induced alterations of lipid metabolism.

5 Lipid accumulation due to impaired NHE3 activity?

Besides being an energy source for the body, unesterified fatty acids are key intermediates in lipid metabolism. They function as second messengers in signal transduction [184] and modulate ion channel activities [185, 186]. Fatty acid uptake into cells is generally mediated by fatty acid binding proteins (FABP) and fatty acid transport proteins (FATP) [187, 188]. Apart from these transport mechanisms, unesterified free fatty acids are capable of crossing cell membranes by the flip-flop mechanism [108] in a protonated form. As shown in various cell types, this transport consequently leads to an intracellular acidification. Hamilton and colleagues demonstrated that addition of FA to the pancreatic β-cell line HIT (subclone T-15) leads to a decrease in intracellular pH that can be reversed by adding albumin [189]. Also primary rat hepatocytes showed increased FA uptake by 45 % during cellular alkalosis and a decrease in FA influx by 30 % in cellular acidosis [190]. Civelek and colleagues exposed primary adipocytes (from epididymal fat pads) to external FA leading to intracellular acidification which could be reversed by addition of albumin [191]. As long as intracellular pH is more alkaline than the pH outside FA uptake via the flip-flop mechanism is increased. Since PEPT1 co-transports di- and tripeptides with protons into the cell, this causes a decrease in intracellular pH. To maintain the proton gradient over the cell membrane, protons are re-exported by the sodium-proton exchanger NHE3. If the di- and tripeptide transporter PEPT1 is absent proton influx is lowered and intracellular pH is increased. Consequently, this promotes fatty acid flip-flop over the cell membrane and enables higher FA uptake. Spanier and colleagues demonstrated a highly increased uptake of the fluorescent-labeled C12 fatty acid (BODYPI-C12) fatty acid in *pept1(lg601)* worms (worms lacking PEPT1). Similar results were observed in wild-type worms treated with the PEPT1 antagonist Lys-[z-NO_2]-Val [1]. Since there is a functional coupling of PEPT1 and NHX-2

(homologue to NHE3) in regulation of the intracellular pH [109], inhibition of NHE3 causes a decrease in FA import.

Amiloride is a potassium-sparing diuretic (Figure 30) blocking sodium channels, e.g epithelial sodium channel (ENaC) or NHEs. It is used for treatment of hypertension and cognitive heart failure. Amiloride acts by inhibiting the renal reabsorption of sodium ions in the late distal convoluted tubules, connecting tubules, and collecting ducts in the kidneys [192]. By this it promotes excretion of water and sodium but preventing loss of potassium.

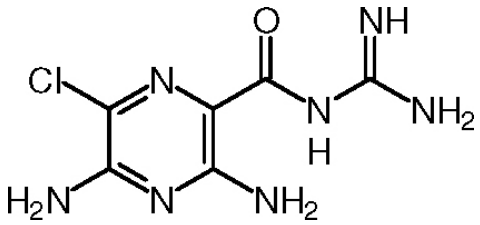

Figure 30: Structure of amiloride.

(http://content.answcdn.com/main/content/img/oxford/oxfordBiochemistry/0198529171.amiloride.1.jpg)

We observed significant weight loss of WT mice treated with 30 µg/ml amiloride in drinking water. This was mainly due to a loss in fat mass. Although unspecific, amiloride was described to inhibit human NHE3 in the fibroblast L cell line (LAP1) with an IC_{50} value of 283 µmol/l [105]. This leads to a surplus of protons outside of the cell and lowering of intracellular pH. Elsing and colleagues showed a decreased FA uptake during cellular acidification that could be reduced by further 57 % when NHE3 was inhibited by amiloride [190]. Since amiloride is not a specific NHE3 inhibitor we used the specific inhibitor S1611 to investigate whether our observations are due to reduced activity of NHE3. But we did not see alterations in weight or fat mass content like during amiloride treatment. Contrary to this, studies in the human intestinal cell line Caco-2 revealed that selective NHE3 inhibition via S1611 (Figure 31A) reduced transepithelial dipeptide uptake suggesting a role in maintenance of pH homeostasis [107]. Our group demonstrated that inhibition of NHX-2 in WT worms via RNAi, or by the specific inhibitor S3226 (Figure 31B) in the worm leads to a reduced FA import into the cells. Like *C. elegans* lacking nhx-2, S3226-treated WT animals also showed a lean phenotype. Additionally, this effect was observed in pept-1 deficient worms that. These animals have increased fat content and also increased

fat granule size. But after inhibition of nhx-2 via RNAi fat content and fat granule size were significantly reduced [1].

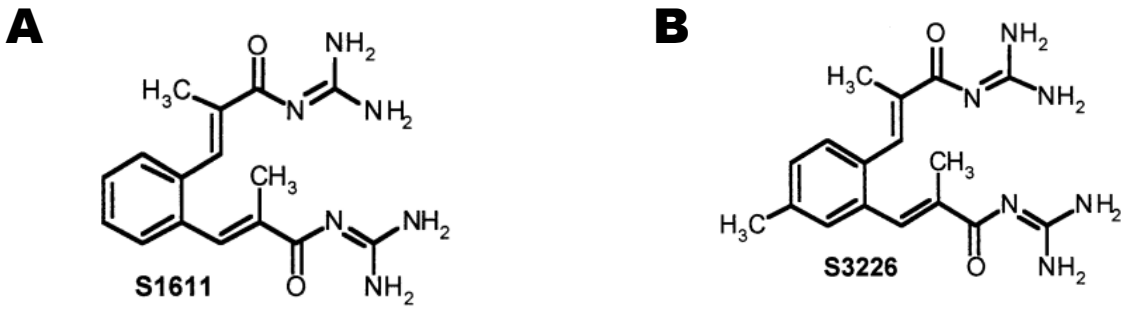

Figure 31: Structures of specific NHE3 inhibitors. (A) S1611 and (B) S3226 (from [105]).

Spanier and colleagues proposed mechanisms underlying fatty acid transport in WT, *pept-1(lg601)* and *nhx-2* RNAi treated *C. elegans*: (i) in WT worms PEPT-1-driven proton influx is neutralized by NHX-2 and FA flip-flop occurs at a low rate, (ii) in pept-1 deficient worms proton influx is reduced leading to an increased intracellular pH and enhanced FA flip-flop. Increased FA uptake results in enlarged lipid granules. (iii) reduced expression of nhx-2 leads to intracellular acidification by pept-1-mediated peptide/proton co-transport. This leads to an reduction in FA uptake finally resulting in smaller fat granules an a lean phenotype [1]. The findings, however, support the notion that PEPT1 and the transmembrane proton gradient essentially affect intestinal uptake of both peptides and fatty acids and moreover, that the fat absorption might be influenced by PEPT1.

Conclusion

Previous studies from our group demonstrated changes in food consumption and partially altered hormones in case of high-protein treatment of WT and *Pept1*$^{-/-}$ mice. Dietary fat was shown to influence food and energy intake, intestinal transit, gastric emptying, the release of gastrointestinal hormones like CCK, GLP-1, PYY and ghrelin, as well as gut morphology and function. Here we wanted to investigate whether and how the intestinal di- and tripeptide transporter PEPT1 affects the lipid metabolism. Studies show a morphological adaptation of the small intestine to an increased amount of dietary fat resulting in increased ileal and jejunal villus height and crypt depths indicating a stimulated cell proliferation. It is known from literature that adipocyte-derived leptin induces IL-6 production and the ensuing IL-6 receptor signaling. In cell culture experiments IL-6 treatment was associated with activation of STAT3, ERK, p38, MEK and JAK2 leading to nuclear translocation of STAT3 – all of these being early events of cell proliferation. We saw elevated leptin and IL-6 (earlier study, data not shown) concentrations in WT mice on HFD. These mice also had increased villus height. Contrary to this, *Pept1*$^{-/-}$ mice on HFD have lowered leptin and IL-6 concentrations. Also villi height in the small intestine is decreased suggesting an impaired adaptation to high-fat feeding. As PEPT1 mediates uptake of di- and tripeptides it is no wonder that concentrations for some plasma amino acids are changed. Among these amino acids taurine was shown to be reduced in *Pept1*$^{-/-}$ mice. Taurine plays a role in lipid metabolism since it is needed for synthesis of bile acids that mediate cholesterol degradation. Furthermore secretion of pancreatic amylase and the gastrointestinal hormone GLP-1 was shown to be altered in *Pept1*$^{-/-}$ mice.

Taken together, *Pept1*$^{-/-}$ mice seem to have a maldigestion resulting from impaired secretion of pancreatic enzymes and bile acids. This may lead to the observed malabsorption of dietary fat and in the end result in a non-obese phenotype.

Appendix

Composition of control and high-fat diet Ssniff, Soest, Germany.

Diet name		Control	48 % High-fat
Product number		**S5745-E720**	**S5745-E722**
Casein	%	24.00	24.00
Maisstärke, pre-gelat.	%	47.79	27.79
Maltodextrin	%	5.60	5.60
Saccharose	%	5.00	5.00
Cellulose	%	5.00	5.00
L-Cystine	%	0.20	0.20
Vitamins	%	1.20	1.20
Trace elements	%	6.00	6.00
Choline-Chloride	%	0.20	0.20
Butylhydroxtoluol	%	0.01	0.01
Soy oil	%	5.00	5.00
Palm oil	%		20.00
Crude protein	%	21.30	21.30
Crude fat	%	5.10	25.10
Crude fibre	%	5.00	5.00
Crude ashes	%	5.30	5.30
Starch	%	46.70	27.20
Sugar	%	6.10	6.10
Nitrogen free extracts	%	58.80	39.10
ME (Atwater)	MJ/kg	15.50	19.80
Protein	kJ%	23.00	18.00
Fat	kJ%	13.00	48.00
Carbohydrates	kJ%	64.00	34.00
Fatty acids			
C12:0	%	0.01	0.01
C14:0	%	0.03	0.22
C16:0	%	0.56	8.88
C18:0	%	0.24	1.19
C20:0	%	0.03	0.13
C16:1	%	0.03	0.13
C18:1	%	1.33	8.75
C18:2 n6	%	2.65	4.67
C18:3 n3	%	0.33	0.43

Abbreviations

aa	amino acids
ALT	alanine aminotransferase
AMP	adenosine monophosphate
AMPK	AMP-activated protein kinase
AST	aspartate aminotransferase
BMI	body-mass index
bps	base pairs
BUN	blood urea nitrogen
Ca^{2+}	calcium ions
°C	degree Celsius
CCK	cholecystokinine
CD	control diet
CYP7A1	cholesterol 7-α hydroxylase
DIO	diet-induced obesity
dL	deci liter
DNA	desoxyribonucleic acid
DNL	*de novo* liposynthesis
EE	energy expenditure
e. g.	for example (lat. exempli gratia)
FABP	fatty acid binding protein
Fe^{3+}	iron ions
Fiaf	fasting-induced adipose factor
FT-IR	Fourier-transform infrared spectroscopy
g	gram
GE	gastric emptying

GF	germ-free
GGT	gamma-glutamyltransferase
GI	gastrointestinal
GIP	gastric inhibitory peptide
GLP-1	glucagon-like peptide 1
GLP-2	glucagon-like peptide 2
Gly-Gln	glycyl-glutamine
Gly-Phe	glycyl-phenylalanine
Gly-Sar	glycyl-sarcosine
h	hour (s)
HDL	high density lipoprotein
HFD	high-fat diet
HPD	high-protein diet
IC_{50}	half maximal inhibitory concentration
IFN-γ	Interferon gamma
IHCL	intrahepatocellular lipids
IR	insulin resistance
KCl	potassium chloride
kJ	kilo Joule
K_m	Michaelis-Menten-constant
KO	knockout
KOH	potassium hydroxide
L	liter
LCFA	long chain fatty acid
LDL	low density lipoprotein
LPS	lipopolysaccharide(s)
MCTT	mouth-to-caecum transit time
mg	milli gram
Mg^{2+}	magnesium ions

$MgSO_4$	magnesium sulphate
min	minute (s)
µl	micro liter
µm	micro meter
µM	micro molar
ml	milli liter
mm	milli meter
mM	milli molar
MRI	magnetic resonance imaging
mRNA	messenger ribonucleic acid
MRS	magnetic resonance spectroscopy
MUFA	mono-unsaturated fatty acid
Na^+	sodium ions
NaCl	sodium chloride
NAFLD	non-alcoholic fatty liver disease
NASH	non-alcoholic steatohepatitis
NEFA	non-esterified fatty acid
NHE3	mammalian sodium-proton exchanger 3
nhx-2	sodium-proton exchanger 3 in *C. elegans*
NL	normal litter
nm	nano meter
NMR	nuclear magnetic resonance
o/n	over night
PBS	phosphate-buffered saline
PCR	polymerase-chain reaction
PEPT1	peptide transporter 1
Pgc-1α	peroxisomal proliferator-activated receptor 1 alpha
PKC	protein kinase C
PL	phospholipids
POT	proton-coupled oligopeptide transporter superfamily
PPAR-α	peroxisome proliferator-activated receptor-α

PTR	peptide transporter family
PUFA	poly-unsaturated fatty acids
RNA	ribonucleic acid
rpm	revolutions per minute
RQ	respiratory quotient
RT	room temperature
SBS	short-bowel syndrome
sec	second (s)
SEM	standard error of the mean
SFA	saturated fatty acids
SL	small litter
SLC	solute carrier
SNP	single nucleotide polymorphism
sOB-R	soluble leptin receptor
TG	triglyceride (s)
TMD	transmembrane domain
TNF-α	tumor necrosis factor alpha
U	units
UCP2	uncoupling protein 2
V_{max}	maximal velocity
VLDL	very low density lipoprotein
WT	wild-type

Amino Acids:

Aad	3-aminoadipic acid	**Leu**	Leucine
Abu	2-aminobutyric acid	**Lys**	Lysine
Ala	Alanine	**Met**	Methionine
bAla	Beta-Alanine	**Orn**	Orithine
Arg	Arginine	**PEtN**	Phospho-Ethanolamine
Asn	Asparagine	**Phe**	Phenylalanine
Asp	Aspartate	**Pro**	Proline
Cit	Citrulline	**Ser**	Serine
Gln	Glutamine	**Tau**	Taurine
Glu	Glutamate	**Thr**	Threonine
Gly	Glycine	**Trp**	Tryptophane
His	Histidine	**Tyr**	Tyrosine
Hyp	Hydroxyproline	**Val**	Valine
Ile	Isoleucine		

References

1. **Spanier, B., et al., *How the intestinal peptide transporter PEPT-1 contributes to an obesity phenotype in Caenorhabditits elegans.* PLoS One, 2009. 4(7): p. e6279.**
2. **McConnell, E.L., A.W. Basit, and S. Murdan, *Measurements of rat and mouse gastrointestinal pH, fluid and lymphoid tissue, and implications for in-vivo experiments.* J Pharm Pharmacol, 2008. 60(1): p. 63-70.**
3. **Asahara, T., et al., *Increased resistance of mice to Salmonella enterica serovar Typhimurium infection by synbiotic administration of Bifidobacteria and transgalactosylated oligosaccharides.* J Appl Microbiol, 2001. 91(6): p. 985-96.**
4. **Smith, H.W., *Observations on the Flora of the Alimentary Tract of Animals and Factors Affecting Its Composition.* J Pathol Bacteriol, 1965. 89: p. 95-122.**
5. **Casteleyn, C., et al., *Surface area assessment of the murine intestinal tract as a prerequisite for oral dose translation from mouse to man.* Lab Anim, 2010. 44(3): p. 176-83.**
6. **Thews G., M.E., Vaupel P., ed. *Anatomie, Physiologie, Pathophysiologie des Menschen*. 1999, Wissenschaftliche Verlagsgesellschaft mbH Stuttgart: Stuttgart.**
7. **Daniel, H., C. Fett, and A. Kratz, *Demonstration and modification of intervillous pH profiles in rat small intestine in vitro.* Am J Physiol, 1989. 257(4 Pt 1): p. G489-95.**
8. **Lucas, M., *Determination of acid surface pH in vivo in rat proximal jejunum.* Gut, 1983. 24(8): p. 734-9.**
9. **McKay, D.M. and A.W. Baird, *Cytokine regulation of epithelial permeability and ion transport.* Gut, 1999. 44(2): p. 283-9.**
10. **Simon-Assmann, P., et al., *In vitro models of intestinal epithelial cell differentiation.* Cell Biol Toxicol, 2007. 23(4): p. 241-56.**
11. **Wright, N.A., *Epithelial stem cell repertoire in the gut: clues to the origin of cell lineages, proliferative units and cancer.* Int J Exp Pathol, 2000. 81(2): p. 117-43.**
12. **van Den Brink, G.R., P. de Santa Barbara, and D.J. Roberts, *Development. Epithelial cell differentiation--a Mather of choice.* Science, 2001. 294(5549): p. 2115-6.**
13. **Porter, E.M., et al., *The multifaceted Paneth cell.* Cell Mol Life Sci, 2002. 59(1): p. 156-70.**
14. **Keshav, S., *Paneth cells: leukocyte-like mediators of innate immunity in the intestine.* J Leukoc Biol, 2006. 80(3): p. 500-8.**
15. **Ouellette, A.J., *IV. Paneth cell antimicrobial peptides and the biology of the mucosal barrier.* Am J Physiol, 1999. 277(2 Pt 1): p. G257-61.**
16. **Freeman, T.C., *Parallel patterns of cell-specific gene expression during enterocyte differentiation and maturation in the small intestine of the rabbit.* Differentiation, 1995. 59(3): p. 179-92.**
17. **Stenling, R. and H.F. Helander, *Stereological studies on the small intestinal epithelium of the rat. 1. The absorptive cells of the normal duodenum and jejunum.* Cell Tissue Res, 1981. 217(1): p. 11-21.**
18. **Steiner, H.Y., F. Naider, and J.M. Becker, *The PTR family: a new group of peptide transporters.* Mol Microbiol, 1995. 16(5): p. 825-34.**
19. **Hediger, M.A., et al., *The ABCs of solute carriers: physiological, pathological and therapeutic implications of human membrane transport proteinsIntroduction.* Pflugers Arch, 2004. 447(5): p. 465-8.**
20. **Daniel, H. and G. Kottra, *The proton oligopeptide cotransporter family SLC15 in physiology and pharmacology.* Pflugers Arch, 2004. 447(5): p. 610-8.**
21. **Boll, M., et al., *Expression cloning of a cDNA from rabbit small intestine related to proton-coupled transport of peptides, beta-lactam antibiotics and ACE-inhibitors.* Pflugers Arch, 1994. 429(1): p. 146-9.**

22. **Fei, Y.J., et al., *Expression cloning of a mammalian proton-coupled oligopeptide transporter.* Nature, 1994. 368(6471): p. 563-6.**
23. **Ogihara, H., et al., *Immuno-localization of H+/peptide cotransporter in rat digestive tract.* Biochem Biophys Res Commun, 1996. 220(3): p. 848-52.**
24. **Terada, T., et al., *Expression profiles of various transporters for oligopeptides, amino acids and organic ions along the human digestive tract.* Biochem Pharmacol, 2005. 70(12): p. 1756-63.**
25. **Ford, D., A. Howard, and B.H. Hirst, *Expression of the peptide transporter hPepT1 in human colon: a potential route for colonic protein nitrogen and drug absorption.* Histochem Cell Biol, 2003. 119(1): p. 37-43.**
26. **Merlin, D., et al., *Colonic epithelial hPepT1 expression occurs in inflammatory bowel disease: transport of bacterial peptides influences expression of MHC class 1 molecules.* Gastroenterology, 2001. 120(7): p. 1666-79.**
27. **Ziegler, T.R., et al., *Distribution of the H+/peptide transporter PepT1 in human intestine: up-regulated expression in the colonic mucosa of patients with short-bowel syndrome.* Am J Clin Nutr, 2002. 75(5): p. 922-30.**
28. **Shen, H., et al., *Localization of PEPT1 and PEPT2 proton-coupled oligopeptide transporter mRNA and protein in rat kidney.* Am J Physiol, 1999. 276(5 Pt 2): p. F658-65.**
29. **Tramonti, G., et al., *Expression and functional characteristics of tubular transporters: P-glycoprotein, PEPT1, and PEPT2 in renal mass reduction and diabetes.* Am J Physiol Renal Physiol, 2006. 291(5): p. F972-80.**
30. **Verri, T., et al., *Molecular and functional characterisation of the zebrafish (Danio rerio) PEPT1-type peptide transporter.* FEBS Lett, 2003. 549(1-3): p. 115-22.**
31. **Zhou, X., et al., *Characterization of an oligopeptide transporter in renal lysosomes.* Biochim Biophys Acta, 2000. 1466(1-2): p. 372-8.**
32. **Thamotharan, M., et al., *An active mechanism for completion of the final stage of protein degradation in the liver, lysosomal transport of dipeptides.* J Biol Chem, 1997. 272(18): p. 11786-90.**
33. **Bockman, D.E., et al., *Localization of peptide transporter in nuclei and lysosomes of the pancreas.* Int J Pancreatol, 1997. 22(3): p. 221-5.**
34. **Groneberg, D.A., et al., *Peptide transport in the mammary gland: expression and distribution of PEPT2 mRNA and protein.* Am J Physiol Endocrinol Metab, 2002. 282(5): p. E1172-9.**
35. **Agu, R.U., et al., *Proton-Coupled Oligopeptide Transporter (Pot) Family Expression in Human Nasal Epithelium and Their Drug Transport Potential.* Mol Pharm, 2011.**
36. **Rubio-Aliaga, I. and H. Daniel, *Peptide transporters and their roles in physiological processes and drug disposition.* Xenobiotica, 2008. 38(7-8): p. 1022-42.**
37. **Knutter, I., et al., *H+-peptide cotransport in the human bile duct epithelium cell line SK-ChA-1.* Am J Physiol Gastrointest Liver Physiol, 2002. 283(1): p. G222-9.**
38. **Doring, F., et al., *Delta-aminolevulinic acid transport by intestinal and renal peptide transporters and its physiological and clinical implications.* J Clin Invest, 1998. 101(12): p. 2761-7.**
39. **Herrera-Ruiz, D., et al., *Spatial expression patterns of peptide transporters in the human and rat gastrointestinal tracts, Caco-2 in vitro cell culture model, and multiple human tissues.* AAPS PharmSci, 2001. 3(1): p. E9.**
40. **Hilgendorf, C., et al., *Expression of thirty-six drug transporter genes in human intestine, liver, kidney, and organotypic cell lines.* Drug Metab Dispos, 2007. 35(8): p. 1333-40.**
41. **Augustine, L.M., et al., *Xenobiotic and endobiotic transporter mRNA expression in the blood-testis barrier.* Drug Metab Dispos, 2005. 33(1): p. 182-9.**
42. **Lu, H. and C. Klaassen, *Tissue distribution and thyroid hormone regulation of Pept1 and Pept2 mRNA in rodents.* Peptides, 2006. 27(4): p. 850-7.**

43. **Zhang, E.Y., et al., *Genetic polymorphisms in human proton-dependent dipeptide transporter PEPT1: implications for the functional role of Pro586.* J Pharmacol Exp Ther, 2004. 310(2): p. 437-45.**
44. **Liang, R., et al., *Human intestinal H+/peptide cotransporter. Cloning, functional expression, and chromosomal localization.* J Biol Chem, 1995. 270(12): p. 6456-63.**
45. **Fei, Y.J., et al., *cDNA structure, genomic organization, and promoter analysis of the mouse intestinal peptide transporter PEPT1.* Biochim Biophys Acta, 2000. 1492(1): p. 145-54.**
46. **Erickson, R.H., et al., *Regional expression and dietary regulation of rat small intestinal peptide and amino acid transporter mRNAs.* Biochem Biophys Res Commun, 1995. 216(1): p. 249-57.**
47. **Doring, F., et al., *Functional analysis of a chimeric mammalian peptide transporter derived from the intestinal and renal isoforms.* J Physiol, 1996. 497 (Pt 3): p. 773-9.**
48. **Doring, F., et al., *Importance of a small N-terminal region in mammalian peptide transporters for substrate affinity and function.* J Membr Biol, 2002. 186(2): p. 55-62.**
49. **Terada, T., et al., *N-terminal halves of rat H+/peptide transporters are responsible for their substrate recognition.* Pharm Res, 2000. 17(1): p. 15-20.**
50. **Daniel, H., *Molecular and integrative physiology of intestinal peptide transport.* Annu Rev Physiol, 2004. 66: p. 361-84.**
51. **Ganapathy, V. and F.H. Leibach, *Role of pH gradient and membrane potential in dipeptide transport in intestinal and renal brush-border membrane vesicles from the rabbit. Studies with L-carnosine and glycyl-L-proline.* J Biol Chem, 1983. 258(23): p. 14189-92.**
52. **Ganapathy, V., Brandsch, M. E., Leibach, F. H., ed. *Intestinal transport of amino acids and peptides.* Physiology of the gastrointestinal tract, ed. J. L. R. . 1994, Raven Press: New York. 1773 - 1794.**
53. **Mackenzie, B., et al., *Mechanisms of the human intestinal H+-coupled oligopeptide transporter hPEPT1.* J Biol Chem, 1996. 271(10): p. 5430-7.**
54. **Steel, A., et al., *Stoichiometry and pH dependence of the rabbit proton-dependent oligopeptide transporter PepT1.* J Physiol, 1997. 498 (Pt 3): p. 563-9.**
55. **Kottra, G., A. Stamfort, and H. Daniel, *PEPT1 as a paradigm for membrane carriers that mediate electrogenic bidirectional transport of anionic, cationic, and neutral substrates.* J Biol Chem, 2002. 277(36): p. 32683-91.**
56. **Amasheh, S., et al., *Transport of charged dipeptides by the intestinal H+/peptide symporter PepT1 expressed in Xenopus laevis oocytes.* J Membr Biol, 1997. 155(3): p. 247-56.**
57. **Lister, N., et al., *Dipeptide transport and hydrolysis in isolated loops of rat small intestine: effects of stereospecificity.* J Physiol, 1995. 484 (Pt 1): p. 173-82.**
58. **Daniel, H., E.L. Morse, and S.A. Adibi, *Determinants of substrate affinity for the oligopeptide/H+ symporter in the renal brush border membrane.* J Biol Chem, 1992. 267(14): p. 9565-73.**
59. **Biegel, A., et al., *Structural requirements for the substrates of the H+/peptide cotransporter PEPT2 determined by three-dimensional quantitative structure-activity relationship analysis.* J Med Chem, 2006. 49(14): p. 4286-96.**
60. **Vig, B.S., et al., *Human PEPT1 pharmacophore distinguishes between dipeptide transport and binding.* J Med Chem, 2006. 49(12): p. 3636-44.**
61. **Meredith, D., et al., *Modified amino acids and peptides as substrates for the intestinal peptide transporter PepT1.* Eur J Biochem, 2000. 267(12): p. 3723-8.**
62. **Carl SM, H.-R.D., Bhardwaj RK, Gudmundsson OS, Knipp G *Mammalian oligopetide transporters.*, in *Drug Transporters: Molecular Characterization and Role in Drug Disposition.* 2007, Wiley Hoboken.**
63. **Rubio-Aliaga, I. and H. Daniel, *Mammalian peptide transporters as targets for drug delivery.* Trends Pharmacol Sci, 2002. 23(9): p. 434-40.**

64. **Brandsch, M., et al., *Calmodulin-dependent modulation of pH sensitivity of the amino acid transport system L in human placental choriocarcinoma cells.* Biochim Biophys Acta, 1994. 1192(2): p. 177-84.**
65. **Muller, U., et al., *Inhibition of the H+/peptide cotransporter in the human intestinal cell line Caco-2 by cyclic AMP.* Biochem Biophys Res Commun, 1996. 218(2): p. 461-5.**
66. **Thamotharan, M., et al., *Mechanism of dipeptide stimulation of its own transport in a human intestinal cell line.* Proc Assoc Am Physicians, 1998. 110(4): p. 361-8.**
67. **Shiraga, T., et al., *Cellular and molecular mechanisms of dietary regulation on rat intestinal H+/Peptide transporter PepT1.* Gastroenterology, 1999. 116(2): p. 354-62.**
68. **Thamotharan, M., et al., *Hormonal regulation of oligopeptide transporter pept-1 in a human intestinal cell line.* Am J Physiol, 1999. 276(4 Pt 1): p. C821-6.**
69. **Buyse, M., et al., *PepT1-mediated epithelial transport of dipeptides and cephalexin is enhanced by luminal leptin in the small intestine.* J Clin Invest, 2001. 108(10): p. 1483-94.**
70. **Ashida, K., et al., *Thyroid hormone regulates the activity and expression of the peptide transporter PEPT1 in Caco-2 cells.* Am J Physiol Gastrointest Liver Physiol, 2002. 282(4): p. G617-23.**
71. **Ashida, K., et al., *Decreased activity and expression of intestinal oligopeptide transporter PEPT1 in rats with hyperthyroidism in vivo.* Pharm Res, 2004. 21(6): p. 969-75.**
72. **Vavricka, S.R., et al., *Tumor necrosis factor-alpha and interferon-gamma increase PepT1 expression and activity in the human colon carcinoma cell line Caco-2/bbe and in mouse intestine.* Pflugers Arch, 2006. 452(1): p. 71-80.**
73. **Marquet, P., et al., *Cryptosporidiosis induces a transient upregulation of the oligopeptides transporter (PepT1) activity in neonatal rats.* Exp Biol Med (Maywood), 2007. 232(3): p. 454-60.**
74. **Hindlet, P., et al., *Reduced intestinal absorption of dipeptides via PepT1 in mice with diet-induced obesity is associated with leptin receptor down-regulation.* J Biol Chem, 2009. 284(11): p. 6801-8.**
75. **Thamotharan, M., et al., *Functional and molecular expression of intestinal oligopeptide transporter (Pept-1) after a brief fast.* Metabolism, 1999. 48(6): p. 681-4.**
76. **Naruhashi, K., et al., *PepT1 mRNA expression is induced by starvation and its level correlates with absorptive transport of cefadroxil longitudinally in the rat intestine.* Pharm Res, 2002. 19(10): p. 1417-23.**
77. **Ihara, T., et al., *Regulation of PepT1 peptide transporter expression in the rat small intestine under malnourished conditions.* Digestion, 2000. 61(1): p. 59-67.**
78. **Howard, A., et al., *Increased expression of specific intestinal amino acid and peptide transporter mRNA in rats fed by TPN is reversed by GLP-2.* J Nutr, 2004. 134(11): p. 2957-64.**
79. **Shimakura, J., et al., *Induction of intestinal peptide transporter 1 expression during fasting is mediated via peroxisome proliferator-activated receptor alpha.* Am J Physiol Gastrointest Liver Physiol, 2006. 291(5): p. G851-6.**
80. **Murer, H., U. Hopfer, and R. Kinne, *Sodium/proton antiport in brush-border-membrane vesicles isolated from rat small intestine and kidney.* Biochem J, 1976. 154(3): p. 597-604.**
81. **Aronson, P.S., and Boron, W. F., ed. *Na+-H+ Exchange, Intracellular pH and Cell Function.* . Vol. 26. 1986, Academic Press: New York.**
82. **Grinstein, S., et al., *Characterization of the activation of Na+/H+ exchange in lymphocytes by phorbol esters: change in cytoplasmic pH dependence of the antiport.* Proc Natl Acad Sci U S A, 1985. 82(5): p. 1429-33.**
83. **Cavet, M.E., et al., *Half-lives of plasma membrane Na(+)/H(+) exchangers NHE1-3: plasma membrane NHE2 has a rapid rate of degradation.* Am J Physiol Cell Physiol, 2001. 281(6): p. C2039-48.**
84. **Pizzonia, J.H., et al., *Immunochemical characterization of Na+/H+ exchanger isoform NHE4.* Am J Physiol, 1998. 275(4 Pt 2): p. F510-7.**

85. Janecki, A.J., et al., *Subcellular redistribution is involved in acute regulation of the brush border Na+/H+ exchanger isoform 3 in human colon adenocarcinoma cell line Caco-2. Protein kinase C-mediated inhibition of the exchanger.* J Biol Chem, 1998. 273(15): p. 8790-8.
86. Szaszi, K., et al., *Clathrin-mediated endocytosis and recycling of the neuron-specific Na+/H+ exchanger NHE5 isoform. Regulation by phosphatidylinositol 3'-kinase and the actin cytoskeleton.* J Biol Chem, 2002. 277(45): p. 42623-32.
87. D'Souza, S., et al., *The epithelial sodium-hydrogen antiporter Na+/H+ exchanger 3 accumulates and is functional in recycling endosomes.* J Biol Chem, 1998. 273(4): p. 2035-43.
88. Brett, C.L., et al., *Human Na(+)/H(+) exchanger isoform 6 is found in recycling endosomes of cells, not in mitochondria.* Am J Physiol Cell Physiol, 2002. 282(5): p. C1031-41.
89. Klanke, C.A., et al., *Molecular cloning and physical and genetic mapping of a novel human Na+/H+ exchanger (NHE5/SLC9A5) to chromosome 16q22.1.* Genomics, 1995. 25(3): p. 615-22.
90. Numata, M., et al., *Identification of a mitochondrial Na+/H+ exchanger.* J Biol Chem, 1998. 273(12): p. 6951-9.
91. Numata, M. and J. Orlowski, *Molecular cloning and characterization of a novel (Na+,K+)/H+ exchanger localized to the trans-Golgi network.* J Biol Chem, 2001. 276(20): p. 17387-94.
92. Nakamura, N., et al., *Four Na+/H+ exchanger isoforms are distributed to Golgi and post-Golgi compartments and are involved in organelle pH regulation.* J Biol Chem, 2005. 280(2): p. 1561-72.
93. de Silva, M.G., et al., *Disruption of a novel member of a sodium/hydrogen exchanger family and DOCK3 is associated with an attention deficit hyperactivity disorder-like phenotype.* J Med Genet, 2003. 40(10): p. 733-40.
94. Goyal, S., G. Vanden Heuvel, and P.S. Aronson, *Renal expression of novel Na+/H+ exchanger isoform NHE8.* Am J Physiol Renal Physiol, 2003. 284(3): p. F467-73.
95. Zachos, N.C., M. Tse, and M. Donowitz, *Molecular physiology of intestinal Na+/H+ exchange.* Annu Rev Physiol, 2005. 67: p. 411-43.
96. Chu, J., S. Chu, and M.H. Montrose, *Apical Na+/H+ exchange near the base of mouse colonic crypts.* Am J Physiol Cell Physiol, 2002. 283(1): p. C358-72.
97. Mennone, A., et al., *Role of sodium/hydrogen exchanger isoform NHE3 in fluid secretion and absorption in mouse and rat cholangiocytes.* Am J Physiol Gastrointest Liver Physiol, 2001. 280(2): p. G247-54.
98. Orlowski, J. and S. Grinstein, *Diversity of the mammalian sodium/proton exchanger SLC9 gene family.* Pflugers Arch, 2004. 447(5): p. 549-65.
99. Seidler B, R.H., Murray A, Orlowski J, Tse CM, et al., *Expression of the Na+/H+ exchanger isoform NHE1–4 mRNA in different epithelial cell types of rat and rabbit gastricmucosa.* Gastroenterology, 1997. 110(A285 (Abstr.)).
100. Bookstein, C., et al., *Na+/H+ exchangers, NHE-1 and NHE-3, of rat intestine. Expression and localization.* J Clin Invest, 1994. 93(1): p. 106-13.
101. Repishti, M., et al., *Human duodenal mucosal brush border Na(+)/H(+) exchangers NHE2 and NHE3 alter net bicarbonate movement.* Am J Physiol Gastrointest Liver Physiol, 2001. 281(1): p. G159-63.
102. Hoogerwerf, W.A., et al., *NHE2 and NHE3 are human and rabbit intestinal brush-border proteins.* Am J Physiol, 1996. 270(1 Pt 1): p. G29-41.
103. Abedin, M.Z., et al., *Characterization of NA+/H+ exchanger isoform (NHE1, NH32 and NHE3) expression in prairie dog gallbladder.* J Membr Biol, 2001. 182(2): p. 123-34.
104. Silviani, V., et al., *Role of the NHE3 isoform of the Na+/H+ exchanger in sodium absorption by the rabbit gallbladder.* Pflugers Arch, 1996. 432(5): p. 791-6.
105. Schwark, J.R., et al., *S3226, a novel inhibitor of Na+/H+ exchanger subtype 3 in various cell types.* Pflugers Arch, 1998. 436(5): p. 797-800.

106. **Furukawa, O., et al., *NHE3 inhibition activates duodenal bicarbonate secretion in the rat.* Am J Physiol Gastrointest Liver Physiol, 2004. 286(1): p. G102-9.**
107. **Thwaites, D.T., et al., *H/dipeptide absorption across the human intestinal epithelium is controlled indirectly via a functional Na/H exchanger.* Gastroenterology, 2002. 122(5): p. 1322-33.**
108. **Hamilton, J.A., *Fatty acid transport: difficult or easy?* J Lipid Res, 1998. 39(3): p. 467-81.**
109. **Nehrke, K., *A reduction in intestinal cell pHi due to loss of the Caenorhabditis elegans Na+/H+ exchanger NHX-2 increases life span.* J Biol Chem, 2003. 278(45): p. 44657-66.**
110. **Reaven, G.M., *Banting lecture 1988. Role of insulin resistance in human disease.* Diabetes, 1988. 37(12): p. 1595-607.**
111. **Collins, S., et al., *Genetic vulnerability to diet-induced obesity in the C57BL/6J mouse: physiological and molecular characteristics.* Physiol Behav, 2004. 81(2): p. 243-8.**
112. **Ganapathy, V.G., N.; Martindale, RG., ed. *Protein digestion and absorption*. In: Physiology of the gastrointestinal tract, ed. J. L. R. . Vol. 4th ed.. 2006, Elsevier;: Burlington:. pp. 1667-1692.**
113. **Meissner, B., et al., *Deletion of the intestinal peptide transporter affects insulin and TOR signaling in Caenorhabditis elegans.* J Biol Chem, 2004. 279(35): p. 36739-45.**
114. **Hu, Y., et al., *Targeted disruption of peptide transporter Pept1 gene in mice significantly reduces dipeptide absorption in intestine.* Mol Pharm, 2008. 5(6): p. 1122-30.**
115. **Nassl, A.M., et al., *The Intestinal Peptide Transporter PEPT1 Is Involved in Food Intake Regulation in Mice Fed a High-Protein Diet.* PLoS One, 2011. 6(10): p. e26407.**
116. **Nassl, A.M., et al., *Amino acid absorption and homeostasis in mice lacking the intestinal peptide transporter PEPT1.* Am J Physiol Gastrointest Liver Physiol, 2011.**
117. **Surwit, R.S., et al., *Diet-induced type II diabetes in C57BL/6J mice.* Diabetes, 1988. 37(9): p. 1163-7.**
118. **West, D.B., et al., *Dietary obesity in nine inbred mouse strains.* Am J Physiol, 1992. 262(6 Pt 2): p. R1025-32.**
119. **Schemmel, R., O. Mickelsen, and J.L. Gill, *Dietary obesity in rats: Body weight and body fat accretion in seven strains of rats.* J Nutr, 1970. 100(9): p. 1041-8.**
120. **West, K.M. and J.M. Kalbfleisch, *Influence of nutritional factors on prevalence of diabetes.* Diabetes, 1971. 20(2): p. 99-108.**
121. **Mills, E., et al., *Hypertension in CB57BL/6J mouse model of non-insulin-dependent diabetes mellitus.* Am J Physiol, 1993. 264(1 Pt 2): p. R73-8.**
122. **Bjursell, M., et al., *Acutely reduced locomotor activity is a major contributor to Western diet-induced obesity in mice.* Am J Physiol Endocrinol Metab, 2008. 294(2): p. E251-60.**
123. **Clegg, M. and A. Shafat, *Energy and macronutrient composition of breakfast affect gastric emptying of lunch and subsequent food intake, satiety and satiation.* Appetite, 2010. 54(3): p. 517-23.**
124. **Clegg, M.E., et al., *Gastrointestinal transit, post-prandial lipaemia and satiety following 3 days high-fat diet in men.* Eur J Clin Nutr, 2011. 65(2): p. 240-6.**
125. **Clegg, M.E. and A. Shafat, *A high-fat diet temporarily accelerates gastrointestinal transit and reduces satiety in men.* Int J Food Sci Nutr, 2011.**
126. **Brownlow, B.S., et al., *The role of motor activity in diet-induced obesity in C57BL/6J mice.* Physiol Behav, 1996. 60(1): p. 37-41.**
127. **Parekh, P.I., et al., *Reversal of diet-induced obesity and diabetes in C57BL/6J mice.* Metabolism, 1998. 47(9): p. 1089-96.**
128. **Surwit, R.S., et al., *Differential effects of fat and sucrose on the development of obesity and diabetes in C57BL/6J and A/J mice.* Metabolism, 1995. 44(5): p. 645-51.**
129. **Rebuffe-Scrive, M., et al., *Regional fat distribution and metabolism in a new mouse model (C57BL/6J) of non-insulin-dependent diabetes mellitus.* Metabolism, 1993. 42(11): p. 1405-9.**

130. **Funkat, A., et al., *Metabolic adaptations of three inbred strains of mice (C57BL/6, DBA/2, and 129T2) in response to a high-fat diet.* J Nutr, 2004. 134(12): p. 3264-9.**
131. **Greenberg, A.S. and M.S. Obin, *Obesity and the role of adipose tissue in inflammation and metabolism.* Am J Clin Nutr, 2006. 83(2): p. 461S-465S.**
132. **Horowitz, J.F., et al., *Effect of short-term fasting on lipid kinetics in lean and obese women.* Am J Physiol, 1999. 276(2 Pt 1): p. E278-84.**
133. **Horowitz, J.F. and S. Klein, *Whole body and abdominal lipolytic sensitivity to epinephrine is suppressed in upper body obese women.* Am J Physiol Endocrinol Metab, 2000. 278(6): p. E1144-52.**
134. **Blaak, E.E., *Fatty acid metabolism in obesity and type 2 diabetes mellitus.* Proc Nutr Soc, 2003. 62(3): p. 753-60.**
135. **Postic, C. and J. Girard, *Contribution of de novo fatty acid synthesis to hepatic steatosis and insulin resistance: lessons from genetically engineered mice.* J Clin Invest, 2008. 118(3): p. 829-38.**
136. **Donnelly, K.L., et al., *Sources of fatty acids stored in liver and secreted via lipoproteins in patients with nonalcoholic fatty liver disease.* J Clin Invest, 2005. 115(5): p. 1343-51.**
137. **Hudgins, L.C., et al., *Relationship between carbohydrate-induced hypertriglyceridemia and fatty acid synthesis in lean and obese subjects.* J Lipid Res, 2000. 41(4): p. 595-604.**
138. **Parks, E.J., *Dietary carbohydrate's effects on lipogenesis and the relationship of lipogenesis to blood insulin and glucose concentrations.* Br J Nutr, 2002. 87 Suppl 2: p. S247-53.**
139. **Farrell, G.C. and C.Z. Larter, *Nonalcoholic fatty liver disease: from steatosis to cirrhosis.* Hepatology, 2006. 43(2 Suppl 1): p. S99-S112.**
140. **Thomas, E.L., et al., *Hepatic triglyceride content and its relation to body adiposity: a magnetic resonance imaging and proton magnetic resonance spectroscopy study.* Gut, 2005. 54(1): p. 122-7.**
141. **Park, S.H., et al., *Body fat distribution and insulin resistance: beyond obesity in nonalcoholic fatty liver disease among overweight men.* J Am Coll Nutr, 2007. 26(4): p. 321-6.**
142. **Lewis, G.F., et al., *Disordered fat storage and mobilization in the pathogenesis of insulin resistance and type 2 diabetes.* Endocr Rev, 2002. 23(2): p. 201-29.**
143. **Huang, X.D., et al., *Serum leptin and soluble leptin receptor in non-alcoholic fatty liver disease.* World J Gastroenterol, 2008. 14(18): p. 2888-93.**
144. **Mantzoros, C.S., *The role of leptin in human obesity and disease: a review of current evidence.* Ann Intern Med, 1999. 130(8): p. 671-80.**
145. **Lord, G., *Role of leptin in immunology.* Nutr Rev, 2002. 60(10 Pt 2): p. S35-8; discussion S68-84, 85-7.**
146. **Matarese, G., S. Moschos, and C.S. Mantzoros, *Leptin in immunology.* J Immunol, 2005. 174(6): p. 3137-42.**
147. **Saxena, N.K., et al., *Leptin in hepatic fibrosis: evidence for increased collagen production in stellate cells and lean littermates of ob/ob mice.* Hepatology, 2002. 35(4): p. 762-71.**
148. **Doi, Y., et al., *Liver enzymes as a predictor for incident diabetes in a Japanese population: the Hisayama study.* Obesity (Silver Spring), 2007. 15(7): p. 1841-50.**
149. **Yu, C., et al., *Deletion of Tis7 protects mice from high-fat diet-induced weight gain and blunts the intestinal adaptive response postresection.* J Nutr, 2010. 140(11): p. 1907-14.**
150. **Thomson, A.B., et al., *Dietary fat content influences uptake of hexoses and lipids into rabbit jejunum following ileal resection.* Digestion, 1986. 35(2): p. 78-88.**
151. **Thomson, A.B., et al., *Dietary fat selectively alters transport properties of rat jejunum.* J Clin Invest, 1986. 77(1): p. 279-88.**
152. **Li, D.F., et al., *Effect of fat sources and combinations on starter pig performance, nutrient digestibility and intestinal morphology.* J Anim Sci, 1990. 68(11): p. 3694-704.**
153. **Goda, T. and S. Takase, *Effect of dietary fat content on microvillus in rat jejunum.* J Nutr Sci Vitaminol (Tokyo), 1994. 40(2): p. 127-36.**

154. **Balint, J.A., M.B. Fried, and C. Imai, *Ileal uptake of oleic acid: evidence for adaptive response to high fat feeding.* Am J Clin Nutr, 1980. 33(11): p. 2276-80.**

155. **Sagher, F.A., et al., *Rat small intestinal morphology and tissue regulatory peptides: effects of high dietary fat.* Br J Nutr, 1991. 65(1): p. 21-8.**

156. **Singh, A., et al., *Adaptive changes of the rat small intestine in response to a high fat diet.* Biochim Biophys Acta, 1972. 260(4): p. 708-15.**

157. **Sukhotnik, I., et al., *Effect of dietary fat on early morphological intestinal adaptation in a rat with short bowel syndrome.* Pediatr Surg Int, 2004. 20(6): p. 419-24.**

158. **Sabb, J.E., P.M. Godfrey, and P.M. Brannon, *Adaptive response of rat pancreatic lipase to dietary fat: effects of amount and type of fat.* J Nutr, 1986. 116(5): p. 892-9.**

159. **Spannagel, A.W., et al., *Adaptation to fat markedly increases pancreatic secretory response to intraduodenal fat in rats.* Am J Physiol, 1996. 270(1 Pt 1): p. G128-35.**

160. **Felig, P., *Amino acid metabolism in man.* Annu Rev Biochem, 1975. 44: p. 933-55.**

161. **Qin, L.Q., et al., *Higher branched-chain amino acid intake is associated with a lower prevalence of being overweight or obese in middle-aged East Asian and Western adults.* J Nutr, 2011. 141(2): p. 249-54.**

162. **Murakami, S., et al., *Effect of taurine on cholesterol metabolism in hamsters: up-regulation of low density lipoprotein (LDL) receptor by taurine.* Life Sci, 2002. 70(20): p. 2355-66.**

163. **Nakaya, Y., et al., *Taurine improves insulin sensitivity in the Otsuka Long-Evans Tokushima Fatty rat, a model of spontaneous type 2 diabetes.* Am J Clin Nutr, 2000. 71(1): p. 54-8.**

164. **Hsu, T.C., et al., *Treatment with taurine attenuates hepatic apoptosis in NZB/W F1 mice fed with a high-cholesterol diet.* J Agric Food Chem, 2008. 56(20): p. 9685-91.**

165. **Chang, Y.Y., et al., *Preventive effects of taurine on development of hepatic steatosis induced by a high-fat/cholesterol dietary habit.* J Agric Food Chem, 2011. 59(1): p. 450-7.**

166. **Li, T., et al., *Transgenic expression of cholesterol 7alpha-hydroxylase in the liver prevents high-fat diet-induced obesity and insulin resistance in mice.* Hepatology, 2010. 52(2): p. 678-90.**

167. **Arjmandi, B.H., et al., *Dietary soluble fiber and cholesterol affect serum cholesterol concentration, hepatic portal venous short-chain fatty acid concentrations and fecal sterol excretion in rats.* J Nutr, 1992. 122(2): p. 246-53.**

168. **Arjmandi, B.H., et al., *Soluble dietary fiber and cholesterol influence in vivo hepatic and intestinal cholesterol biosynthesis in rats.* J Nutr, 1992. 122(7): p. 1559-65.**

169. **Buhman, K.K., et al., *Dietary psyllium increases fecal bile acid excretion, total steroid excretion and bile acid biosynthesis in rats.* J Nutr, 1998. 128(7): p. 1199-203.**

170. **Moore, W.E. and L.V. Holdeman, *Human fecal flora: the normal flora of 20 Japanese-Hawaiians.* Appl Microbiol, 1974. 27(5): p. 961-79.**

171. **Vrieze, A., et al., *The environment within: how gut microbiota may influence metabolism and body composition.* Diabetologia, 2010. 53(4): p. 606-13.**

172. **Berg, R.D., *The indigenous gastrointestinal microflora.* Trends Microbiol, 1996. 4(11): p. 430-5.**

173. **Zengler, K., et al., *Cultivating the uncultured.* Proc Natl Acad Sci U S A, 2002. 99(24): p. 15681-6.**

174. **Favier, C.F., et al., *Molecular monitoring of succession of bacterial communities in human neonates.* Appl Environ Microbiol, 2002. 68(1): p. 219-26.**

175. **Sefcikova, Z., et al., *Developmental changes in gut microbiota and enzyme activity predict obesity risk in rats arising from reduced nests.* Physiol Res, 2011. 60(2): p. 337-46.**

176. **Edwards, C.A. and A.M. Parrett, *Intestinal flora during the first months of life: new perspectives.* Br J Nutr, 2002. 88 Suppl 1: p. S11-8.**

177. **Hopkins, M.J., R. Sharp, and G.T. Macfarlane, *Age and disease related changes in intestinal bacterial populations assessed by cell culture, 16S rRNA abundance, and community cellular fatty acid profiles.* Gut, 2001. 48(2): p. 198-205.**

178. **Zoetendal, E.G., Akkermans, A.D.L., Akkermans-van Vliet W.M., de Visser J.A.G.M., de Vos W.M., *The host genotype affects the bacterial community in the human gastrointestinal tract.* Microbial. Ecol. Health Dis., 2001. 13(3): p. 129-134.**
179. **Sullivan, A., C. Edlund, and C.E. Nord, *Effect of antimicrobial agents on the ecological balance of human microflora.* Lancet Infect Dis, 2001. 1(2): p. 101-14.**
180. **DiBaise, J.K., et al., *Gut microbiota and its possible relationship with obesity.* Mayo Clin Proc, 2008. 83(4): p. 460-9.**
181. **Turnbaugh, P.J., et al., *An obesity-associated gut microbiome with increased capacity for energy harvest.* Nature, 2006. 444(7122): p. 1027-31.**
182. **Backhed, F., et al., *Mechanisms underlying the resistance to diet-induced obesity in germ-free mice.* Proc Natl Acad Sci U S A, 2007. 104(3): p. 979-84.**
183. **Buhman, K.K., et al., *Inhibition of Hedgehog signaling protects adult mice from diet-induced weight gain.* J Nutr, 2004. 134(11): p. 2979-84.**
184. **Nishizuka, Y., *Intracellular signaling by hydrolysis of phospholipids and activation of protein kinase C.* Science, 1992. 258(5082): p. 607-14.**
185. **Huang, J.M., H. Xian, and M. Bacaner, *Long-chain fatty acids activate calcium channels in ventricular myocytes.* Proc Natl Acad Sci U S A, 1992. 89(14): p. 6452-6.**
186. **Ordway, R.W., J.V. Walsh, Jr., and J.J. Singer, *Arachidonic acid and other fatty acids directly activate potassium channels in smooth muscle cells.* Science, 1989. 244(4909): p. 1176-9.**
187. **Hamilton, J.A., *New insights into the roles of proteins and lipids in membrane transport of fatty acids.* Prostaglandins Leukot Essent Fatty Acids, 2007. 77(5-6): p. 355-61.**
188. **Schaffer, J.E., *Fatty acid transport: the roads taken.* Am J Physiol Endocrinol Metab, 2002. 282(2): p. E239-46.**
189. **Hamilton, J.A., et al., *Changes in internal pH caused by movement of fatty acids into and out of clonal pancreatic beta-cells (HIT).* J Biol Chem, 1994. 269(33): p. 20852-6.**
190. **Elsing, C., A. Kassner, and W. Stremmel, *Effect of surface and intracellular pH on hepatocellular fatty acid uptake.* Am J Physiol, 1996. 271(6 Pt 1): p. G1067-73.**
191. **Civelek, V.N., et al., *Intracellular pH in adipocytes: effects of free fatty acid diffusion across the plasma membrane, lipolytic agonists, and insulin.* Proc Natl Acad Sci U S A, 1996. 93(19): p. 10139-44.**
192. **Loffing, J. and B. Kaissling, *Sodium and calcium transport pathways along the mammalian distal nephron: from rabbit to human.* Am J Physiol Renal Physiol, 2003. 284(4): p. F628-43.**

Acknowledgement

An dieser Stelle möchte ich mich bei allen herzlich bedanken, die zum Gelingen meiner Doktorarbeit beigetragen haben:

Ich möchte mich bei Prof. Dr. Hannelore Daniel bedanken, dass sie mir die Möglichkeit gegeben hat meine Doktorarbeit an ihren Lehrstuhl anzufertigen.

Danke auch an Prof. Dr. Hans Hauner als meinen Zweitbetreuer.

Besonders möchte ich mich bei Ronny Scheundel bedanken, der mich immer wieder zuverlässig mit Mäusen versorgt hat und mir auch sonst mit Rat und Tat zur Seite stand.

Ein großer Dank gilt auch Dr. Tamara Zietek und Dr. Christian Scherling, die mir mit konstruktiven Gesprächen und verschiedenen Analysen eine große Hilfe waren.

Außerdem gilt mein Dank Ramona Pais, Tobias Ludwig und Christoph Dahlhoff, die mir bei den Mausexperimenten immer wieder geholfen haben. Ohne euch hätte ich die große Anzahl der Tiere nie durchmessen können.

Ich möchte mich auch bei der ganzen AG Klingenspor für die Einweisungen an diversen Geräten und die konstruktiven Gespräche bedanken. Mein besonderer Dank gilt Nadine Rink, Florian Bolze und Katrin Seyfart, die mir eine sehr große Hilfe im Tierstall waren, sowie Sabine Mocek, die immer ein zuverlässiger Ansprechpartner für die Bombenkalorimetrie und die FT-IR war.

Danke auch an unsere Tierpflegerinnen, Aline Lukacs, Anna Bhandari, Christina Reim und Patricia Izidoro-Ziehlke. Ohne euch würde der Tierstall nicht funktionieren.

Ferner möchte ich mich bei Heike, Karen, Chantal, Andre und Christoph bedanken. Unsere Koch-, Grill- und Cocktailabende sind mir immer eine willkommene Abwechslung zum Arbeitsstress.

Acknowledgement

Ein ganz großes Dankeschön geht an Frederic Lemnitzer, der mich immer wieder aufgebaut und motiviert hat durchzuhalten und weiter zu machen, meine Doktorarbeit korrekturgelesen und mir bei sämtlichen Abbildungen geholfen hat. Ohne dich hätte ich diese Zeit niemals durchgestanden.

Danke auch an meine Eltern, die mein Studium und damit meine Doktorarbeit ermöglicht und mich bei jedem meiner vielen Tiefpunkte in dieser Zeit immer wieder motiviert haben durchzuhalten.

Last but not least, danke den knapp 200 Mäusen, die ihr Leben im Namen der Wissenschaft gelassen und mein Projekt ermöglicht haben.

Curriculum vitae

Personal data

Name:	Dominika Johanna Kolodziejczak
Date of birth:	5th December 1981
Place of birth:	Katowice, Poland
Nationality:	German

School education

09 – 12/1988	primary school Katowice, Polen
01 – 07/1989	primary school Reit im Winkl
1989 – 1990	primary school Augsburg Oberhausen
1990 – 1992	primary school Süd Königsbrunn
1992 – 2001	Gymnasium Königsbrunn
July 2001	Abitur

University education

2001 – 2007	Studies of Biology, University of Constance
2006 – 2007	Diploma thesis at the group of Prof. Dr. Stefan Weiß, Gene Center Munich, LMU
2007 – 2008	research associate at the Gene Center Munich, LMU
2008 – 2011	PhD in Nutrition Physiology at the group of Prof. Dr. Hannelore Daniel, Molecular Nutrition Unit, TUM

Additional Qualification

11 - 20.02.08	Internship at the veterinary institute, Georg-August University, Göttingen Isolation of ovine enterocytes from duodenum

8/2005 - 9/2005	Internship at the Institute of toxicology, Heinrich-Heine University, Düsseldorf Cultivation and immunfluorescence microscopy of *C. elegans*
6/2005 - 7/2005	Internship at the Institute of pharmacology, University of Cologne Caco-2 cell culture, RNA isolation from mouse tissue
8/2004 - 9/2004	Internship at the Eurofins Analytik GmbH, Labor Dr. Hallermayer, Augsburg Microbiological analyses of food and drinks
2/2004 - 4/2004	Internship at the Firma Synlab®, Medizinisches Versorgungszentrum für Laboratoriumsdiagnostik, Augburg Microbiological und biochemical analyses of human blood, urine, stool samples

List of scientific publications

2009 Vana K, Zuber C, Pflanz H, **Kolodziejczak D,** Zemora G, Bergmann AK, Weiss S. LRP/LR as an alternative promising target in therapy of prion diseases, Alzheimer's disease and cancer. Infect Disord Drug Targets. 2009 Feb; 9(1):69-80.

2010 **Kolodziejczak D**, Da Costa Dias B, Zuber C, Jovanovic K, Omar A, Beck J, Vana K, Mbazima V, Richt J, Brenig B, Weiss SF. Prion interaction with the 37-kDa/67-kDa laminin receptor on enterocytes as a cellular model for intestinal uptake of prions. J Mol Biol. 2010 Sep 17; 402(2):293-300.

2013 Lemnitzer F, Raschbichler V, **Kolodziejczak D**, Israel L, Imhof A, Bailer SM, Koszinowski U, and Ruzsics Z. Mouse cytomegalovirus egress protein pM50 interacts with cellular endophilin-A2. Cell Microbiol. 2013 Feb; 15(2):335-51

2013 **Kolodziejczak D**, Spanier B, Pais R, Kraiczy J, Stelzl T, Gedrich K, Scherling C, Zietek T, Daniel H. Mice lacking the intestinal peptide transporter display reduced energy intake and a subtle maldigestion/-absorption that protects them from diet-induced obesity. Am J Phys Gastro. Accepted.

Oral communications

10/2008 1st GRK1482 meeting, Hohenkammer, Germany

07/2009 2nd GRK1482 meeting, Freising, Germany

12/2009 GRK1482 networking day, Freising, Germany

10/2010 3rd GRK1482 meeting, Seeon, Germany

Poster presentations

12/2011 D. Kolodziejczak, B. Spanier, H. Hauner, H. Daniel. The role of PEPT1 in control of lipid metabolism. Freising, Germany.

Hiermit versichere ich, Dominika Johanna Kolodziejczak, dass ich die vorliegende Arbeit

Phenotyping of PEPT1-deficient mice on the background of a high fat-diet induced obesity

selbständig verfasst und keine anderen als die angegebenen Quellen und Hilfsmittel benutzt habe.

Diese Arbeit hat in gleicher oder ähnlicher Form noch keiner andern Prüfungsbehörde vorgelegen.

Ort, Datum

Unterschrift